Bootstrapping $N_f = 4$ conformal QED$_3$

Soner Albayrak[,1,2] Rajeev S. Erramilli[,1] Zhijin Li[,1] David Poland[,1] and Yuan Xin[1]

[1]*Department of Physics, Yale University, New Haven, Connecticut 06511, USA*
[2]*Institute of Physics, University of Amsterdam, Amsterdam 1098 XH, Netherlands*

We present the results of a conformal bootstrap study of the presumed unitary IR fixed point of quantum electrodynamics in three dimensions (QED$_3$) coupled to $N_f = 4$ two-component Dirac fermions. Specifically, we study the four-point correlators of the $SU(4)$ adjoint fermion bilinear r and the monopole of lowest topological charge $\mathcal{M}_{1/2}$. Most notably, the scaling dimensions of the fermion bilinear r and the monopole $\mathcal{M}_{1/2}$ are found to be constrained into a closed island with a combination of spectrum assumptions inspired by the $1/N_f$ perturbative results as well as a novel interval positivity constraint on the next-lowest-charge monopole $\mathcal{M}_1$. Bounds in this island on the $SU(4)$ and topological $U(1)_t$ conserved current central charges c_J, c_J^t, as well as on the stress tensor central charge c_T, are comfortably consistent with the perturbative results. Together with the scaling dimensions, this suggests that a part of estimates from the $1/N_f$ expansion—even at $N_f = 4$—provide a self-consistent solution to the bootstrap crossing equations, despite some of our assumptions not being strictly justified.

I. INTRODUCTION

Quantum electrodynamics in three dimensions (QED$_3$) has been extensively studied over the past decades, partially motivated by qualitative similarities with four dimensional quantum chromodynamics. The gauge coupling in QED$_3$ has positive mass dimension, and so the theory is asymptotically free and strongly coupled in the infrared (IR) limit. The IR phase of QED$_3$ depends on the number of electrons N_f.[1] In the large N_f limit, the theory can be solved using a $1/N_f$ expansion, which suggests a renormalization group flow to an IR fixed point [1,2]. The pure $U(1)$ gauge theory with $N_f = 0$ is expected to be confined in the IR due to a proliferation of monopoles [3,4]. Schwinger-Dyson equation analysis [5,6] and some lattice simulations [7] suggest that at small N_f, the IR phase of QED$_3$ has its chiral symmetry spontaneously broken (χSB),

$$SU(N_f) \to SU(N_f/2) \times SU(N_f/2) \times U(1),$$

due to the dynamical generation of a fermion mass. It is expected that there is a critical flavor number N_f^* which separates the conformal phase from the χSB phase.

QED$_3$ also has various fundamental applications in condensed matter physics. In particular, $N_f = 4$ QED$_3$ has been utilized to describe high-temperature superconductors, or more generally Dirac spin liquids [8–13]. $N_f = 2$ QED$_3$ has been proposed to be part of the 3D fermion-boson duality web and is an effective theory for the deconfined quantum critical point, see [14] for a comprehensive review.

A crucial unanswered question in these studies is the value of the critical flavor number N_f^* of QED$_3$. Various approaches have been used to estimate N_f^* [1,2,15–45][2]; however, there is no general consensus to what the actual value should be. Estimates range from 0 all the way up to 10.[3] The problem is made worse by the fact that the theory is actually strongly coupled near N_f^*, rendering the estimations of perturbative approaches unreliable. Lattice simulations do offer a nonperturbative approach, but their results remain inconsistent between each other. In particular, some lattice simulations indicate that there is no χSB for any $N_f > 0$ [41–44] and that the low energy limit of QED$_3$ coupled with massless fermions is always

---

[1]In this work, the flavor number refers to N_f two-component Dirac fermions, and we will assume N_f is even to avoid the parity anomaly.

[2]Some of these studies focused on QED$_3$ with a noncompact gauge group $\mathbb{R}$, in which the monopole contributions have been suppressed. At small N_f its low energy dynamics may be different from compact QED$_3$.

[3]See [36] for more details on this discrepancy.

conformal. This assertion stands in contrast to other lattice results which observed χSB at $N_f = 2$ and a conformal phase at $N_f \geq 4$ [37–40]. A subtle issue in the study of $N_f = 2$ QED$_3$ by lattice simulations is the violation of conformality by a small nonunitary factor, as this could not be distinguished from the standard conformal phase due to the finiteness of practical lattice simulations. For instance, [43] measures the scaling dimension of the monopole with lowest unit of topological charge in $N_f = 2$ QED$_3$, and according to the bootstrap result [45], their data requires a weakly relevant singlet scalar, indicating that the theory is slightly below the conformal window in the so-called merger and annihilation scenario for the loss of conformality in QED$_3$ [18,23,24,46–48].[4]

The modern conformal bootstrap [49,50] provides a powerful nonperturbative approach to study conformal QED$_3$, free of the subtleties of the perturbative and lattice computations, and poised to be able to answer puzzles such as the value of the critical N_f^*. Bootstrap studies of QED$_3$ have been initiated in [51,52] by focusing on the monopole operators in QED$_3$. In 3D, $U(1)$ gauge theories have a unique property of admitting a topological symmetry $U(1)_t$, whose nontrivial representations are constructed by the monopole operators. From bootstrap point of view, the power of the monopole operators is that they let us distinguish QED$_3$ from e.g. the $SU(N_c)$ QCD$_3$. Moreover, monopole operators are known to play important roles in QED$_3$ with small N_f. For instance, in $N_f = 2$ QED$_3$ which is a part of the 3D boson-fermion duality web [14], the monopoles provide dual descriptions of the gauge invariant composite operators made from elementary fermions. In [51], the authors obtained bootstrap bounds on the scaling dimensions of the leading charge $q = 1/2$ and $q = 1$ monopoles close to saturation, but these bounds were quite sensitive to the gap assumptions, especially to what the authors refer to as Δ_2 (which we will refer to as $\Delta_{S_{(220)}}$), which will also play an important role in our study.

Other encouraging results towards bootstrapping conformal QED$_3$ have been obtained by bootstrapping $SU(N_f)$ adjoint fermion bilinear scalars [53]; these operators are the leading gauge-invariant operators with a nontrivial $SU(4)$ representation, and therefore can give us a view into the flavor symmetry of this theory. The study [53] found bootstrap bounds with sharp kinks for $N_f > 2$: for large N_f, the location of the kink approaches free fermion theory; for large but finite N_f, the location is close to the perturbative predictions of conformal QED$_3$; and for sufficiently small N_f the kink disappears, implying some

critical $N_f^* \in (2, 3)$. The lowest singlet operator approaches marginality condition near N_f^*, consistent with the merger and annihilation mechanism [18,23,24,46–48] for the loss of conformality in QED$_3$. However, it has been proved in [54] that the kinks in the singlet bounds are wholly $SO(N)$ symmetric and cannot literally be identified with conformal QED$_3$, while they may correspond to the conformal QED$_3$ through $SO(N)$ symmetry enhancement in the bootstrap bounds [54,55]. Another set of studies focused on the $SU(N)$ adjoint bilinears in scalar QED$_3$ [56,57], with similarly promising results (including isolated regions at large N_f or in $d = 2 + \epsilon$ which may contain the scalar QED$_3$ solution [56]).

A natural next step would be to bootstrap crossing equations of both the monopoles and the $SU(4)$ adjoint fermion bilinears; this was recently pursued in [58]. The authors make assumptions inspired by the constraints of lattice implementations, based on which they obtain lower bounds on the dimension of the leading monopole $\Delta_{\mathcal{M}_{1/2}}$ in order to reach the IR fixed point of $N_f = 4$ QED$_3$ on a triangular lattice $\Delta_{\mathcal{M}_{1/2}} > 1.046$ or kagome lattice $\Delta_{\mathcal{M}_{1/2}} > 1.105$. The bounds are consistent with recent Monte Carlo estimates [41,43,59] but they exclude the large N_f expansion prediction $\Delta_{\mathcal{M}_{1/2}} \approx 1.022$.

In this work we will provide a more comprehensive bootstrap study for $N_f = 4$ conformal QED$_3$. An important element of our analysis is that the crossing equations of single correlators with the $SU(4)$-adjoint fermion bilinear operator r and the monopole operator with lowest unit of topological charge $\mathcal{M}_{1/2}$ have enhanced $SO(15)$ and $SO(12)$ symmetry, respectively. A direct consequence of the $SO(N)$ symmetry enhancement of the crossing equations is that suitable gap assumptions are necessary to obtain bootstrap results for non-$SO(N)$ symmetric theories, e.g. conformal QED$_3$. We will use the fermion bilinear bootstrap to demonstrate the gap dependence of the bootstrap bounds, and show that interesting results for $N_f = 4$ conformal QED$_3$ can be obtained after introducing gap assumptions inspired by the perturbative results. Our most interesting results are obtained from the monopole bootstrap, presented in Sec. IV C, in which the scaling dimensions of operators r and $\mathcal{M}_{1/2}$ are restricted into a closed island after introducing an *interval positivity* assumption, along with some input about gaps in the monopole spectrum. Parity symmetry also plays a critical role in generating the monopole bootstrap results. Our bootstrap results suggest that part of the perturbative conformal field theory (CFT) data of $N_f = 4$ conformal QED$_3$ provides a consistent solutions to the crossing equations.

The paper is organized as follows. In Sec. II we briefly review the perturbative results on conformal QED$_3$, which provide useful guides for our bootstrap studies. In Sec. III we explain the gap dependence of the $SU(4)$ adjoint bootstrap bounds caused by the $SO(15)$ symmetry

---

[4]In the merger and annihilation scenario for the loss of conformality in QED$_3$, we expect the fixed point of QED$_3$ to merge with another fixed point as we continuously vary N_f down to N_f^* from above, and these points annihilate one another below N_f^*. A candidate theory for the other fixed point is the so-called *QED Gross Neveu Yukawa* (QED$_3$-GNY) fixed point.

enhancement in the crossing equations and show that interesting results can be obtained after introducing gap assumptions inspired by the perturbative results. In Sec. IV we revisit the monopole bootstrap. We explain the $SO(12)$ symmetry enhancement in the crossing equations and show that parity symmetry can help to restrict the CFT data in a closed region consistent with the results from $1/N_f$ expansions. In Sec. V we study the mixed correlator bootstrap with fermion bilinear operator r and the monopole $\mathcal{M}_{1/2}$. Conclusions and discussions are given in Sec. VI. Technical details related to the bootstrap studies are provided in Appendices.

II. PERTURBATIVE RESULTS FOR CONFORMAL QED3

QED3 can be understood pertubatively in the large N_f limit, where one can identify a conformal fixed point and solve conformal QED3 analytically in a $1/N_f$ expansion. At small N_f this expansion breaks down and the theory becomes strongly coupled, making perturbative estimates of the theory as well as the critical flavor number N_f^* harder to calculate. One of the main objectives of this work is to test whether the results from perturbative computations can be consistent with constraints from the conformal bootstrap.

In Euclidean signature, the QED3 action, i.e. the action of a $U(1)$ gauge theory coupled to N_f massless charged two-component Dirac fermions, is

$$S = \int d^3x \left(\frac{1}{4e^2} F^{\mu\nu} F_{\mu\nu} - \sum_{i=1}^{N_f} \bar{\psi}_i \sigma^\mu (\partial_\mu + iA_\mu) \psi^i \right), \quad (2.1)$$

where e is the $U(1)$ gauge coupling constant, A_μ is the gauge field with field strength $F_{\mu\nu} = \partial_\mu A_\nu - \partial_\nu A_\mu$, and ψ^i are the N_f fermions in the fundamental representation of the flavor symmetry $SU(N_f)$. The gamma matrices associated with two-component Dirac fermions are given by the Pauli matrices $\sigma^\mu, \mu = 1, 2, 3$. Besides the flavor symmetry $SU(N_f)$, the theory also has a $U(1)_t$ global symmetry associated with a conserved current

$$J_\mu^t = \frac{1}{4\pi} \epsilon_{\mu\nu\rho} F^{\nu\rho}. \quad (2.2)$$

The current J_μ^t is conserved due to the Bianchi identity of the $U(1)$ gauge field, i.e. $dF = 0$. The local operators charged under $U(1)_t$ are the monopole operators corresponding to the nontrivial topology of the $U(1)$ gauge field. The $U(1)_t$ charges q of the monopole operators are quantized according to the Dirac quantization condition. We will follow the normalization of monopole operators in [51,52], in which $2q \in \mathbb{Z}$.

Due to the contributions from fermionic zero modes in the topological gauge field configurations, the monopole operators also construct nontrivial representations of the flavor symmetry $SU(N_f)$. According to their charges under topological $U(1)_t$, the local gauge invariant operators in QED3 can be separated into two parts: the $U(1)_t$ charged monopole operators and the composite operators made from products of fundamental fields which are neutral under topological $U(1)_t$.

A. Scaling dimensions of low-lying gauge invariant operators with $U(1)_t$ charge $q = 0$

In large N_f QED3, a set of local gauge invariant operators can be constructed out of the fundamental fields ψ_i, A_μ and their derivatives. These operators do not correspond to any nontrivial topology of $U(1)$ gauge field and are neutral ($q = 0$) under the topological $U(1)_t$; however, they form nontrivial representations of the flavor symmetry $SU(N_f)$. In this work, we will be interested in the fermion bilinear operator $r \equiv \bar{\psi}_i \psi^j - \frac{1}{N_f} \delta_i^j \bar{\psi}_k \psi^k$ with $N_f = 4$, which forms an $SU(4)$ adjoint representation. The operator product expansion (OPE) of $r \times r$ can be decomposed into $SU(N_f)$ irreducible representations (irreps):

$$(211) \otimes (211) = (000)^+ \oplus (211)^+ \oplus (211)^- \oplus (220)^+$$
$$\oplus (310)^- \oplus (332)^- \oplus (422)^+, \quad (2.3)$$

where the ith number in the vector (abc) denotes the number of boxes in the ith line in the Young diagram of the representation, e.g. (211) is the adjoint representation. The superscripts $+/-$ denote even/odd spin selection rules. Since r forms a real representation of $SU(4)$, only real representations can appear in the right hand side (rhs) of above equation; for instance, only the real combination of (310) and (332) can appear in the $r \times r$ OPE, which will be denoted by $(310)_R$ throughout this paper.

Another important fact to take into account is the parity symmetry. The fermion bilinear scalar is parity odd, and so all the operators in the rhs of (2.3) are parity even. The lowest parity-even operators in these sectors are constructed from fermion quadrilinear operators or their mixing with the gauge kinetic operator F^2. These four-fermion operators play important roles in solving the conformal QED3 crossing equations. The scaling dimensions of these operators have been computed using $1/N_f$ expansion in previous studies [1,2,12,60–65], which we now summarize.

The scaling dimension of the parity odd $SU(N_f)$ adjoint fermion bilinear scalar has been computed to the order $1/N_f^2$ [61]:

$$\Delta_{(211)} = 2 - \frac{64}{3\pi^2 N_f} + \frac{256(28 - 3\pi^2)}{9\pi^4 N_f^2}. \quad (2.4a)$$

The $SU(N_f)$ singlet four-fermion operator $(\bar{\psi}_i\psi^i)^2$ has scaling dimension of 4 at tree level, identical to the $U(1)$ gauge kinetic term $F_{\mu\nu}F^{\mu\nu}$. They can mix with each other through quantum loop corrections; the scaling dimensions of the resultant two operators at order $1/N_f$ are

$$\Delta^{\pm}_{(000)} = 4 + \frac{64(2 \pm \sqrt{7})}{3\pi^2 N_f}. \qquad (2.4b)$$

We expect that the singlet operator with negative anomalous dimension $\Delta_S < 4$ plays an important role in the loss of conformality in QED$_3$. For sufficiently small N_f, Δ_S approaches the marginality condition $\Delta_S = 3$ from above and eventually generates an RG flow, dissolving the IR fixed point of QED$_3$ below N_f^*. Above N_f^*, the singlet four-fermion coupling can also generate a UV fixed point, whose UV completion is given by the QED$_3$-Gross-Neveu-Yukawa model. In this work, we will only focus on the QED$_3$ IR fixed point, and assume that $N_f^* < 4$, as indicated by previous bootstrap studies and some lattice simulations.

The scaling dimension of the lowest scalar in the parity even (220) sector has been computed in [63,65] at the order $1/N_f$ to be

$$\Delta_{(220)} = 4 - \frac{64}{\pi^2 N_f}, \qquad (2.4c)$$

this operator will play an important role in bootstrap computations. Meanwhile, the scaling dimension of the parity even adjoint scalar[5] is

$$\Delta_{(211)} = 4 + \frac{8(25 \pm \sqrt{2317})}{3\pi^2 N_f}, \qquad (2.4d)$$

where the two operators differ by the contraction of the flavor indices at tree level [65]. Note that with $N_f = 4$ the two operators have scaling dimensions about 2.44 and 8.94, respectively! Clearly, these first order corrections to the scaling dimensions of these four-fermion operators are significant, and so these results should be taken cautiously: it would be interesting to know if the higher order corrections can improve the behavior of these perturbative expansions. In [63] the author also computed the scaling dimension of lowest parity even scalar in the (422) sector

$$\Delta_{(422)} = 4 + \frac{64}{3\pi^2 N_f}. \qquad (2.4e)$$

We would like to briefly comment on the convergence of the perturbative results in Eq. (2.4). For the parity odd

---

[5]We remind the reader that Eq. (2.4d) is for the *parity even* scalar, whereas the result in Eq. (2.4a) is for the *parity odd* operator r, which is also in the (211) sector.

fermion bilinear adjoint operator, the second order correction is quite small, being only 5.4% of the first order correction. Meanwhile, for the lowest scalars in the parity even (220) and (211) sectors, the first order corrections at $N_f = 4$ are nearly 40% of the tree level results. The $1/N_f$ perturbative results obtained in [65] suggest that the convergence becomes worse for composite operators with more fermions. It is currently unclear how well the leading order results can estimate scaling dimensions of four fermion operators in these sectors: as noted previously, it would be quite useful to compute higher order corrections to clarify this issue. For the $SU(N_f)$ adjoint fermion bilinear scalar, Monte Carlo simulations in [41,59] have computed the scaling dimension of r, which is consistent with the leading order results even for $N_f = 4$; however, there are significant error bars in the estimates, which cannot exclude a potentially notable correction to the current result.

B. Conserved charges in conformal QED$_3$

Conserved currents play fundamental roles in the study of CFTs. In conformal QED$_3$, there are three such currents: the stress tensor $T_{\mu\nu}$ and two global symmetry currents, $J^j_{\mu,i}$ and J^t_μ, the latter of which are associated with the $SU(N_f)$ flavor symmetry and the topological $U(1)_t$ symmetry, respectively. The two-point functions of these conserved currents (in the normalization of [65]) are

$$\langle T_{\mu\nu}(x_1)T_{\lambda\rho}(x_2)\rangle = c_T \frac{3}{16\pi^2(x_{12}^2)^3} I_{\mu\nu,\lambda\rho}(x_{12}), \qquad (2.5a)$$

$$\langle J^j_{\mu,i}(x_1)J^l_{\nu,k}(x_2)\rangle = c_J \frac{1}{8\pi^2(x_{12}^2)^2} I_{\mu\nu}(x_{12})\left(\delta^l_i\delta^j_k - \frac{1}{N_f}\delta^j_i\delta^l_k\right), \qquad (2.5b)$$

$$\langle J^t_\mu(x_1)J^t_\nu(x_2)\rangle = c_J^t \frac{1}{8\pi^2(x_{12}^2)^2} I_{\mu\nu}(x_{12}), \qquad (2.5c)$$

where c_x are the central charges and the tensor structures are defined through

$$I_{\mu\nu}(x) \equiv \delta_{\mu\nu} - 2\frac{x_\mu x_\nu}{x^2}, \qquad (2.6a)$$

$$I_{\mu\nu,\lambda\rho}(x) \equiv \frac{1}{2}(I_{\mu\lambda}(x)I_{\nu\rho}(x) + I_{\mu\rho}(x)I_{\nu\lambda}(x)) - \frac{1}{3}\delta_{\mu\nu}\delta_{\lambda\rho} \qquad (2.6b)$$

for convenience. The above central charges have been computed to subleading order in the $1/N_f$ expansion in [26][6]:

---

[6]These central charges have also been studied in [66,67].

$$c_T = c_{T0}\left(1 + \frac{0.7193}{N_f} + O\left(1/N_f^2\right)\right), \tag{2.7a}$$

$$c_J = c_{J0}\left(1 + \frac{0.1429}{N_f} + O\left(1/N_f^2\right)\right), \tag{2.7b}$$

$$c_J^t = \frac{6.4846}{N_f}\left(1 - \frac{0.1429}{N_f} + O\left(1/N_f^2\right)\right). \tag{2.7c}$$

Here c_{T0} and c_{J0} are the contributions from the free fermions to the central charges, which are equal to 1 in our normalization.

It is worth mentioning one other result from [26], on c_T and c_J in QCD$_3$ with an $SU(N_c)$ Yang-Mills gauge field coupled with quarks in the fundamental representation of the color group:

$$c_T = N_c c_{T0}\left(1 + \frac{0.7193}{N_f}\frac{N_c^2 - 1}{N_c} + O\left(1/N_f^2\right)\right), \tag{2.8a}$$

$$c_J = N_c c_{J0}\left(1 + \frac{0.1429}{N_f}\frac{N_c^2 - 1}{N_c} + O\left(1/N_f^2\right)\right). \tag{2.8b}$$

Compared with QED$_3$, c_T, and c_J in QCD$_3$ with gauge group $SU(N_c)$ have an additional factor of N_c, due to the color degrees of freedom carried by the fermions. The non-Abelian gauge fields also contain more degrees of freedom than the $U(1)$ gauge field, which increase the subleading order corrections in c_T and c_J. This provides a key differentiation between QED$_3$ and QCD$_3$, which otherwise might be hard to distinguish in bootstrap studies just by looking at their low-lying spectrum.

C. Large N_f expansion of the monopole spectrum in QED$_3$

Monopole operators in QED$_3$ have been studied in various works [52,68–71]. Their quantum numbers (Δ_i, q_i, R_i) consist of their scaling dimension Δ_i, their topological charge q_i under $U(1)_t$ symmetry, and their $SU(4)$ representation R_i. We will be particularly interested in the monopoles $\mathcal{M}_{1/2}$ and $\mathcal{M}_1$ carrying the lowest topological charges $q = 1/2$ and $q = 1$,[7] which, respectively, sit in (110) and (220) representations of $SU(4)$. The scaling dimensions of these monopole operators were computed in [70,71] to subleading order in the large N_f expansion. The authors computed the free energy on $S^2 \times \mathbb{R}$ in the presence of a monopole flux in the IR limit $e^2 N_f \to \infty$. The scaling dimensions of the monopole operators on $\mathbb{R}^3$ are then given by the energies of the monopole states on $S^2 \times \mathbb{R}$ through the state-operator

---

[7]In this work we will follow the conventions and the normalization used in [69,70].

correspondence. For the monopoles $\mathcal{M}_{1/2}$ and $\mathcal{M}_1$, their scaling dimensions are [71]

$$\Delta_{\mathcal{M}_{1/2}} = 0.26510 N_f - 0.038138(5) + O(1/N_f), \tag{2.9a}$$

$$\Delta_{\mathcal{M}_1} = 0.67315 N_f - 0.19340(3) + O(1/N_f). \tag{2.9b}$$

At $N_f = 4$, the above formulas give $\Delta_{\mathcal{M}_{1/2}} \simeq 1.022$, $\Delta_{\mathcal{M}_1} \simeq 2.499$. The subleading corrections are fairly small compared with the leading terms, even at small $N_f = 4$.

The OPE of the monopole operators $\mathcal{M}_{1/2} \times \mathcal{M}_{1/2}$ plays a key role in our bootstrap study. There are an infinity family of operators with topological charge $q = 1$ appearing in this OPE. Like the monopoles $\mathcal{M}_{1/2}$ and $\mathcal{M}_1$, these operators can be constructed by applying fermionic creation operators on the monopole vacuum with 4π background magnetic flux. Our bootstrap study will make important use of the topological charge 1 spectrum appearing in the $\mathcal{M}_{1/2} \times \mathcal{M}_{1/2}$ OPE, which we discuss in more detail below.

States or operators with topological charge q can be explicitly constructed in the free theory limit $e^2 N_f \to 0$ using a formalism developed in [52]. To construct these states, one first chooses a monopole vacuum with background magnetic flux $4\pi q$ uniformly distributed in the 2D sphere of the Lorentzian spacetime $S^2 \times \mathbb{R}$. Then the spectrum with topological charge q can be obtained by constructing the gauge invariant states of free massless fermions ψ^i in this background. The building blocks of a generic state are the fermionic modes in the classical solutions of the fermion field, which can be obtained by solving the Dirac equation $(i\nabla + \mathcal{A})\psi = 0$ in the monopole vacuum, giving a mode expansion

$$\psi^i(t, x) = \sum_{m=1/2-q}^{q-1/2} c_{q-1/2,m}^{i,\dagger} C_{q,q-1/2,m}(x)$$
$$+ \sum_{j>q-1/2,m} (a_{jm}^{i,\dagger} A_{qjm}(x)e^{i\lambda_j t} + b_{jm}^i B_{qjm}(x)e^{-i\lambda_j t}), \tag{2.10}$$

where q is an overall label of the family of states on the same monopole background, and each fermion mode is labeled by the flavor indices i and total angular momentum quantum numbers j and m. The operators $a_{jm}^{i,\dagger}$, $b_{jm,i}^\dagger$, and $c_{q-1/2,m}^{i,\dagger}$ are fermion creation operators, and their corresponding coefficients A_{qjm}, B_{qjm}, and $C_{q,q-1/2,m}$, are spinor spherical harmonics. Specifically, $a_{jm}^{i,\dagger}$ ($b_{jm,i}^\dagger$) corresponds to (anti)particles, whereas $c_{q-1/2,m}^{i,\dagger}$ corresponds to fermion zero modes; furthermore, each $a_{jm}^{i,\dagger}$ and $c_{q-1/2,m}^{i,\dagger}$ ($b_{jm,i}^\dagger$) mode transforms in the (anti)fundamental representation of the $SU(N)$ group, and carry gauge $U(1)$ charge $+1$ (-1).

TABLE I.　Quantum numbers of the bare monopole with topological charge q and the fermionic creation operators, adapted from [52].

	Energy/scaling dimension	Spin	Gauge charge	$SU(N)$ irrep
$a^{i,\dagger}_{jm}$	$\sqrt{(j+1/2)^2 - q^2}$	$j(\geq q+1/2)$	$+1$	**N**
$b^{i,\dagger}_{jm,i}$	$\sqrt{(j+1/2)^2 - q^2}$	$j(\geq q+1/2)$	-1	$\bar{\mathbf{N}}$
$c^{i,\dagger}_{q-1/2,m}$	0	$q-1/2$	$+1$	**N**
M_{bare}	Δ_{bare}	0	$-qN$	1

The quantum numbers of the creation operators are given in Table I.[8] See [52] for more details on the monopole vacuum and fermionic creation operators.

In principle the fermionic creation operators in Table I allow us to construct any states or operators in the topological charge q sector. There is a subtle issue that the above microstate construction is based on the free fermions in the UV limit $e^2 N_f \to 0$ of QED$_3$, while the theory we are interested in corresponds to its IR fixed point, which relates to the $e^2 N_f \to \infty$ limit. Nevertheless, there is evidence from the thermal computation which suggests that the states have significant overlaps between the two different limits [52].

We then set out to construct as completely as possible the low-lying states of $N_f = 4$ QED$_3$. Our strategy is the following:

(1) We first set a maximum energy threshold $\Delta_{\max}$, and exhaust all possible combinations of creation operators $a^{i,\dagger}_{jm}$, $b^\dagger_{jm,i}$, and $c^{i,\dagger}_{q-1/2,m}$, with the constraint that the net gauge charge is zero.

(2) We decompose states created by each sequence of $a^{i,\dagger}_{jm}$, $b^\dagger_{jm,i}$, and $c^{i,\dagger}_{q-1/2,m}$ operators into irreps of the product group of spin and flavor symmetries $SU(2) \times SU(4)$.

(3) Within the sectors of the same $SU(2) \times SU(4)$ irreps, we antisymmetrize the fermion creation operators, and collect the linearly independent states.

(4) After obtaining all possible states created by the fermion modes, it is straightforward to get the scaling dimension, spin, $SU(4)$ irreps and parity of the corresponding operators.

More details of our procedure can be found in Appendix C, and we present the results in Table II. Here, we would like to briefly comment on the data in Table II: it describes the low-lying spectrum predicted by the large N_f mode expansion, where some entries are improved wherever results about subleading corrections in $1/N_f$ are available. Additionally, there is a possible caveat of the above

procedure that it does not include operators created by gauge fields. Therefore we need to add the operators constructed from gauge fields by hand. Pure gauge field operators include the topological current $J^{t\mu}$, $F^{\mu\nu}F_{\mu\nu}$, and their composite operators. $J^{t\mu}$ is already added to the table by hand, whereas $F^{\mu\nu}F_{\mu\nu}$ mixes with the $SU(4)$ singlet four-fermion operator. It is of course also possible to have composite operators between $J^{t\mu}$ and operators constructed from the fermion modes, which are annotated with a *. We will frequently refer to this table when introducing assumptions on the spectrum in our bootstrap equations.

III. $SU(4)$ ADJOINT FERMION BILINEAR BOOTSTRAP

The fermion bilinear scalar $r^j_i \equiv \bar{\psi}_i \psi^j - \frac{1}{N_f}\delta^j_i \bar{\psi}_k \psi^k$ is one of the lowest-dimension gauge-invariant operators in QED$_3$, making it a natural candidate for bootstrap studies of IR fixed points of gauge theories coupled with fermions; see e.g. [53,54,72–74]. A main challenge in the fermion bilinear bootstrap comes from the $SO(N_f^2 - 1)$ symmetry enhancement in the crossing equations [54,55]. To bootstrap conformal QED$_3$ with a proper $SU(N_f)$ symmetry, one has to resolve the $SO(N_f^2 - 1)$ symmetry enhancement in the crossing equations. In this section, we will describe how the $SO(N_f^2 - 1)$ symmetry enhancement can be slightly broken by introducing gap assumptions inspired by the perturbative $N_f = 4$ conformal QED$_3$ spectrum, and the resulting bootstrap bounds have kinks which could conjecturally be connected to $N_f = 4$ conformal QED$_3$. Nevertheless, the positions of the kinks are sensitive to the gap assumptions, so even under this conjecture more input needs to be given or more constraints need to be imposed in order to extract the physical solution of QED$_3$.

A. Crossing equations with different symmetries and gap dependence

In certain theories, there exists an $SO(N)$ symmetry enhancement of the crossing equations which affect general single correlator bootstrap bounds [54,55,75]. In particular, there is a unique map up to normalization which transforms the $SU(N_f)$ adjoint crossing equation into the $SO(N_f^2 - 1)$ vector crossing equations; see [55,57]. Here we will

---

[8]The energy of the bare monopole is the Casimir energy of the fermion fields

$$\Delta_{\text{bare}} = -N \sum_{j=q-1/2}^{\infty} d_j \lambda_j,$$

where $d_j = 2j + 1$ is the degeneracy. The infinite sum is treated by ζ-function regularization to give a finite answer.

TABLE II. A summary of estimates for the low-lying spectrum appearing in our bootstrap crossing equations obtained using the large N_f expansion. The $SO(2)$ irrep, $SU(4)$ irrep, spin, the lowest 2 or 3 scaling dimensions, and the OPE channels that the operators contribute to are shown for each type of operators. The dimensions correspond to the scaling dimension of operators constructed using the fermion mode creation operators, J^t, and their composition. Whenever subleading order corrections are available in the literature, we added them as well. The dimension is annotated with * if the corresponding operator is a composite operator involving J^t. Note that the $SO(2)$ irrep encodes both the $U(1)$ charge and the parity information: the $SO(2)$ irreps S and A have $U(1)$ charge $q = 0$ and are parity even and odd, respectively, whereas the $SO(2)$ irreps V and T have the respective $U(1)$ charges $q = 1/2$ and $q = 1$ while they can have either parity. Special operators are highlighted in the table using square brackets.

$SO(2)$ rep	$SU(4)$ rep	Spin-j	Δ_1	Δ_2	OPE
S	(000) (Singlet)	0	$4 + \frac{64(2\pm\sqrt{7})}{3\pi^2 N_f} = \frac{6.510}{3.651}$	5.00*	$\lambda_{rrO}, \lambda_{MMO}$
S	(211) (Adj)	0	$4 + \frac{8(25\pm\sqrt{2317})}{3\pi^2 N_f} = \frac{8.940}{2.437}$	5.00*	λ_{rrO}
S	(211) (Adj)	1	$2.00 \; [J_f]$	4.00	$\lambda_{rrO}, \lambda_{MMO}$
S	(220) (AĀ)	0	$4 - \frac{64}{\pi^2 N_f} = 2.379$	6.00	$\lambda_{rrO}, \lambda_{MMO}$
S	$(310)_R$ (SĀ)	1	5.00	6.00	λ_{rrO}
S	(422) (SS̄)	0	$4 + \frac{64}{3\pi^2 N_f} = 4.540$	6.00	λ_{rrO}
A	(000) (Singlet)	1	$2.00 \; [J^t]$	3.00	λ_{MMO}
A	(211) (Adj)	0	$2 - \frac{64}{3\pi^2 N_f} + \frac{256(28-3\pi^2)}{9\pi^4 N_f^2} = 1.43 \; [r]$	4.00	λ_{MMO}
A	(220) (AĀ)	1	4.00	6.00	λ_{MMO}
T	(000) (Singlet)	0	4.424	6.156	λ_{MMO}
T	(211) (Adj)	1	2.692	4.424	λ_{MMO}
T	(220) (AĀ)	0	$2.499 \; [M_1]$	6.156	λ_{MMO}
V	(110) (Anti)	0	$1.022 \; [M_{1/2}]$	3.888	λ_{rMO}
V	(110) (Anti)	1	2.474	3.060*	λ_{rMO}
V	(200) (Sym)	0	3.888	4.474*	λ_{rMO}
V	(200) (Sym)	1	2.474	3.888	λ_{rMO}
V	(321) (AAdj)	0	3.888	5.303	λ_{rMO}
V	(321) (AAdj)	1	3.888	4.924	λ_{rMO}

follow [54] and provide a more detailed study of its effect on the bootstrap bounds.

The operators that can appear in the $r \times r$ OPE are provided in (2.3). The crossing equations of the four-point correlator $\langle r(x_1) r(x_2) r(x_3) r(x_4) \rangle$ can be written in the vector form

$$\sum_{\mathcal{O}\in\ell^+} \lambda_{\mathcal{O}}^2 \vec{V}_{(000)}^+ + \sum_{\mathcal{O}\in\ell^+} \lambda_{\mathcal{O}}^2 \vec{V}_{(211)}^+ + \sum_{\mathcal{O}\in\ell^-} \lambda_{\mathcal{O}}^2 \vec{V}_{(211)}^-$$

$$+ \sum_{\mathcal{O}\in\ell^-} \lambda_{\mathcal{O}}^2 \vec{V}_{(310)_R}^- + \sum_{\mathcal{O}\in\ell^+} \lambda_{\mathcal{O}}^2 \vec{V}_{(220)}^+ + \sum_{\mathcal{O}\in\ell^+} \lambda_{\mathcal{O}}^2 \vec{V}_{(422)}^+ = 0,$$

(3.1)

where the vector $\vec{V}_R^\pm$ is a 6-component vector corresponding to the $SU(4)$ representation R with even/odd spin.[9] The crossing equations can be captured by a 6×6 matrix:

$$\mathcal{M}_{SU(4)\text{-ad}} = \begin{pmatrix} 0 & 0 & 0 & -F & F & F \\ 0 & \frac{1}{2}F & 0 & 0 & -\frac{1}{2}F & \frac{1}{6}F \\ 0 & -F & -F & \frac{1}{4}F & \frac{1}{2}F & \frac{1}{6}F \\ F & -4F & 0 & 0 & \frac{16}{3}F & \frac{16}{15}F \\ H & -H & 0 & -H & -\frac{2}{3}H & -\frac{14}{15}H \\ 0 & H & -H & \frac{1}{4}H & \frac{1}{2}H & -\frac{7}{6}H \end{pmatrix},$$

(3.2)

where the columns of the matrix correspond to the vectors $\vec{V}_R^\pm$ in the order

$$\mathcal{M}_{SU(4)\text{-ad}}$$
$$= \left(\vec{V}_{(000)}^+, \vec{V}_{(211)}^+, \vec{V}_{(211)}^-, \vec{V}_{(310)_R}^-, \vec{V}_{(220)}^+, \vec{V}_{(422)}^+ \right)_{SU(4)\text{-ad}},$$

(3.3)

and the variables F, H denote the symmetrized/antisymmetrized conformal blocks

$$F = v^{\Delta_r} g_{\Delta,\ell}(u, v) - u^{\Delta_r} g_{\Delta,\ell}(v, u),$$ (3.4a)

---

[9]The vector $\vec{V}_{(310)_R}$ corresponds to the real combination of $\vec{V}_{(310)}$ and $\vec{V}_{(332)}$.

$$H = v^{\Delta_r} g_{\Delta,\ell}(u,v) + u^{\Delta_r} g_{\Delta,\ell}(v,u). \qquad (3.4\text{b})$$

A notable property of the above $SU(4)$ adjoint crossing equations is that they admit a unique (up to normalization) transformation $\mathcal{T}_{SU(4)\text{-ad}}$

$$\mathcal{T}_{SU(4)\text{-ad}} = \begin{pmatrix} 1 & \frac{226}{119} & \frac{4}{7} & 0 & 0 & 0 \\ -1 & \frac{894}{119} & -\frac{4}{7} & 1 & 0 & 0 \\ 0 & 0 & 0 & 0 & 1 & \frac{4}{7} \end{pmatrix}, \qquad (3.5)$$

which maps the $SU(4)$ adjoint crossing equations to the $SO(15)$ vector crossing equations

$$\mathcal{M}_{SO(15)} = (\vec{V}_S^+, \vec{V}_T^+, \vec{V}_A^-)_{SO(15)} = \begin{pmatrix} 0 & F & -F \\ F & \frac{13}{15}F & F \\ H & -\frac{17}{15}H & -H \end{pmatrix},$$
$$(3.6)$$

in which S, T, A represent the singlet, traceless symmetric, and antisymmetric representations of $SO(15)$, respectively.

The action of $\mathcal{T}_{SU(4)\text{-ad}}$ is

$$(\mathcal{T} \cdot \mathcal{M})_{SU(4)\text{-ad}}$$
$$= \begin{pmatrix} 0 & \frac{45}{119}F & -\frac{4}{7}F & -\frac{6}{7}F & \frac{40}{119}F & \frac{24}{17}F \\ F & \frac{39}{119}F & \frac{4}{7}F & \frac{6}{7}F & \frac{104}{357}F & \frac{104}{85}F \\ H & -\frac{3}{7}H & -\frac{4}{7}H & -\frac{6}{7}H & -\frac{8}{21}H & -\frac{8}{5}H \end{pmatrix}, \qquad (3.7)$$

which can be briefly expressed in a vector form

$$\mathcal{T}_{SU(4)\text{-ad}} \cdot \left(\vec{V}_{(000)}^+, \vec{V}_{(211)}^+, \vec{V}_{(211)}^-, \vec{V}_{(310)_R}^-, \vec{V}_{(220)}^+, \vec{V}_{(422)}^+ \right)_{SU(4)\text{-ad}}$$
$$= (\vec{V}_S^+, x_1\vec{V}_T^+, x_2\vec{V}_A^-, x_3\vec{V}_A^-, x_4\vec{V}_T^+, x_5\vec{V}_T^+)_{SO(15)}, \qquad (3.8)$$

with positive coefficients x_i

$$\vec{x} = \left(\frac{45}{119}, \frac{4}{7}, \frac{6}{7}, \frac{40}{119}, \frac{24}{17} \right). \qquad (3.9)$$

We will show that the positivity of these coefficients is critical in the bootstrap algorithm.

We can summarize the above by saying that the transformation $\mathcal{T}_{SU(4)\text{-ad}}$ maps the channels of the $SU(4)$ adjoint crossing equations $\mathcal{M}_{SU(4)\text{-ad}}$ to the channels of the $SO(15)$ vector crossing equations $\mathcal{M}_{SO(15)}$ through the branching rules

SO(15)   **SU(4)**

$$S \leftrightarrow (000)^+, \qquad (3.10\text{a})$$

$$T \leftrightarrow (211)^+ \oplus (220)^+ \oplus (422)^+, \qquad (3.10\text{b})$$

$$A \leftrightarrow (211)^- \oplus (310)_R^-. \qquad (3.10\text{c})$$

The goal of the conformal bootstrap algorithm is to find linear functionals

$$\vec{\beta} \equiv (\beta_1, \beta_2, \beta_3, \beta_4, \beta_5, \beta_6)$$

whose action on the crossing equations $\mathcal{M}_{SU(4)\text{-ad}}$ satisfies

$$\vec{\beta} \cdot \mathcal{M}_{SU(4)\text{-ad}} = \left(\beta_{(000)}^+, \beta_{(211)}^+, \beta_{(211)}^-, \beta_{(310)_R}^-, \beta_{(220)}^+, \beta_{(422)}^+ \right)$$
$$\succeq 0_{1\times 6}, \ \forall \Delta \geq \Delta_{R_i,\ell}^*, \qquad (3.11)$$

where $\Delta_{R_i,\ell}^*$ is the assumed minimum scaling dimension of any spin ℓ operator in the R_i representation of $SU(4)$.[10] Due to the algebraic relation (3.8), any linear functional $\vec{\alpha} \equiv (\alpha_1, \alpha_2, \alpha_3)$ satisfying the $SO(15)$ bootstrap equations

$$\vec{\alpha} \cdot \mathcal{M}_{SO(15)} = \vec{\alpha} \cdot (\vec{V}_S^+, \vec{V}_T^+, \vec{V}_A^-)_{SO(15)}$$
$$= (\alpha_S^+, \alpha_T^+, \alpha_A^-) \succeq 0_{1\times 3}, \quad \forall \Delta \geq \Delta_{S/T/A,\ell}^*, \qquad (3.12)$$

can be used to construct linear functionals in the $SU(4)$ adjoint bootstrap

$$\vec{\beta}_{1\times 6} = \vec{\alpha}_{1\times 3} \cdot (\mathcal{T}_{SU(4)\text{-ad}})_{3\times 6}, \qquad (3.13)$$

which also satisfies the $SU(4)$ adjoint bootstrap equations

$$\vec{\beta} \cdot \mathcal{M}_{SU(4)\text{-ad}} = (\vec{\alpha} \cdot \mathcal{T}_{SU(4)\text{-ad}}) \cdot \mathcal{M}_{SU(4)\text{-ad}},$$
$$= \vec{\alpha} \cdot (\vec{V}_S^+, x_1\vec{V}_T^+, x_2\vec{V}_A^-, x_3\vec{V}_A^-, x_4\vec{V}_T^+, x_5\vec{V}_T^+)_{SO(15)},$$
$$= (\alpha_S^+, x_1\alpha_T^+, x_2\alpha_A^-, x_3\alpha_A^-, x_4\alpha_T^+, x_5\alpha_T^+) \succeq 0_{1\times 6}, \quad \forall \Delta \geq \Delta_{R_i,\ell}^*, \qquad (3.14)$$

given that the gap assumptions $\Delta_{R_i,\ell}^*$ are consistent with those in the $SO(15)$ vector bootstrap $\Delta_{S/T/A,\ell}^*$ following the branching rules (3.10). Note in the second line we have employed the identity (3.8) and the positivity condition in the third line follows from the positivity of $\alpha_{S/T/A}^\pm$ owing to the positive coefficients x_i.

The relation (3.14) suggests that the bounds from $SU(4)$-adjoint bootstrap cannot be weaker than that from the $SO(15)$ vector bootstrap, i.e. $\Delta_{SO(15)-v}^* \geq \Delta_{SU(4)-ad}^*$,

---

[10]$\Delta_{R_i,\ell}^*$ is either the unitary bound or a specific value above the unitary bound.

because any linear functional that excludes some CFT data in the $SO(15)$ vector bootstrap must exclude the same data in the $SU(4)$-adjoint bootstrap. On the other hand, because any four-point correlator of the $SO(15)$ vectors can be decomposed into four-point correlators of the $SU(4)$ adjoint scalar, the inverse is true, i.e. $\Delta^*_{SO(15)-v} \leq \Delta^*_{SU(4)-ad}$. Therefore we have exactly the same bounds from $SO(15)$ vector bootstrap and $SU(4)$-adjoint bootstrap computations, $\Delta^*_{SO(15)-v} = \Delta^*_{SU(4)-ad}$, under the condition that sectors on both sides that are related by the branching rules (3.10) have the same gap assumptions.

The above arguments show that due to the algebraic relation (3.8), the $SU(4)$ adjoint bootstrap problem with suitably related gap assumptions is equivalent to the $SO(15)$ vector bootstrap and admits the same solutions. The differences between the two bootstrap setups come from the gap assumptions $\Delta^*_{R_i,\ell}$. To illustrate, let us consider the upper bounds on the scaling dimensions of the lowest nonidentity singlet scalar Δ_0, without imposing any gap assumptions besides the unitary bounds in other sectors; i.e. our assumptions are

$$\Delta_{(000),\ell=0} \geq \Delta_0, \quad \Delta_{\text{other sectors}} \geq \text{unitary bounds} \quad (3.15)$$

in the $SU(4)$ adjoint bootstrap and

$$\Delta_{S,\ell=0} \geq \Delta_0, \quad \Delta_{\text{other sectors}} \geq \text{unitary bounds} \quad (3.16)$$

in the $SO(15)$ vector bootstrap. The two sets of assumptions are consistent with the $SO(15) \to SU(4)$ branching rules (3.10). In consequence the singlet bounds obtained from the $SU(4)$ adjoint bootstrap and $SO(15)$ vector bootstrap are exactly the same.

Another interesting example is given by the upper bound on the scaling dimension of the lowest $SO(15)$ traceless symmetric scalar Δ_1 obtained from the $SO(15)$ vector bootstrap. Without imposing any extra gap assumptions, the assumptions are

$$\Delta_{T,\ell=0} \geq \Delta_1, \quad \Delta_{\text{other sectors}} \geq \text{unitary bounds.} \quad (3.17)$$

In the $SU(4)$ adjoint bootstrap, if we want to get the upper bound on the scaling dimension of the lowest scalar in a sector like the (422) representation without imposing extra gap assumptions, then the assumptions are

$$\Delta_{(422),\ell=0} \geq \Delta_1, \quad \Delta_{\text{other sectors}} \geq \text{unitary bounds.} \quad (3.18)$$

According to the branching rule (3.10b), the $SO(15)$ assumptions in (3.17) are actually equivalent to

$$\Delta_{T,\ell=0} \to \begin{cases} \Delta_{(422),\ell=0} \geq \Delta_1 \\ \Delta_{(220),\ell=0} \geq \Delta_1 \,, \\ \Delta_{(211),\ell=0} \geq \Delta_1 \end{cases}$$

$$\Delta_{\text{other sectors}} \geq \text{unitary bounds,} \quad (3.19)$$

which is stronger than the assumptions (3.18) in the $SU(4)$ adjoint bootstrap. Consequently, the upper bound on the scaling dimensions of the lowest (422) scalar in the $SU(4)$ adjoint bootstrap is weaker than the bound on the lowest traceless symmetric scalar in the $SO(15)$ vector bootstrap.[11] Nevertheless, the two bounds coincide with each other if we impose the assumption that the scalars in the three sectors (422), (220), and (211) all have the same minimum scaling dimension Δ_1.

The symmetry enhancement (3.8) thus leads to a surprising fact that, in the single correlator bootstrap, although the crossing equations admit $SU(4)$ symmetry, it cannot be distinguished from an $SO(15)$ symmetry at the crossing equation level. The constraints specific to $SU(4)$ symmetric theories can only be obtained from the gap assumptions that break the $SO(15)$ symmetry explicitly. This suggests that the gap assumptions in the bootstrap conditions are the only ingredients that we may resort to to carve out the parameter space of non-$SO(N)$ symmetric CFTs, while the role of the non-$SO(N)$ symmetric crossing equations is to provide access to individual sectors branched from the $SO(N)$ representations. Our bootstrap bounds for non-$SO(N)$ symmetric theories are obtained based on non-$SO(N)$ symmetric gap assumptions, and the bounds directly rely on the magnitudes of gaps in certain sectors; i.e. they are gap dependent.

For the ambitious bootstrap dream which aims to completely solve the IR fixed points of gauge theories, this gap dependence could be a serious problem. One hopes that the bootstrap bounds can provide numerical solutions of targeted theories with only a few reliable and general assumptions. On the other hand, the gap dependence of the bootstrap bounds indicates that the physical solutions may not saturate the bootstrap bounds unless there are sufficiently precise gaps input to the bootstrap equations. Below we will show several examples of the gap dependence of the bootstrap bounds and study possible approaches to partially resolve this problem.

B. $SU(4)$ adjoint bootstrap results

In this section we study the constraints on the CFT data of $N_f = 4$ conformal QED$_3$ by bootstrapping the $SU(4)$

---

[11]In principle, it is possible that there could be no solution to the crossing equations between the two gap sets (3.17) and (3.19). In this case, the two bootstrap boundary conditions (3.17) and (3.19) can actually generate the same bootstrap bound. In this work, we find the bootstrap bounds with such different boundary conditions are indeed different at finite derivative order Λ.

adjoint fermion bilinear scalars. The main results are that the bootstrap approach indeed can provide nontrivial constraints on the putative CFT data of the theory, and after imposing certain gaps inspired by the QED_3 spectrum, there are prominent kinks in the bootstrap bounds on scaling dimensions of operators in different $SU(4)$ representations, indicating the existence of a special solution to the crossing equations containing an $SU(4)$ adjoint scalar. Notably, the dimension of this scalar is near the perturbative and lattice results of $N_f = 4$ QED_3. However, as discussed above, the precise locations of these kinks are gap dependent, and consequently we need more information or constraints to pin down the underlying theories of these kinks using the conformal bootstrap and to firmly establish their connection to QED_3.

The fermion bilinear scalar r is parity odd in QED_3 and the operators appearing in the $r \times r$ OPE are parity even. The lowest scalars on the rhs of (3.10) are parity even four-fermion operators, which have scaling dimensions $4 \pm O(1/N_f^2)$ and break $SO(N_f^2 - 1)$ symmetry by their $1/N_f$ corrections, see Table II for details on the subleading corrections of the scaling dimensions of these four-fermion operators. Another notable factor breaking the $SO(15)$ symmetry appears on the rhs of (3.10c): in the $(211)^-$ sector, the lowest operator is the spin-1 conserved current corresponding to the $SU(4)$ symmetry, while in the $(310)_R^-$ sector, the lowest spin-1 operator has scaling dimension $5 \pm O(1/N_f)$. Its subleading correction is not known yet, while the scaling dimension of this operator is expected to be notably higher than the unitary bound.

In Fig. 1 we show the bootstrap bounds on the scaling dimension of the lowest scalar in the $S\bar{S}$ sector. The lightest blue shadowed region denotes the bootstrap bound obtained from the $SU(4)$ adjoint bootstrap without imposing any gap assumptions. The bootstrap bound is smooth without any significant structure, nevertheless, it is already quite interesting even without any extra input information specific to QED_3. The red dot represents the $1/N_f$ perturbative results for the scaling dimensions of the fermion bilinear r (at order $1/N_f^2$) and the leading scalar in the $S\bar{S}$ sector (at order $1/N_f$). The perturbative data is notably above the bootstrap bounds and cannot belong to a unitary CFT, which suggests that at least one of the operators will receive significant higher order corrections.

The green dashed line gives the bootstrap bound on the lowest traceless symmetric scalar from the $SO(15)$ vector bootstrap. The same bound appears in the $SU(4)$ adjoint bootstrap if the sectors on the rhs of (3.10b) have the same gap assumptions, due to the bound coincidence explained previously. The bootstrap bound shows a sharp kink near $\Delta_r \sim 1.35$, close to the expected scaling dimension of the $SU(4)$ adjoint fermion bilinear scalar in $N_f = 4$ QED_3. Comparing with the lightest blue shadowed region, the gap assumption helps to rule out the regions on the left of the
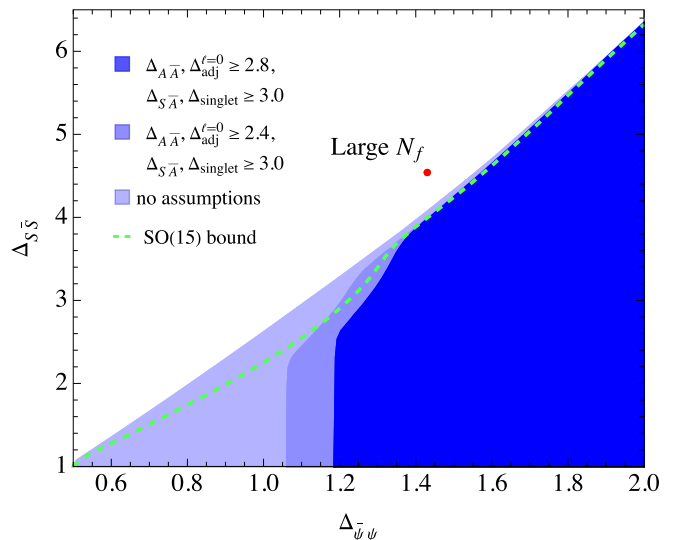

FIG. 1. Upper bounds ($\Lambda = 31$) on the scaling dimension of the lowest scalar in the (422) representation under various conditions: no gaps (lightest blue region), gaps 2.4 in the $(211)^+$ and $(220)^+$ sectors and 3.0 in the $(422)^+$ and $(310)_R^-$ sectors (light blue), gaps 2.8 in the $(211)^+$ and $(220)^+$ sectors and 3.0 in the $(422)^+$ and $(310)_R^-$ sectors (dark blue). The green line denotes the upper bound on the scaling dimension of the lowest $SO(15)$ traceless symmetric scalar obtained from the $SO(15)$ vector bootstrap, which is identical to the $SU(4)$ adjoint bootstrap bound on the scaling dimensions of the four-fermion scalars on the rhs of (3.10b) with the assumption that these four-fermion scalars have the same scaling dimension. In the physical spectrum of $N_f = 4$ QED_3, this assumption is violated by subleading $1/N_f$ corrections. The kink near ($\Delta_{\bar{\psi}\psi} \simeq 1.35$, $\Delta_{S\bar{S}} \simeq 3.7$) in the green dashed line remains in the $SU(4)$ adjoint bootstrap bound after introducing different gaps inspired by the $1/N_f$ perturbative results. Nevertheless, the position of this kink depends on the gaps. The red dot denotes the $1/N_f$ perturbative results on the scaling dimensions of the $SU(4)$ adjoint fermion bilinear and the lowest scalar in the (422) representation.

kink, while the bootstrap bound to the right of the kink is only mildly modified. This shows heuristically how the gap assumptions help in forming the kink structure in the $SU(4)$ adjoint bootstrap bound, and it indicates that a special solution stands out under the constraints posed by the gap assumptions.

The $SO(15)$ vector bootstrap bounds can be obtained in the $SU(4)$ adjoint bootstrap with the $SO(15)$ symmetric gap assumptions given in (3.19). In $N_f = 4$ QED_3, this is only satisfied by the tree-level scaling dimensions of four-fermion operators on the rhs of (3.10b). In the physical spectrum of $N_f = 4$ QED_3, these four-fermion scalars have different higher order corrections, which are summarized in Table II. After taking this difference into account, the gap assumptions in (3.19) need to be sightly modified and the bootstrap bound, especially the position of the kink will be shifted.
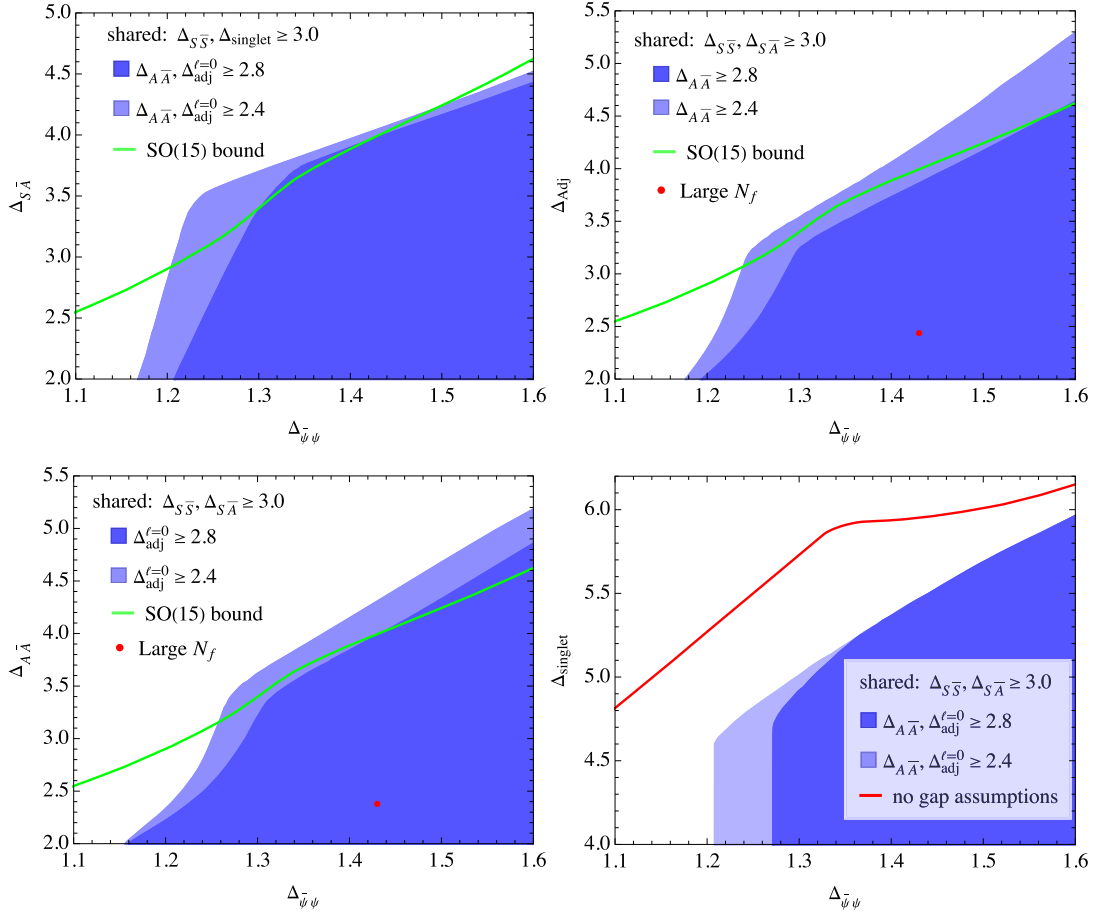
FIG. 2. The (light) blue regions give bootstrap bounds ($\Lambda = 31$) on the scaling dimensions of lowest operators in the $S\bar{A}$ (upper left), $Adj_{\ell=0}$ (upper right), $A\bar{A}$ (lower left), and singlet (lower right) representations of $SU(4)$ with certain gap assumptions. The green lines denote the upper bound on the scaling dimension of the lowest $SO(15)$ traceless symmetric scalar obtained from the $SO(15)$ vector bootstrap. The red line in the lower right plot represents the $SU(4)$ singlet upper bound without any gap assumptions, which coincides with the singlet upper bound from the $SO(15)$ vector bootstrap. The red dots denote the large N_f perturbative results. In the gap assumptions, we require the lowest operators in the $R = \{S\bar{A}, S\bar{S}, \text{singlet}\}$ sectors are all irrelevant $\Delta_R > 3$; while the lowest scalars in the $R = \{A\bar{A}, Adj_{\ell=0}\}$ sectors are above $\Delta_R > 2.4$ (light blue) or $\Delta_R > 2.8$ (blue).

According to the $1/N_f$ perturbative results in Table II, at order $O(1/N_f)$ the lowest scalars in the (211) and (220) representations have scaling dimensions $\Delta \sim 2.4$, while the higher order corrections are expected to be significant, as shown in Fig. 1 for the leading scalar in the (422) representation. In Fig. 1 we tested the gaps $\Delta > 2.4$ (light blue region) and $\Delta > 2.8$ (dark blue region) in both the (211) and (220) sectors.[12] In addition, we also imposed the gaps $\Delta > 3$ for the lowest operators in the parity even

singlet and $S\bar{A}$ sectors. In the new bootstrap bounds with these gaps there are vertical left cuts caused by the gaps $\Delta > 2.4$ or $\Delta > 2.8$ in the (211) and (220) sectors. The prominent kinks remain in the new bootstrap bounds, while their positions are slightly shifted in comparison with the kink in the $SO(15)$ vector bootstrap bound.

In Fig. 2 we show more bootstrap bounds on the scaling dimensions of operators in different representations of $SU(4)$. Generally the bootstrap bounds of nonsinglet operators show prominent kinks near the kink of the $SO(15)$ vector bootstrap bound, and the positions of the kinks depend on the gaps. Note the upper-left plot of Fig. 2 gives an upper bound on the lowest spin 1 operator in the $S\bar{A}$ sector. Its branching rule is given in (3.10c), which is part of the spin 1 operator in the antisymmetric representation of $SO(15)$ symmetry. So its bound is independent of

---

[12]A natural choice of the gaps in these sectors is the irrelevance condition $\Delta > 3$, which can affect whether QED$_3$ can be realized in lattice models [58]. However, for reasons that will be explained in our monopole bootstrap study, we chose to a make a slightly more conservative gap assumption $\Delta > 2.8$ instead. The bounds with gaps $\Delta > 3$ in the (211) and (220) sectors have slightly stronger but similar shapes as the bounds shown in this work.

the bound of the $SO(15)$ traceless-symmetric scalar given by the green line. Interestingly, it still shows a sharp kink with Δ_r close to the kink in the green line.

The kink in the singlet sector (right bottom) is less significant in comparison with the nonsinglet sectors. Nevertheless, a mild kinklike structure appears in the dark blue shadowed region, obtained after imposing gaps $\Delta >$ 2.8 in the Adj and $A\bar{A}$ sectors. An interesting fact here is that after imposing gaps $\Delta > 3$ in the $S\bar{A}$ and $S\bar{S}$ sectors, the singlet upper bound decreases significantly in comparison to the singlet upper bound without any gap assumptions (red line). The singlet upper bound has been observed to be significantly weaker than the expected value $\Delta_{\text{singlet}} \in (3, 4)$ in interesting physical theories. By introducing gaps inspired by the QED_3 spectrum which break the $SU(4) \rightarrow SO(15)$ symmetry enhancement (3.10), the singlet bound can be notably improved. The gap in the $S\bar{A}$ sector is especially helpful to resolve the $SO(15)$ symmetry enhancement in that its dimension is much higher than the unitary bound of spin 1 currents which forbids a conserved current for $SO(15)$ symmetry. According to the large N_f spectrum in Table II and the bootstrap bounds in Fig. 2, we expect that a stronger gap in this sector is also allowed and that the singlet upper bound can potentially be improved further.

We emphasize that gap assumptions, even those such in Figs. 1 and 2 which only slightly break the $SO(15) \rightarrow SU(4)$ relations (3.10), play a critical role in bootstrapping a specific theory such as conformal $N_f = 4$ QED_3. With insufficient gap assumptions, many undesired potential solutions to the $SU(4)$ or $SO(15)$ crossing equations may still be around, obscuring a physical solution (which may relate to a kink structure). Recently the authors of [58] observed that the kink in the $SU(4)$ adjoint scalar bootstrap singlet bound smooths out and perhaps disappears when one imposes a gap in only the spin-1 $S\bar{A}$ sector. We do not view this as a major surprise since it is not clear that a single $S\bar{A}$ gap is sufficient to pick out the conformal $N_f = 4$ QED_3 solution. For several sectors shown in Figs. 1 and 2, when we use gaps inspired by the perturbative expectations for $N_f = 4$ QED_3, the kinks remain and some become even sharper compared with those first found in [53].

Figure 3 shows the bootstrap bounds on another two important physical quantities in CFTs, the stress tensor central charge c_T and the $SU(4)$ conserved current central charge c_J. In the plot we have imposed the gap assumptions $\Delta > 2.8$ in the Adj and $A\bar{A}$ sectors and $\Delta > 3$ in the singlet and $S\bar{A}$ sectors. Besides, we also assume the second $S\bar{S}$ scalar satisfies $\Delta_{S\bar{S}'} > 4.5$, which leads to a lower cut in the bootstrap bound. The second lowest $S\bar{S}$ scalar has a scaling dimension of 6 in the large N_f limit, see Table II. The gap $\Delta'_{S\bar{S}} > 4.5$ for the second $S\bar{S}$ scalar is slightly above the scaling dimension of the lowest $S\bar{S}$ scalar near the kink at $\Delta_{\bar{\psi}\psi} \sim 1.35$. This gap introduced a lower cut in the bound on the scaling dimension of the lowest scalar in the $S\bar{S}$ sector. Contours denoting the $1/N_f$ perturbative results on c_T and c_J given in Eq. (2.7) are highlighted in Fig. 3, which are remarkably close to the bootstrap lower bounds on c_T and c_J near the kink.

$$\Delta_{S_{(000)}}^{\ell=0} \geqslant 3.0, \; \Delta_{S_{(310)}}^{\ell=0} \geqslant 3.0, \; \Delta_{S_{(220)}}^{\ell=0} \geqslant 2.8, \; \Delta_{S_{(211)}}^{\ell=0} \geqslant 2.8, \; \Delta_{S\bar{S}'} \geqslant 4.5$$
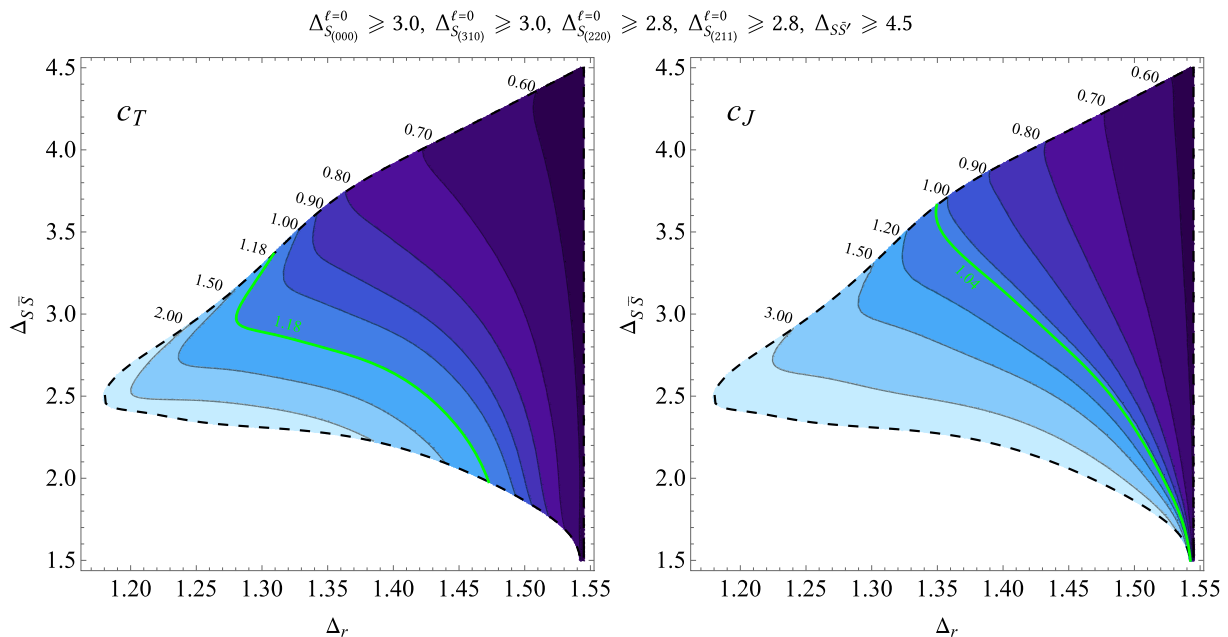

FIG. 3. Contour plots of the stress tensor central charge c_T (left panel) and the $SU(4)$ conserved current central charge c_J (right panel). The bounds are obtained at $\Lambda = 21$ with the gap assumptions: $\Delta_R > 3$ for the lowest operators in the $SU(4)$ representations $R = \{\text{singlet}, S\bar{A}\}$, $\Delta_R > 2.8$ for the lowest scalars in the $R = \{A\bar{A}, \text{Adj}\}$ representations, and the second lowest scalar in the $S\bar{S}$ sector is above 4.5. The green contours denote the values of c_T and c_J in $N_f = 4$ conformal QED_3 obtained from the $1/N_f$ expansion.

The bounds on c_T and c_J shown in Fig. 3 are especially interesting for bootstrap studies of conformal QED$_3$. A widely recognized difficulty in bootstrapping conformal gauge theories is how to distinguish theories with different gauge groups and matter representations. The conformal bootstrap focuses on gauge invariant operators, in which information about the gauge group has been obscured and the low-lying operators can be similar in different gauge theories. For instance, the $SU(N_f)$ adjoint fermion bilinear operators and four-fermion operators also exist in $SU(N_c)$ gauge theories coupled to N_f fundamental fermions. Without extra constraints on the gauge interactions, it is difficult for the bootstrap algorithm to distinguish the scaling dimensions of operators in conformal QED$_3$ from those in other gauge theories. In this sense, it is not surprising that by introducing a gap on the second $S\bar{S}$ scalar, the lower region is not carved out significantly. Information about the gauge group actually appears in the central charges c_T and c_J. The central charges can be viewed as rough measures of the number of degrees of freedom, which are significantly affected by the rank of gauge groups and their representations.

In [26] the central charges c_T and c_J in $SU(N_c)$ gauge theories coupled to N_f fundamental fermions were computed perturbatively, which gives at leading order N_c times of the central charges of N_f flavor QED$_3$. Therefore the central charges c_T and c_J provide critical parameters to distinguish QED$_3$ from 3D Yang-Mills theories. Going back to the bootstrap bounds on c_T and c_J in Fig. 3, the lower bounds on c_T and c_J near the kink are close to the perturbative results of QED$_3$, while significantly lower than the central charges of QCD$_3$, giving evidence that the underlying theory of the kink could be QED$_3$ or a similar $U(1)$ gauge theory. Moreover, near the lower cut caused by the gap for the second $S\bar{S}$ scalar, c_T and c_J have much stronger lower bounds. This region may be excluded at higher Λ and does not clearly appear to correspond to any physical theories. Alternatively this region may contain solutions of certain Yang-Mills gauge theories with scaling dimensions $(\Delta_r, \Delta_{S\bar{S}})$ in between the kink and lower cut, which cannot be excluded by the gap $\Delta_{S\bar{S}'} > 4.5$ for the second $S\bar{S}$ scalar and have central charges c_T and c_J significantly larger than those of QED$_3$. By inputting upper bounds on the central charges, the bootstrap solutions near the lower cut of the $\Delta_{S\bar{S}}$ allowed region can be excluded. The central charges may thus play a more efficient role in excluding Yang-Mills gauge theory solutions compared with imposing gap assumptions in the spectrum.

In consideration of the special role that the central charges play in the bootstrap bounds, it would be very interesting to bootstrap mixed correlators between $SU(4)$ adjoint fermion bilinears and $SU(4)$ conserved currents. The roles of conserved currents in the 3D numerical bootstrap have been studied in [76–78]. Another motivation to study mixed correlators involving the $SU(4)$ conserved currents is that they may play an interesting role in resolving the bootstrap bound coincidence caused by the algebraic relation between the crossing equations of $SU(4)$ adjoint scalars and the $SO(15)$ vector scalars (see [54] for more discussions). We leave this direction for future study.

IV. MONOPOLE SINGLE CORRELATOR BOOTSTRAP REVISITED

As noted in the introduction, monopole operators are particularly interesting in studying conformal QED$_3$, since the topological $U(1)_t$ symmetry provides an opportunity to distinguish conformal QED$_3$ from QCD$_3$ with $SU(N_c)$ gauge interactions, which are otherwise difficult for the bootstrap to distinguish just based on their flavor symmetries and the perturbative gauge invariant spectrum.[13] Bootstrap studies of the monopole four-point correlator in this theory were performed previously in [51,52]. The key results were that after imposing certain gaps, the bootstrap bounds show kinklike structures. Nevertheless, the kinks are gap dependent, meaning it may be hard to pin down the conformal QED$_3$ solution with the monopole bootstrap and just a few reliable and general assumptions. We will focus our attention on a less ambitious but still nontrivial task, which is to test the perturbative and lattice results of conformal QED$_3$ using the monopole bootstrap.

Along the way, we will show an algebraic relation between the crossing equations of the four-point functions of the monopole operator $\mathcal{M}_{1/2}$ and the crossing equations of the $SO(12)$ vector scalar, which in turn leads to a coincidence of bootstrap bounds between the monopole bootstrap and the $SO(12)$ vector bootstrap. We find that gaps inspired by the perturbative spectrum which take advantage of parity symmetry can play an important role in resolving this $SO(12)$ symmetry enhancement in the bootstrap bounds and in carving out peninsula structures. Based on these, we will introduce *interval positivity* constraints in the bootstrap setup, with which the allowed parameter space can be further isolated into a closed island.

A. Single correlator crossing equations of the monopole operator $\mathcal{M}_{1/2}$

The crossing equations for the monopole four-point correlator were computed in [51]. The monopole $\mathcal{M}_{1/2}$ with lowest $U(1)_t$ charge $q = \frac{1}{2}$ forms the (110) representation of $SU(4)$. This monopole operator is not parity definite: parity flips the sign of the $U(1)$ gauge flux and maps the monopole operator $\mathcal{M}_{1/2}$ to the antimonopole $\mathcal{M}_{-1/2}$. It is convenient to rewrite the $U(1)_t$ charged

---

[13]QCD$_3$ theories which contain $U(1)$ factors, e.g. $U(N_c)$ QCD$_3$, also contain monopole operators charged under the topological $U(1)^t$ generated by the current $J^t_\mu = \epsilon_{\mu\nu\rho}\mathrm{tr}(F^{\nu\rho})$. Both the monopole spectrum and central charges have a strong dependence on N_c [70], which can be useful for distinguishing these theories.

monopole ($\mathcal{M}_{1/2}$) and antimonopole ($\mathcal{M}_{-1/2}$) operators in an $SO(2)$ vector form $\mathcal{M}^a_{1/2}$ with

$$\mathcal{M}^{a=1}_{1/2} = (\mathcal{M}_{1/2} + \mathcal{M}_{-1/2})/2,$$
$$\mathcal{M}^{a=2}_{1/2} = -i(\mathcal{M}_{1/2} - \mathcal{M}_{-1/2})/2, \quad (4.1)$$

where the $SU(4)$ indices have been assumed implicitly. Note that these are now parity definite. Our crossing equations are of the monopole four-point correlator

$$\langle \mathcal{M}^a_{1/2}(x_1)\mathcal{M}^b_{1/2}(x_2)\mathcal{M}^c_{1/2}(x_3)\mathcal{M}^d_{1/2}(x_4)\rangle. \quad (4.2)$$

There are nine sectors with different $SU(4) \times SO(2)$ representations or parity charge which appear in the OPE of $\mathcal{M}^a_{1/2} \times \mathcal{M}^b_{1/2}$. We can understand the algebraic structure of the crossing equations from (4.2) with the tensor product of the monopole's $SU(4)$ and $SO(2)$ representations:

$$SU(4)\colon (110) \otimes (110) = (000) \oplus (211) \oplus (220),$$
$$SO(2)\colon V \otimes V = S \oplus T \oplus A, \quad (4.3)$$

where V, S, T, A denote vector, singlet, traceless-symmetric tensor, and antisymmetric tensor representations of $SO(2)$. The S and A sectors are isomorphic for $SO(2)$, but they have different spin selection rules and parity charges; see Table III.

The crossing equations can be summarized by the vector equation

TABLE III. Spin selection rules ($\ell^\pm$) and parity charges ($P^\pm$) for the monopole crossing equations. There are no definite parity charges in the T sectors.

	(000)	(211)	(220)
S	l^+, P^+	ℓ^-, P^+	ℓ^+, P^+
A	ℓ^-, P^-	ℓ^+, P^-	ℓ^-, P^-
T	ℓ^+	ℓ^-	ℓ^+

$$\sum_{\mathcal{O},i}\lambda^2_{\mathcal{O}}\vec{V}^\pm_{S_i} + \sum_{\mathcal{O},i}\lambda^2_{\mathcal{O}}\vec{V}^\pm_{A_i} + \sum_{\mathcal{O},i}\lambda^2_{\mathcal{O}}\vec{V}^\mp_{T_i} = 0, \quad (4.4)$$

in which the vector $\vec{V}^\pm_{R_i}$ has an even/odd spin selection rule and its subscript R_i denotes a sector with $SO(2)$ representation $R = S/A/T$ and $SU(4)$ representation $i = (000), (211),$ or (220). The vectors $\vec{V}$ have nine components and the crossing equations

$$\mathcal{M}_{\text{monopole}} \equiv \left(\vec{V}^+_{S_{(000)}}, \vec{V}^-_{S_{(211)}}, \vec{V}^+_{S_{(220)}}, \vec{V}^-_{A_{(000)}}, \vec{V}^+_{A_{(211)}},\right.$$
$$\left.\vec{A}^-_{A_{(220)}}, \vec{V}^+_{T_{(000)}}, \vec{V}^-_{T_{(211)}}, \vec{V}^+_{T_{(220)}}\right)_{\text{monopole}} \quad (4.5)$$

can be written in a 9×9 square matrix form, as expected in the single correlator bootstrap with general global symmetries [79]:

$$\mathcal{M}_{\text{monopole}} = \begin{pmatrix} 0 & 0 & 0 & 0 & F & -F & 0 & -F & F \\ 0 & 0 & 0 & -F & -F & -\frac{2}{3}F & F & F & \frac{2}{3}F \\ 0 & -F & F & 0 & -F & F & 0 & 0 & 0 \\ F & F & \frac{2}{3}F & F & F & \frac{2}{3}F & 0 & 0 & 0 \\ F & -F & -\frac{4}{3}F & -F & F & \frac{4}{3}F & -2F & 2F & \frac{8}{3}F \\ 0 & 0 & 0 & -H & H & \frac{4}{3}H & H & -H & -\frac{4}{3}H \\ H & -H & -\frac{4}{3}H & H & -H & -\frac{4}{3}H & 0 & 0 & 0 \\ 0 & -H & H & 0 & H & -H & 0 & 2H & -2H \\ H & H & \frac{2}{3}H & -H & -H & -\frac{2}{3}H & -2H & -2H & -\frac{4}{3}H \end{pmatrix}, \quad (4.6)$$

where F/H are the symmetrized/antisymmetrized conformal block functions (3.4).

It turns out that there is a relation which maps the above crossing equations (4.6) onto the much simpler $SO(12)$ vector crossing equations, which was not noted in previous monopole bootstrap works [51,52]. Following the procedure discovered in [54], there is a 3×9 matrix

$$\mathcal{T}_{\text{monopole}} = \begin{pmatrix} 1 & \frac{19}{154} & \frac{75}{154} & \frac{5}{308} & -\frac{5}{308} & 0 & 0 & 0 & 0 \\ 0 & \frac{40}{77} & \frac{12}{77} & \frac{62}{77} & \frac{15}{77} & 0 & 0 & 0 & 0 \\ 0 & 0 & 0 & 0 & 0 & \frac{5}{11} & \frac{15}{22} & \frac{1}{11} & \frac{7}{22} \end{pmatrix}, \quad (4.7)$$

which can transform the monopole crossing equations into the $SO(12)$ vector four-point crossing equations

$$\mathcal{M}_{SO(12)} = (\vec{V}_S^+, \vec{V}_T^+, \vec{V}_A^-)_{SO(12)} = \begin{pmatrix} 0 & F & -F \\ F & \frac{5}{6}F & F \\ H & -\frac{7}{6}H & -H \end{pmatrix}. \tag{4.8}$$

Its action on the monopole crossing equations gives

$$(\mathcal{T} \cdot \mathcal{M})_{\text{monopole}} = \begin{pmatrix} 0 & -\frac{5}{11}F & \frac{40}{77}F & -\frac{1}{11}F & \frac{30}{77}F & -\frac{20}{33}F & \frac{12}{77}F & -\frac{10}{11}F & \frac{80}{77}F \\ F & \frac{5}{11}F & \frac{100}{231}F & \frac{1}{11}F & \frac{25}{77}F & \frac{20}{33}F & \frac{10}{77}F & \frac{10}{11}F & \frac{200}{231}F \\ H & -\frac{5}{11}H & -\frac{20}{33}H & -\frac{1}{11}H & -\frac{5}{11}H & -\frac{20}{33}H & -\frac{2}{11}H & -\frac{10}{11}H & -\frac{40}{33}H \end{pmatrix}, \tag{4.9}$$

which can be briefly written in the vector form

$$\left[\mathcal{T} \cdot \left(\vec{V}_{S(000)}^+, \vec{V}_{S(211)}^-, \vec{V}_{S(220)}^+, \vec{V}_{A(000)}^-, \vec{V}_{A(211)}^+, \vec{A}_{A(220)}^-, \vec{V}_{T(000)}^+, \vec{V}_{T(211)}^-, \vec{V}_{T(220)}^+ \right) \right]_{\text{monopole}}$$
$$= \left(\vec{V}_S^+, x_1 \vec{V}_A^-, x_2 \vec{V}_T^+, x_3 \vec{V}_A^-, x_4 \vec{V}_T^+, x_5 \vec{V}_A^-, x_6 \vec{V}_T^+, x_7 \vec{V}_A^-, x_8 \vec{V}_T^+ \right)_{SO(12)}, \tag{4.10}$$

with positive coefficients x_i

$$\vec{x} = \left\{ \frac{5}{11}, \frac{40}{77}, \frac{1}{11}, \frac{30}{77}, \frac{20}{33}, \frac{12}{77}, \frac{10}{11}, \frac{80}{77} \right\}. \tag{4.11}$$

Therefore the transformation $\mathcal{T}_{\text{monopole}}$ maps the monopole crossing equations into the $SO(12)$ vector crossing equations, combined with the $SO(12) \rightarrow SU(4) \times SO(2)$ branching rules

SO(12)   **SU(4) × SO(2)**

$$S \leftrightarrow S_{(000)}, \tag{4.12a}$$

$$T \leftrightarrow S_{(220)} \oplus A_{(211)} \oplus T_{(000)} \oplus T_{(220)}, \tag{4.12b}$$

$$A \leftrightarrow S_{(211)} \oplus A_{(000)} \oplus A_{(220)} \oplus T_{(211)}. \tag{4.12c}$$

Note that only even (odd) spins appear in the S, T (A) sectors of $SO(12)$, consistent with the spin selection rules of the different $SU(4) \times SO(2)$ representations shown in Table III.

Positivity of x_i implies that the coefficients in the $N_f = 4, q = 1/2$ monopole crossing equations have the same positivity properties as in the $SO(12)$ vector crossing equations. This agrees with the results in [54,55] that in general for a scalar in a representation with N^* degrees of freedom, its four-point crossing equations relate to the $SO(N^*)$ vector crossing equations through a unique linear transformation. As proved in [54] and the Sec. III A of this paper, this relation combined with suitable boundary conditions can lead to coincidences between the monopole and $SO(12)$ vector bootstrap bounds. Indeed one can show that the bootstrap bound on the lowest nonunit scalar in the

$S_{(000)}$ sector coincides with the singlet bound in $SO(12)$ vector bootstrap. Such a bound coincidence can be broken using non-$SO(N^*)$ symmetric boundary conditions in the bootstrap implementation.

It is very interesting to compare the branching rules in the monopole crossing equations (4.12) with those in the $SU(4)$ adjoint fermion bilinear crossing equations (3.10). A major difference is that in (3.10) all the operators on the rhs are parity even, while in (4.12), the $SU(4) \times SO(2)$ representations branched from $SO(12)$ A or T sectors contain both parity even and parity odd representations, as well as $T_{\vec{x}}$ monopole sectors without a definite parity charge. Specifically, the lowest scalar in the $S_{(220)}$ sector is a parity even four-fermion operator while the lowest scalar in the $A_{(211)}$ sector is just the parity odd fermion bilinear r, which have quite different scaling dimensions. The lowest scalars in the $T_{(000)}$ and $T_{(220)}$ sectors also have rather different scaling dimensions at leading order, see Table II. Similar differences appear in the branching rule of the $SO(12)$ A sector (4.12c). This is different from the fermion bilinear r crossing equations (3.10), in which the $SO(15)$ symmetry enhancement is broken only at the subleading order $O(1/N_f)$. Therefore, the monopole crossing equations perhaps provide the strongest way to break the $SO(N)$ symmetry enhancement appearing in bootstrap studies for gauge theories with smaller symmetry.

Based on the above facts, it is possible to introduce highly restrictive gap assumptions in the QED$_3$ monopole bootstrap. Perturbative calculations can provide valuable guidance on the possible gaps in different sectors. However, one needs to use this information carefully as the CFT data may receive notable higher order corrections. On the other hand, the monopole bootstrap can provide a

nonperturbative check on whether the perturbative (or lattice) results can be consistent with conformality and unitarity.

B. Monopole bootstrap bounds with gaps inspired by QED$_3$ spectrum

In this section we explore bootstrap constraints from the crossing equations of the four-point correlator $\langle \mathcal{M}_{1/2} \mathcal{M}_{1/2} \mathcal{M}_{1/2} \mathcal{M}_{1/2} \rangle$. The symmetry enhancement of the crossing equations (4.10) strongly affects the monopole bootstrap bounds. Both singlet and nonsinglet bounds coincide with the $SO(12)$ vector bootstrap results unless the symmetry is strongly broken by gap assumptions. However, interesting bootstrap results can be obtained after introducing gap assumptions inspired by the perturbative spectrum of QED$_3$, shown in Table II.

In Fig. 4, we show the bootstrap bounds on the scaling dimensions of the lowest scalars in the $S_{(220)}$ (left panel) and $T_{(220)}$ (right panel) sectors without imposing any gap assumptions. The bootstrap bounds are close to straight lines in the regions away from the unitary bound $\Delta = 1/2$. A direct consequence is that by imposing a gap Δ^* for the lowest scalar in $S_{(220)}$ sector: $\Delta_{S_{(220)}} \geq \Delta^*$, there will be a minimal $\Delta_{\mathcal{M}_{1/2}}$ in the bootstrap allowed region proportional to the gap Δ^*. This explains the $S_{(220)}$-gap dependent bootstrap bounds observed in [51]. The red dots in Fig. 4 denote the $1/N_f$ perturbative results, which locate in the physically allowed regions and are well consistent with the bootstrap bounds without imposing any gap assumptions.

The lowest scalar in the $S_{(220)}$ sector is the four-fermion operator with scaling dimension $\Delta \simeq 2.4$ at subleading order in the $1/N_f$ expansion, see Table II. Its scaling dimension is expected to receive notable corrections from higher order terms. An interesting question is whether this operator is relevant or not. Assuming the lowest scalar in the $S_{(220)}$ sector is irrelevant, the bootstrap bound in Fig. 4 introduces a
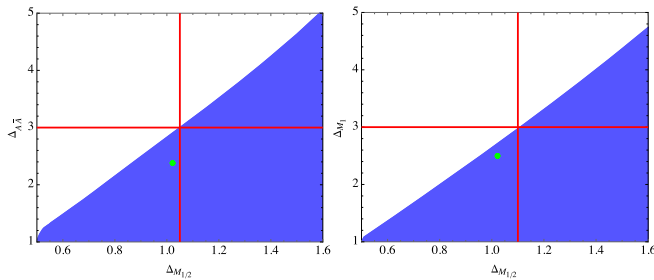

FIG. 4. Bounds on the scaling dimensions of the lowest scalar in the $S_{(220)}$ sector (left) and the charge 1 monopole in the $T_{(220)}$ sector (right) at $\Lambda = 31$. The green dots denote the $1/N_f$ perturbative predictions. The axes highlighted with red color are positioned at the intersection of the bounds and $\Delta_{A\bar{A}}, \Delta_{M_1} = 3$. Note that the perturbative results are ruled out if we assume $\Delta \geq 3$ in either sector.

lower cut on the scaling dimension of the monopole $\mathcal{M}_{1/2}$: $\Delta_{\mathcal{M}_{1/2}} > 1.05$ at $\Lambda = 31$. This is consistent with the lattice result [43] but excludes the perturbative prediction at subleading order $\Delta_{\mathcal{M}_{1/2}} \simeq 1.022$. We do not have solid evidence on the relevance of the lowest scalar in the $S_{(220)}$ sector and we will adopt a weaker gap assumption in the $S_{(220)}$ sector with which the perturbative result on $\Delta_{\mathcal{M}_{1/2}}$ is still in the allowed region of the bootstrap bound.

Due to the gap dependence of the bootstrap bound, it is likely too much to hope that our current bootstrap setup can *solve* the $N_f = 4$ conformal QED$_3$ as a special solution saturating the bootstrap bound. However, it is still interesting to know whether by imposing gaps inspired by the perturbative monopole spectrum, will the bootstrap bounds converge to the region near perturbative CFT data of $N_f = 4$ conformal QED$_3$ or completely exclude it? In the monopole spectrum, the subleading order corrections on the scaling dimensions of the low-lying monopole operators have been shown to be small: only 3.6% (7.2%) of the leading term for $\mathcal{M}_{1/2}$ ($\mathcal{M}_1$). If this is also true for higher order corrections, i.e. the large N_f expansion is still converging, then the current perturbative results should be close to the physical spectrum. In contrast, subleading order corrections of the four-fermion operators are more significant and the perturbative results have been shown in Fig. 1 to be not reliable. The readers should be reminded that our assumptions on the gap 2.8 in the $S_{(220)}$ sector and the monopole spectrum have not been strictly established yet and the bootstrap computations should be considered as numerical experiments before more solid evidence on these assumptions can be obtained.

In Fig. 5 we show the bootstrap bound on the scaling dimension of the lowest parity odd $SU(4)$ adjoint scalar r in the $A_{(211)}$ sector. To obtain the result, we have imposed gaps $\Delta_{S_{(000)}} \geq 3.0$, $\Delta_{S_{(220)}} \geq 2.8$, $\Delta_{T_{(000)}} \geq 4.0$, and $\Delta_{A'_{(211)}} \geq 3.0$ for the second lowest scalar in the $A_{(211)}$ sector. In the conformal phase of QED$_3$, the lowest parity even singlet scalar is expected to be irrelevant. The gap $\Delta_{S_{(220)}} \geq 2.8$ is weaker than the marginality condition and it can generate a lower cut on $\Delta_{\mathcal{M}_{1/2}}$ below the perturbative result 1.022. The gap in $\Delta_{T_{(000)}}$ can affect the upper bound in Fig. 5. A weaker gap in this sector gives a higher upper bound on Δ_r. According to the $1/N_f$ expansion results in Table II, the leading order result gives $\Delta_{T_{(000)}} \simeq 4.42$, so the gap $\Delta_{T_{(000)}} \geq 4.0$ actually assumes the higher order corrections will not reduce the scaling dimension drastically. The next scalar in the parity odd $A_{(211)}$ sector can be constructed by contracting the spin indices of the $SU(4)$ conserved current and the topological $U(1)_t$ conserved current $J_\mu^f J^{t\mu}$, which has a scaling dimension of 4 in the large N_f limit. We assume this operator remains irrelevant at $N_f = 4$. The gap in this sector can affect the lower bound on Δ_r.
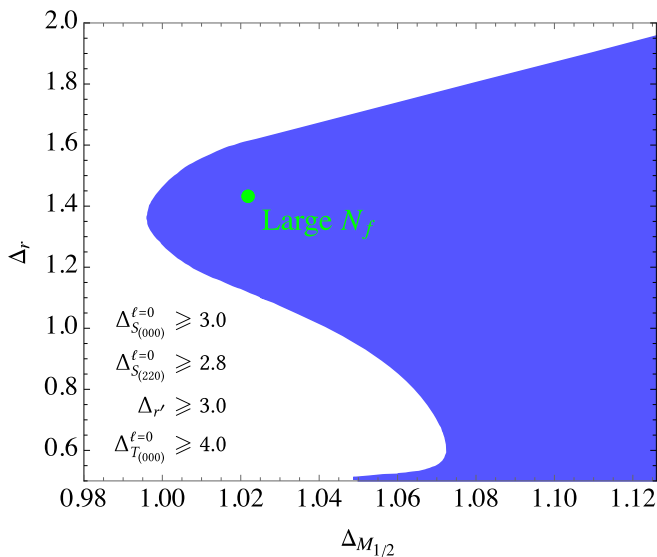
FIG. 5. Bootstrap bound on the scaling dimensions of the monopole $\mathcal{M}_{1/2}$ and adjoint fermion bilinear operator r at $\Lambda = 31$. To get this bound, we assumed the scaling dimensions of the lowest parity even singlet scalar and second parity odd $SU(4)$ adjoint scalar are irrelevant, the lowest scalar in the $A_{(220)}$ sector is above $\Delta > 2.8$, and the lowest scalar in the $T_{(000)}$ sector has scaling dimension $\Delta > 4.0$. The green dot denotes the large N_f expansion estimate.

The three sectors with gaps, $S_{(220)}$, $A_{(211)}$, and $T_{(000)}$, together with the isolated operator r, appear in the $SO(12) \rightarrow SU(4) \times SO(2)$ branching rule (4.12b). In the physical spectrum of $N_f = 4$ QED$_3$, the lowest scalars in these four sectors have rather different scaling dimensions, as they carry different charges under the parity symmetry. Therefore, the spectrum in the monopole bootstrap strongly breaks the enhanced $SO(12)$ symmetry in the algebraic relation (4.12b)! In contrast, in the $SU(4)$ adjoint crossing equations, all the operators appearing in the $SO(15) \rightarrow SU(4)$ branching rule (3.10b) are parity even and the lowest operators in these sectors have the same scaling dimensions at the leading order. The $SO(15)$ symmetry is only broken mildly by the higher order $1/N_f$ corrections.

With the above gap assumptions, the bootstrap bound on the scaling dimension of the lowest parity odd $SU(4)$ adjoint scalar forms an interesting peninsula structure and the $1/N_f$ expansion results locate near the tip of the peninsula. Due to the special role of parity symmetry, the monopole bootstrap combined with gap assumptions inspired by the large N_f QED$_3$ spectrum is more effective at carving out the CFT parameter space as compared with the $SU(4)$ fermion bilinear bootstrap shown in Fig. 3.

We would like to make two remarks about the results in Fig. 5. First the bound has a clear gap dependence. The boundary in different directions is determined by the gaps in certain sectors. Due to this fact, our current bootstrap setup cannot be used to *solve* the target theory without extra

specific input. We think this is a general problem for the bootstrap studies of non-$SO(N)$ vector scalars with scaling dimensions notably above the unitary bound. Another fact that the readers should keep in mind is that though we have pushed the bootstrap numerical precision to $\Lambda = 31$, the bound is far from converged. This fact can be seen in Fig. 6. In the top two panels of Fig. 6, we show the extrapolations of the bootstrap bounds at different Λ with fixed $\Delta_r = 1.43$ or $\Delta_{\mathcal{M}_{1/2}} = 1.022$. It requires a much higher Λ to have the lower or upper bounds close to the optimal bounds in the linear extrapolations. In the lower two panels of Fig. 6, we show the extrapolations of the lower bounds on the central charges of the $SU(4)$ conserved current and the topological $U(1)_t$ conserved current with fixed $\{\Delta_{\mathcal{M}_{1/2}}, \Delta_r\} = \{1.022, 1.43\}$. Interestingly, the $SU(4)$ conserved current central charge bound has a large Λ extrapolation at $c_J \simeq 0.95$, not far from the $1/N_f$ perturbative prediction $c_J \simeq 1.04$. Similarly, the $U(1)_t$ conserved current central charge has a large Λ extrapolation at $c_J^t \simeq 1.50$, and the $1/N_f$ expansion at subleading order predicts $c_J \simeq 1.56$. Extrapolation of the stress tensor central charge goes to $c_T \simeq 0.89$ at large Λ, which is somewhat lower than the $1/N_f$ expansion result $c_T \simeq 1.18$. This is consistent with the observation that the bootstrap bounds in the singlet sectors are relatively weaker than those in the nonsinglet sectors.

C. Closed islands from monopole single correlator bootstrap with interval positivity assumptions

In the last section we have shown that nontrivial peninsula structures show up if we break the $SO(12) \rightarrow SU(4) \times U(1)_t$ symmetry enhancement by physically inspired gap assumptions. There we did not impose any assumptions on the spectrum in the $T_{(220)}$ sector. As a part of the branching rule (4.12b), the spectrum in this sector also plays an important role in the monopole bootstrap.

The $N_f = 4$ QED$_3$ spectrum in the $T_{(220)}$ sector is shown in Table II. According to the $1/N_f$ expansion at subleading order, the lowest charge 1 monopole operator in the $T_{(220)}$ sector has scaling dimension $\Delta_{\mathcal{M}_1} \simeq 2.5$. An interesting fact is that the second scalar in this sector has a significantly higher scaling dimension at leading order $\Delta_{\mathcal{M}_1'}^0 \simeq 6.16$. To take advantage of this big gap while still allowing uncertainty about the precise value of $\Delta_{\mathcal{M}_1}$, we employ an *interval positivity* assumption, namely, we assume an upper bound on the dimension of the lowest charge 1 monopole operator, $\Delta_{\mathcal{M}_1} \leq \Delta_{\mathcal{M}_1}^{max}$, together with a lower bound on the dimension of the next operator in the same channel $\Delta_{\mathcal{M}_1'} \geq \Delta_{\mathcal{M}_1'}^{min} > \Delta_{\mathcal{M}_1}^{max}$. Assumptions of this type can be efficiently studied with a modification to the bootstrap algorithm, see Appendix E for more details.

We refer to the perturbative results given in Table II when making assumptions on $\Delta_{\mathcal{M}_1}^{max}$ and $\Delta_{\mathcal{M}_1'}^{min}$. Specifically, we
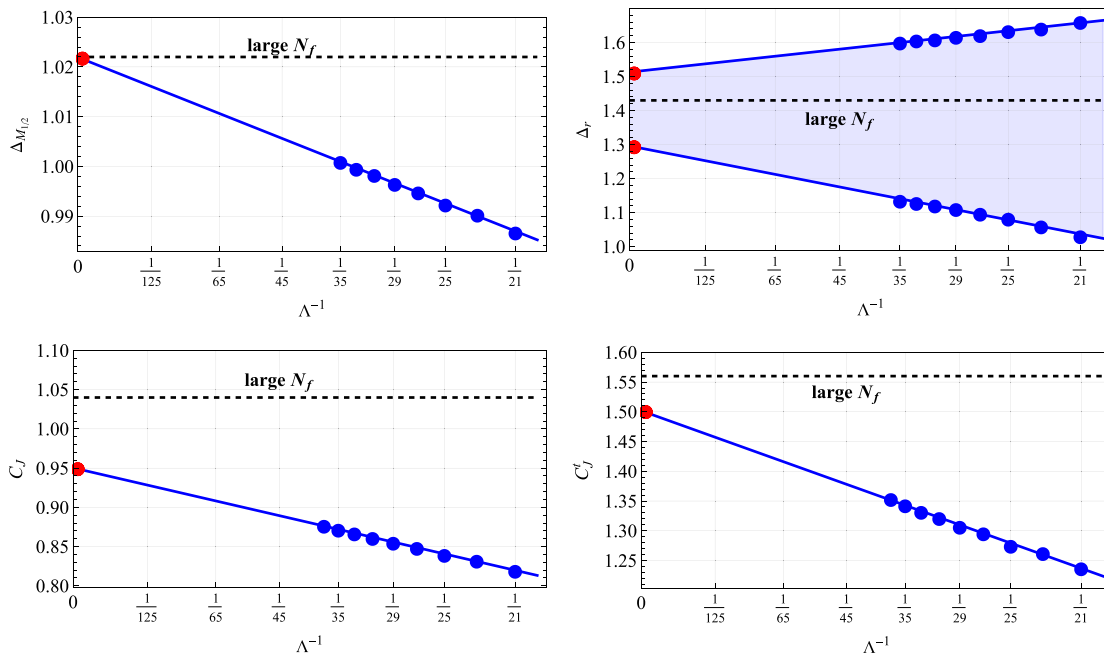
FIG. 6. Upper left: extrapolations of the bootstrap bounds on scaling dimensions of $\Delta_{M_{1/2}}$ with fixed $\Delta_r = 1.43$. Upper right: extrapolations of the bootstrap bounds on scaling dimensions of Δ_r with fixed $\Delta_{M_{1/2}} = 1.022$. Lower left: extrapolations of the central charge of the $SU(4)$ conserved current at fixed $\Delta_{M_{1/2}} = 1.022$ and $\Delta_r = 1.43$. Lower right: extrapolations of the central charge of topological $U(1)_t$ conserved current at fixed $\Delta_{M_{1/2}} = 1.022$ and $\Delta_r = 1.43$. The red dots denote the extrapolation's prediction at $\Lambda = \infty$, and black dashed lines denote the large-N_f perturbation theory prediction.

take $\Delta_{\mathcal{M}_1'}^{\min} = 5.0 < \Delta_{\mathcal{M}_1'}^0 \simeq 6.16$, and will test gaps $\Delta_{\mathcal{M}_1}^{\max} = 2.5, 2.6$, which are inspired by the $1/N_f$ expansion result $\Delta_{\mathcal{M}_1} \simeq 2.5$. The *interval positivity* assumptions can provide surprisingly strong constraints on the CFT data. We will then compare the bootstrap results with the perturbative and lattice CFT data of $N_f = 4$ QED$_3$.

Bootstrap results with these different interval positivity assumptions are shown in Fig. 7. Remarkably, with these gap assumptions inspired by the perturbative $N_f = 4$ QED$_3$ spectrum, the CFT data $(\Delta_{\mathcal{M}_{1/2}}, \Delta_r)$ can be restricted into closed islands! The shapes of the islands are gap dependent and become very small if we take $\Delta_{\mathcal{M}_1}^{\max} = 2.4$ and disappear with smaller $\Delta_{\mathcal{M}_1}^{\max}$. The island is still closed at $\Delta_{\mathcal{M}_1}^{\max} = 2.65(\Lambda = 31)$, extending to a maximum $\Delta_{\mathcal{M}_{1/2}} \simeq 1.4$. Note that the bounds shown in the plot are computed with relatively high numerical precision ($\Lambda = 31$), however, they are not well converged yet and are actually affected by the issue of slow convergence. This can be qualitatively seen through the linear extrapolation of the bound to the large Λ limit. In Fig. 8, we show the maximum values of $\Delta_{\mathcal{M}_{1/2}}$ at fixed $\Delta_r = 1.43$ in the islands computed at different values of Λ, and their linear extrapolation to $\Lambda = \infty$. Surprisingly, if we set the gap $\Delta_{\mathcal{M}_1}^{\max}$ at the perturbative estimate $\Delta_{\mathcal{M}_1}^{\max} = 2.5(\simeq \Delta_{\mathcal{M}_1})$, the upper bound on $\Delta_{\mathcal{M}_{1/2}}$ extrapolates to $\Delta_{\mathcal{M}_{1/2}} \simeq 1.04$, close to the perturbative result $\Delta_{\mathcal{M}_{1/2}} \simeq 1.02$. The left part of the island

coincides with the tip of the peninsula structure in Fig. 5, in which the minimum $\Delta_{\mathcal{M}_{1/2}}$ with fixed $\Delta_r = 1.43$ extrapolates to $\Delta_{\mathcal{M}_{1/2}} \simeq 1.02$, as shown in Fig. 6. Therefore with the interval positivity assumptions $\Delta_{\mathcal{M}_1} \leq 2.5$, $\Delta_{\mathcal{M}_1'} \geq 5.0$, our bootstrap implementation gives a closed island in $(\Delta_{\mathcal{M}_{1/2}}, \Delta_r)$, which shrinks to a rather small region consistent with the perturbative predictions.

Here we would like to remind the readers that the gap $\Delta_{A_{(220)}} \geq 2.8$, which effectively determines the minimum $\Delta_{\mathcal{M}_{1/2}}$, is chosen by hand (but without tuning), and the agreement between the linear extrapolation of the left edge of the bootstrap result and the perturbative result could be considered accidental. On the other hand, the assumed maximum value 2.5 for $\Delta_{\mathcal{M}_1}$, which affects the maximum $\Delta_{\mathcal{M}_{1/2}}$ in the island, is coming from the perturbative result at subleading order. These gaps together conspiratorially restrict the CFT data close to the perturbative QED$_3$ spectrum. If we relax the maximum of $\Delta_{\mathcal{M}_1}$ to 2.6, then the left part of the closed island remains the same, while its right side increases to $\Delta_{\mathcal{M}_{1/2}} \simeq 1.25$ ($\Lambda = 31$), which overlaps with the lattice results enclosed by the red dashed rectangle in Fig. 7. However, the right part of the island shrinks a lot at higher Λ. The linear extrapolation of the maximum $\Delta_{\mathcal{M}_{1/2}}$ at fixed $\Delta_r = 1.43$ in the islands gives the estimate $\Delta_{\mathcal{M}_{1/2}} \simeq 1.14$ at $\Lambda = \infty$, which marginally excludes the lattice results.
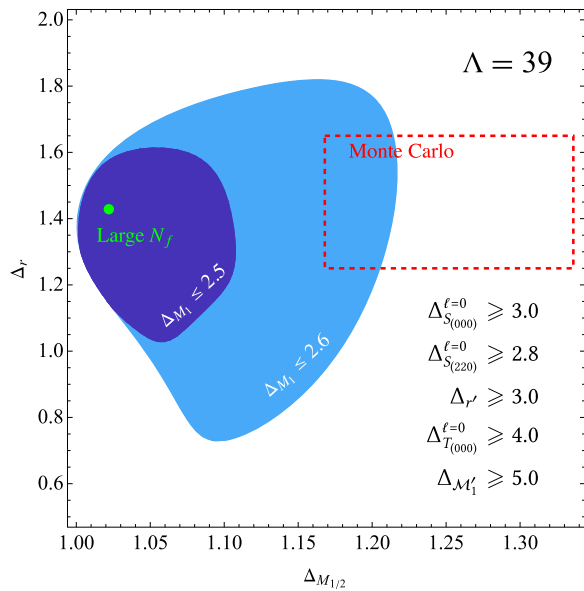
FIG. 7. Bounds on the scaling dimensions of $(\Delta_{\mathcal{M}_{1/2}}, \Delta_r)$ with the same gaps as in Fig. 5 along with the interval positivity assumptions: $\Delta_{\mathcal{M}'_1} \geq 5.0$ and $\Delta_{\mathcal{M}_1} \leq 2.5, 2.6$. We used $\Lambda = 39$ in the bootstrap computations.

More restrictive constraints come from the lower bounds on the central charges c_J, c_J^t, and c_T, which are shown in Fig. 9. The large N_f perturbative results on the central charges are given by the green contours. Inside the contours the central charges have lower bounds below the perturbative results. In the right part of the island with $\Delta_{\mathcal{M}_{1/2}} > 1.15$, the lower bounds on conserved current central charges quickly increase to the range $c_J > 1.5$ and $c_J^t > 2.5$, significantly above the $1/N_f$ perturbative results at subleading order $c_J \simeq 1.04$ and $c_J^t \simeq 1.56$. Such big discrepancies are unlikely to be explained by the higher order corrections, which indicate the bootstrap bounds in Fig. 9 are inconsistent with the lattice results on $N_f = 4$ QED$_3$. Nevertheless, this contradiction should not be simply interpreted to exclude the lattice results, as our bootstrap bounds are gap dependent. By relaxing the gap assumptions, e.g. using an interval positivity assumption with $\Delta_{\mathcal{M}_1}^{\max} > 2.6$ in the bootstrap implementation, one can obtain weaker bootstrap bounds in which the lattice results locate in the allowed region. In the next subsection we will study additional bootstrap bounds with different gap assumptions which provide some necessary conditions for the lattice results to be physical. Here the roles of central charges are quite reminiscent of their roles in Fig. 3, where in comparison with the allowed parameter space of the operator scaling dimensions, bounds on the central charges provide more restrictive constraints for conformal QED$_3$.

The above numerical experiment is surprising to us in two aspects. From the bootstrap point of view, it is a
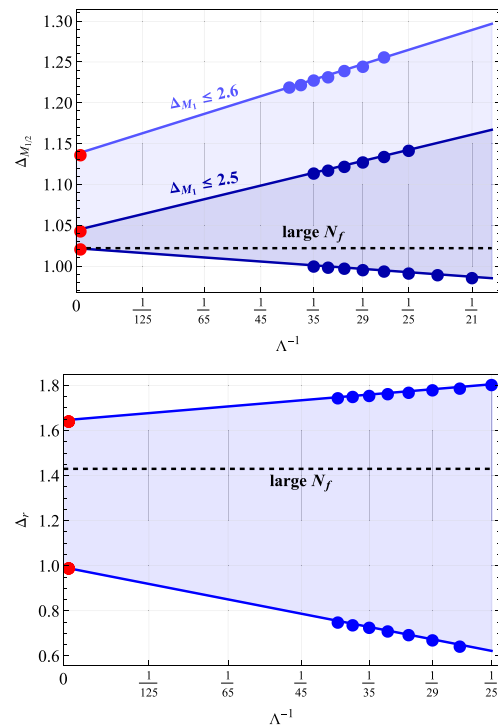

FIG. 8. Top panel: extrapolations of the maximum $\Delta_{\mathcal{M}_{1/2}}$ at fixed $\Delta_r = 1.43$ in the islands with gaps $\Delta_{\mathcal{M}_1} \leq 2.5, 2.6$. Bottom panel: extrapolations of the upper and lower bounds on the scaling dimension Δ_r in the island with $\Delta_{\mathcal{M}_1}^{\max} = 2.6$, at fixed $\Delta_{\mathcal{M}_{1/2}} = 1.08$, which is the center of the range $\Delta_{\mathcal{M}_{1/2}} \in (1.02, 1.14)$ obtained from the large Λ extrapolation. The red dots denote the $1/N_f$ perturbative results for $\Delta_{\mathcal{M}_{1/2}}$ and Δ_r.

welcome surprise that the bootstrap algorithm, though affected by the gap-dependence problem, can effectively capture a special solution which is rather close to the perturbative estimates of $N_f = 4$ QED$_3$. Note that, due to the parity symmetry, operators in different sectors have diversified scaling dimensions; the conserved current central charges also have notable differences both in their physical meanings and magnitudes. Therefore it is highly nontrivial that several of these properties can be simultaneously satisfied by the bootstrap constraints. From the QED$_3$ side, we do not have solid evidence on the gap 2.8 in the $A_{(220)}$ sector, and the current perturbative results on the monopole spectrum and central charges may still receive notable higher order corrections. In this sense, it is surprising that the perturbative CFT data taken at face value can seemingly provide a consistent solution to the bootstrap equations.

Since our bootstrap results are gap dependent, their physical relevance relies on the validity of the gap assumptions in our bootstrap implementation. Given our gap assumptions are consistent or close to the physical spectrum, then our bootstrap results are closely relevant to the physical solution of $N_f = 4$ conformal QED$_3$, which have significant meanings both for understanding the IR

$$\Delta_{S_{(000)}}^{\ell=0} \geqslant 3.0,\ \Delta_{S_{(220)}}^{\ell=0} \geqslant 2.8,\ \Delta_{r'} \geqslant 3.0, \Delta_{T_{(000)}}^{\ell=0} \geqslant 4.0,\ \Delta_{\mathcal{M}_1} \leqslant 2.6,\ \Delta_{\mathcal{M}_1'} \geqslant 5.0$$
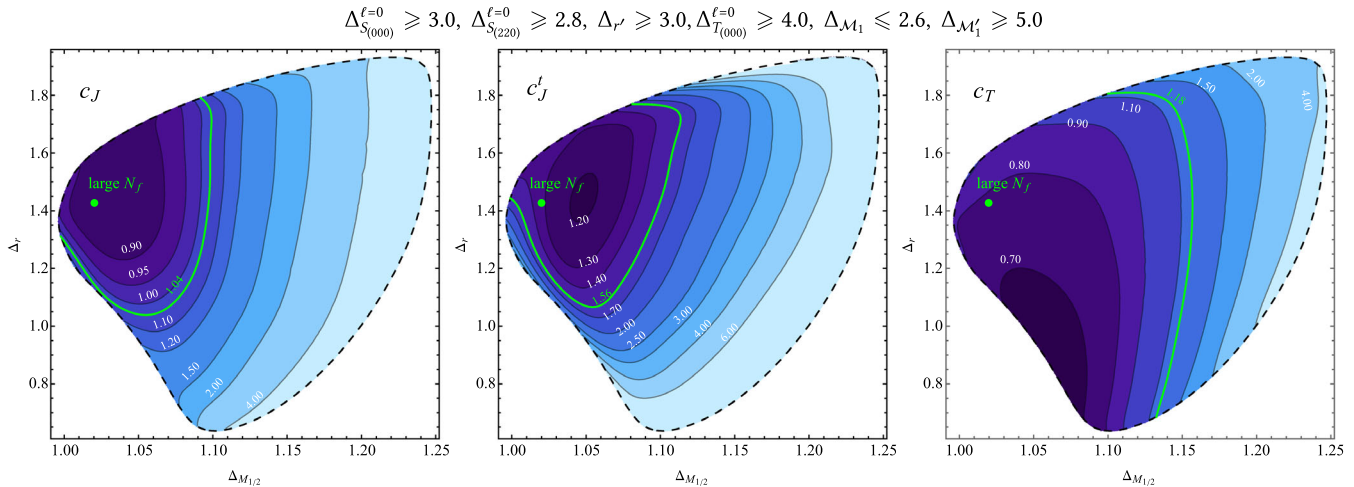

FIG. 9. Lower bounds ($\Lambda = 31$) on the $SU(4)$ conserved current central charge c_J (left), topological $U(1)_t$ conserved current central charge c_J^t (middle), and the stress tensor central charge c_T (right), inside the island of Fig. 7 with the interval positivity assumption $\Delta_{\mathcal{M}_1}^{\max} = 2.60$ (other gap assumptions are the same as in Fig. 7). The green contours denote the $1/N_f$ perturbative results at subleading order: $c_J = 1.04$, $c_J^t = 1.56$, and $c_T = 1.18$. For the $(\Delta_{\mathcal{M}_{1/2}}, \Delta_r)$ inside the green contours, the bounds on the central charges are consistent with the perturbative results, while in the right part of the island, they are significantly higher than the perturbative results.

phases of QED$_3$ and its applications in condensed matter systems. On the other hand, we cannot exclude the possibility, although less likely, that few of our gap assumptions strongly violate the physical spectrum, and the coincidences between our bootstrap results and perturbative CFT data are purely accidental. To verify the two possibilities, we suggest to compute the CFT data using other nonperturbative approaches, e.g. the lattice simulations. The scaling dimensions of the lowest scalar in $A_{(220)}$ and the charge 1 monopole operators are especially important in our bootstrap setup. Reliable estimations of these operators can verify whether our assumptions are consistent with the physical spectrum.

D. Bound on the charge 1 monopole operator $\mathcal{M}_1$ and the lattice results

In this subsection we study the bootstrap bounds on the scaling dimension of charge 1 monopole operator $\mathcal{M}_1$ and the bounds on the central charges in the resulting allowed region. The results will explain why the interval positivity assumptions can generate closed islands. We will additionally provide more comparisons between the bootstrap bounds and the lattice results. Since our bootstrap results are gap dependent and the gap assumptions are not strictly established yet, our results cannot verify or exclude the lattice results by themselves. Nevertheless, they can provide strong necessary conditions for the lattice results to be physical.

First let us consider the bootstrap bounds on the scaling dimension of the lowest charge 1 monopole operator $\mathcal{M}_1$. The results are shown in Fig. 10. To get the bounds we used the gap assumptions $\Delta_{S_{(000)}} \geq 3.0$ and $\Delta_{\mathcal{M}_1'} \geq 5.0$ for the second lowest charge 1 monopole $\mathcal{M}_1'$. The bootstrap

bounds change notably with different gaps $\Delta_{A\bar{A}} \geq \Delta^*$ for the lowest scalar in the $S_{(220)}$ sector. The most interesting point in Fig. 10 is that the bootstrap allowed region forms a wave structure when the $S_{(220)}$ gap is in the range $\Delta^* \leq 3$. The $1/N_f$ perturbative results locate near the tip of the bootstrap bound associated with the gap $\Delta^* = 2.8$. For larger gaps $\Delta^* \geq 3.2$ the wave structure disappears. The wave structures in the $\mathcal{M}_1$ bootstrap bounds are reminiscent of the bootstrap bound on the 3D critical Ising model
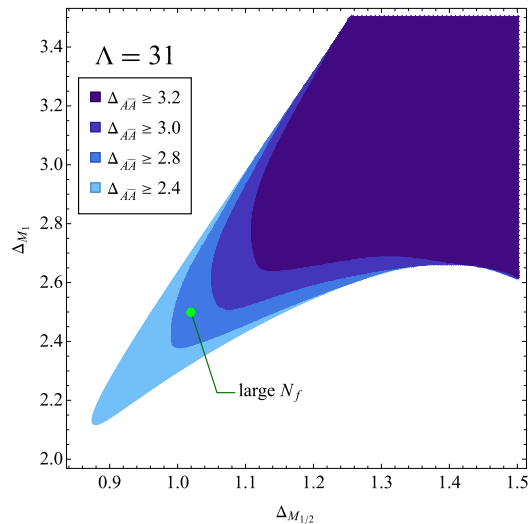

FIG. 10. Bootstrap bounds on the scaling dimension of the lowest charge 1 monopole $\mathcal{M}_1$ at $\Lambda = 31$. To get the bounds, we have employed gap assumptions on the lowest parity even singlet scalar $\Delta_{S_{(000)}} \geq 3.0$, the second lowest charge 1 monopole operator $\mathcal{M}_1'$ in the $T_{(220)}$ sector $\Delta_{\mathcal{M}_1'} \geq 5.0$, and the lowest scalar in the $S_{(220)}$ sector $\Delta_{A\bar{A}} \geq 2.4, 2.8, 3.0, 3.2$.
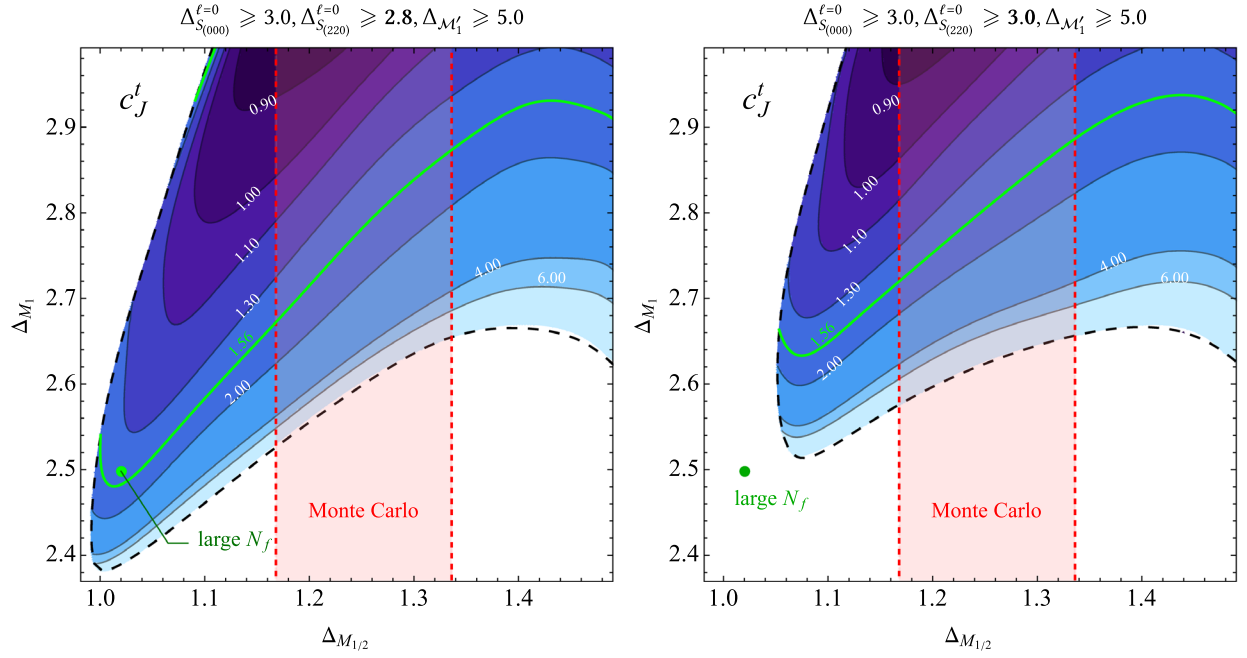
FIG. 11. Lower bounds on the topological $U(1)_t$ central charge c_J^t with different gap assumptions at $\Lambda = 31$. The green dot denotes the perturbative results of the monopole scaling dimensions $(\Delta_{\mathcal{M}_{1/2}}, \Delta_{\mathcal{M}_1}) \simeq (1.022, 2.499)$, and the green line shows the contour $c_J^t = 1.56$ predicted by the $1/N_f$ expansion. The lattice value $\Delta_{\mathcal{M}_{1/2}} = 1.252(84)$ [43] is given by the pink shaded region.

with a gap on the second $\mathbb{Z}_2$ even scalar [80], while the gaps imposed here are not fully justified as our knowledge of $N_f = 4$ QED$_3$ is limited. Due to the wave structure in Fig. 10, the interval positivity condition $\Delta_{\mathcal{M}_1} \leq \Delta_{\mathcal{M}_1}^{\max}$ truncates the tip of the wave structure below $\Delta_{\mathcal{M}_1}^{\max}$, which disconnects from the right part of the bulk region and forms a closed island. Bootstrap bounds on the scaling dimension of the monopole $\mathcal{M}_1$ were first presented in [51], in which the authors introduced a weaker gap assumption on the scaling dimension of the second lowest monopole $\mathcal{M}_1'$ and the bootstrap bound shows a weaker peninsula structure. The sharp wave structure we see here cannot appear unless the stronger gap assumption on $\Delta_{\mathcal{M}_1'}$ is imposed.

In Fig. 11, we also present the lower bound on the topological conserved current central charge c_J^t inside the wave structure, where its $1/N_f$ perturbative prediction is given by the green contour. Similar to the results in Fig. 9, the central charge c_J^t has a much higher lower bound in the right part of the allowed region. According to the c_J^t lower bound, it requires the scaling dimension of the monopole $\mathcal{M}_1$ to be above $\Delta_{\mathcal{M}_1} \geq 2.67$, or even higher values for the $\Delta_{\mathcal{M}_{1/2}}$ in the range predicted by the lattice results [43].

V. BOOTSTRAPPING MIXED CORRELATORS WITH $\mathcal{M}_{1/2}$ AND r

We have shown that the single correlator bootstrap results can provide strong constraints on the conformal $N_f = 4$ QED$_3$. To improve the bootstrap results, the key is

to find a more restrictive bootstrap implementation. A straightforward generalization of our work is to bootstrap mixed correlators with multiple operators in $N_f = 4$ QED$_3$. In this section, we perform a mixed correlator bootstrap study of conformal $N_f = 4$ QED$_3$ with an emphasis on the two low-lying scalars r and $\mathcal{M}_{1/2}$. We will show that this bootstrap setup indeed can significantly improve the lower cuts of the closed islands obtained in Sec. IV C.[14]

Bounds on the scaling dimensions of the operators $\mathcal{M}_{1/2}$ and r obtained from the $r - \mathcal{M}_{1/2}$ mixed correlator bootstrap are shown in Fig. 12. Details on the mixed correlator bootstrap implementation are presented in Appendix D. In the mixed correlator bootstrap, we used the same gap assumptions as in the monopole single correlator bootstrap, including the *interval positivity* assumption. In addition, we also required that the lowest scalar in the $S\bar{S}$, i.e. (422), representation of the $SU(4)$ flavor symmetry is irrelevant. Compared with the single correlator bootstrap bound, the mixed correlator bootstrap significantly improves the lower bound on the scaling dimension of Δ_r in the closed island: $\Delta_r \geq 1.12$ at $\Lambda = 27$.

The large N_f prediction and fermion bilinear bootstrap bounds on the scaling dimension of the lowest scalar in the $S\bar{S}$ sector were shown in Fig. 1, from which we expect the

---

[14] A similar study of the same mixed correlators was also performed in [58], which obtained general constraints on the possible stable critical phases of Dirac spin liquids on triangular and kagome lattices.
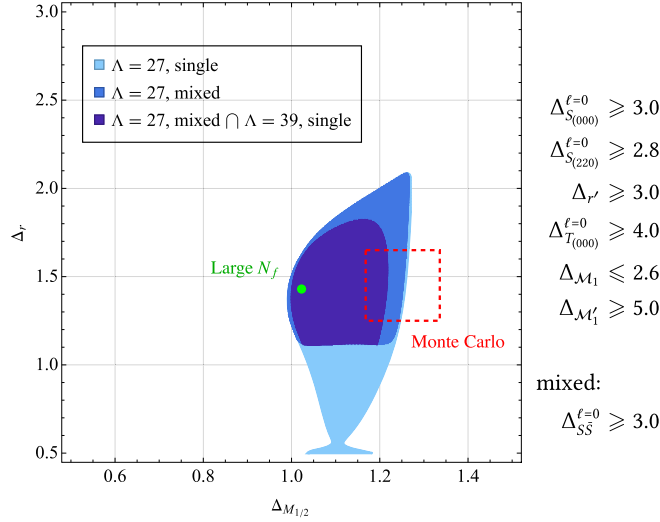
FIG. 12. Bounds on the scaling dimensions of $(\Delta_{\mathcal{M}_{1/2}}, \Delta_r)$ with the interval positivity assumption $\Delta_{\mathcal{M}_1} \leq 2.60$, comparing monopole single correlator bootstrap results with the monopole-adjoint mixed correlator bootstrap results at $\Lambda = 27$.
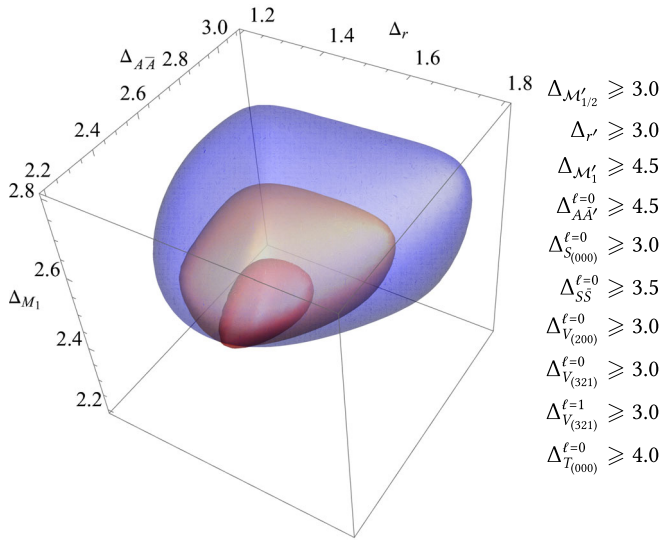

FIG. 13. Bounds on the scaling dimension of $(\Delta_r, \Delta_{A\bar{A}}, \Delta_{\mathcal{M}_1})$ from the monopole-adjoint mixed correlator bootstrap ($\Lambda = 19$) at fixed $\Delta_{\mathcal{M}_{1/2}}$. The islands in the plot, from the largest to the smallest, correspond to $\Delta_{\mathcal{M}_{1/2}} = 1.06$, 1.02, and 0.98, respectively. The full dynamical version of this three-dimensional plot is included in the attached *Mathematica* notebook.

gap 3.0 is a reliable assumption. Moreover, the fermion bilinear bootstrap bound on $\Delta_{S\bar{S}}$ in Fig. 1 explains why the we can obtain a stronger minimum on Δ_r after introducing the gap $\Delta_{S\bar{S}} \geq 3.0$: the upper bound on $\Delta_{S\bar{S}}$ cannot be higher than 3 for $\Delta_r < 1.12$. This provides a nice example which illustrates how the mixed correlator bootstrap can help to get stronger bounds with reliable assumptions. The bootstrap bounds in certain sectors are more restrictive and

TABLE IV. The ranges of scaling dimensions of the adjoint fermion bilinear r, lowest charge 1 monopole $\mathcal{M}_1$, and the lowest $A\bar{A}$-rep scalar, in the three-dimensional islands of fixed $\Delta_{\mathcal{M}_{1/2}}$ values. The islands and the gap assumptions are shown in Fig. 13. The island corresponding to the large-N_f value of $\Delta_{\mathcal{M}_{1/2}}$ is highlighted in bold font. See the body of this paper for further discussion of these values.

$\Delta_{\mathcal{M}_{1/2}}$	Δ_r	$\Delta_{\mathcal{M}_1}$	$\Delta_{A\bar{A}}$
0.98	(1.36, 1.52)	(2.27, 2.46)	(2.43, 2.76)
1.02	**(1.30, 1.66)**	**(2.28, 2.60)**	**(2.39, 2.91)**
1.06	(1.26, 1.79)	(2.29, 2.75)	(2.33, 3.06)

the mixed correlator bootstrap implementation can help to exploit the constraints in these sectors. We expect there are extra sectors, especially in the $\mathcal{M}_{1/2}$ and $\mathcal{M}_1$ mixed correlator setup, which can provide strong constraints on the CFT data with reliable gap assumptions. We hope to give a more systematic study of these constraints in our next work.

In the bootstrap studies of $N_f = 4$ conformal QED$_3$, several operators in different sectors play important roles. Their scaling dimensions relate to higher dimensional structures in the parameter space of CFT data. In Fig. 13 we make a first attempt to map out such a higher dimensional structure at $\Lambda = 19$. Specifically we show the closed 3D allowed region in the space $(\Delta_r, \Delta_{\mathcal{M}_1}, \Delta_{A\bar{A}})$ with different fixed scaling dimensions of $\mathcal{M}_{1/2}$, $\Delta_{\mathcal{M}_{1/2}} = 0.98$, 1.02, 1.06, making a set of plausible gap assumptions. The bootstrap allowed regions are 3D slices of a more complicated higher dimensional geometric structure and so have interesting shapes. The ranges of the islands with different fixed $\Delta_{\mathcal{M}_{1/2}}$ have been summarized in Table IV. In particular, by taking the large N_f result $\Delta_{\mathcal{M}_{1/2}} \simeq 1.02$, the perturbative predictions of $\Delta_r \simeq 1.43$ and $\Delta_{\mathcal{M}_1} \simeq 2.50$ are located inside the 3D island. The large N_f prediction of $\Delta_{A\bar{A}} \simeq 2.38$ is slightly outside of the island, while the gap $\Delta_{A\bar{A}} \geq 2.8$ used in other sections is consistent with the range of $\Delta_{A\bar{A}}$ in the 3D island.

VI. CONCLUSIONS AND DISCUSSIONS

The broad goal of the conformal bootstrap project is to find and classify CFTs. On the other hand, nonsupersymmetric gauge theories have so far shown resistance to being solved numerically using bootstrap methods.[15] In this work we have attempted to study the presumed IR fixed point of $N_f = 4$ QED$_3$ using the conformal bootstrap. Most notably, we found that after imposing some assumptions inspired by perturbative computations for $N_f = 4$

---

[15]However, remarkable progress towards numerically solving conformal gauge theories with extended supersymmetry has been made in the recent work [81,82].

TABLE V. A summary of the ranges of scaling dimensions of the lowest charge-1/2 monopole $\mathcal{M}_{1/2}$ and the $SU(4)$ adjoint fermion bilinear r in different setups. The shared gap assumptions are shown in Fig. 7, and the assumptions specific to the different setups are presented in the first row.

Setup	$\Delta_{\mathcal{M}_{1/2}}$ range	Δ_r range
$\Lambda = 39$ single $\Delta_{\mathcal{M}_1} \leq 2.50$	(1.00, 1.10)	(1.03, 1.61)
$\Lambda = 39$ single $\Delta_{\mathcal{M}_1} \leq 2.60$	(1.00, 1.22)	(0.73, 1.81)
$\cap \begin{cases} \Lambda = 39 \text{ single} \\ \Lambda = 27 \text{ mixed} \end{cases}$ $\begin{cases} \Delta_{\mathcal{M}_1} \leq 2.60 \\ \Delta_{s\bar{s}} \geq 3.50 \end{cases}$	(1.00, 1.22)	(1.12, 1.81)
$\Lambda = 31$ single $\begin{cases} \Delta_{\mathcal{M}_1} \leq 2.60 \\ c_J^t \leq 2 \end{cases}$.	(1.00, 1.14)	(0.98, 1.77)

QED$_3$ we can obtain a closed island in parameter space. The ranges of the islands under different bootstrap setups are summarized in Table V. Promisingly, bounds in this island on the scaling dimensions $\Delta_{\mathcal{M}_{1/2}}, \Delta_{\mathcal{M}_1}, \Delta_r$ as well as on the central charges $c_J, c_J^t,$ and c_T are consistent with their $1/N_f$ perturbative results, which in turn are close to saturating the bootstrap bounds. It is important to be clear that the physical relevance of these results relies on the validity of the gap assumptions used in our bootstrap computations, but nevertheless we believe our work has progressed our understanding of $N_f = 4$ conformal QED$_3$.

A major challenge in getting precise results from the QED$_3$ bootstrap is the notable sensitivity of the bounds to assumed gaps in the spectrum, closely connected to the symmetry-enhancement phenomena discussed in [54,55]. The crossing equations of the single four-point correlators $\langle rrrr \rangle$ and $\langle \mathcal{M}_{1/2} \mathcal{M}_{1/2} \mathcal{M}_{1/2} \mathcal{M}_{1/2} \rangle$ have positivity properties that can be mapped to the crossing equations of $SO(15)$ and $SO(12)$ vectors, respectively. To bootstrap non-$SO(N)$ symmetric theories, one has to impose gap assumptions which explicitly break the $SO(N)$ symmetries, and intriguing kinks and peninsulas which appear in the bootstrap bounds show a clear dependence on these gap assumptions. Despite this gap sensitivity, we believe that these discontinuities could still be of physical relevance to our understanding of QED$_3$ in the sense that they could be directly connected to the physical QED$_3$ solution through larger geometrical structures in scaling-dimension space. We have gained some confidence in this interpretation by inputting a set of gap assumptions inspired by the perturbative spectrum, and seeing that lower bounds on the stress tensor and current central charges near these kinks are nicely compatible with their estimated values from $1/N_f$ perturbation theory. In particular, this makes it seem unlikely that the kinks are

related to non-Abelian gauge theories, which have significantly larger values of the central charges.

The parity symmetry of $N_f = 4$ QED$_3$ makes the monopole bootstrap particularly effective in separating QED$_3$ from other solutions to crossing equations. Operators appearing in the $\mathcal{M}_{\pm 1/2} \times \mathcal{M}_{\pm 1/2}$ OPE carry different parity charges depending on their representations of $SU(4) \times U(1)_t$, and their scaling dimensions strongly break the $SU(4) \times U(1)_t \to SO(12)$ relation between the crossing equations. In contrast, in the fermion bilinear bootstrap, operators in different sectors branched from $SO(N)$ representations have the same parity charges and their scaling dimensions only differ by loop corrections in the $1/N_f$ expansion. By inputting gap assumptions inspired by the $N_f = 4$ QED$_3$ perturbative spectrum, in particular an expected large gap until the second charge 1 monopole, we are able to find a sharp peninsula structure in $(\Delta_{\mathcal{M}_{1/2}}, \Delta_{\mathcal{M}_1})$ whose narrow tip coincides neatly with the perturbative estimates of the theory. The peninsula structure remains gap dependent, and the gap assumption in the $S_{(2,2,0)}$ sector is particularly important as it determines the minimum value of $\Delta_{\mathcal{M}_{1/2}}$. As emphasized recently in [58], the leading operator in this sector is also physically important because its relevance or irrelevance determines whether QED$_3$ can be reached in lattice systems. We found that a gap $\Delta_{S_{(2,2,0)}} \geq 2.8$ allows for a nice consistency with $1/N_f$ perturbation theory, while irrelevance of this operator implies that uncomputed $1/N_f$ corrections to $(\Delta_{\mathcal{M}_{1/2}}, \Delta_{\mathcal{M}_1})$ should be of the same order as computed ones. It will be important in future work to determine which of these scenarios is correct.

Adopting the assumption that we should take perturbation theory at least somewhat seriously, our most notable results are obtained by imposing an *interval positivity* assumption $\Delta_{\mathcal{M}_1} \leq 2.6$, that $\Delta_{\mathcal{M}_1}$ required to be near or below its subleading perturbative estimate $\Delta_{\mathcal{M}_1} \approx 2.5$, which in turn restricts the peninsula structure to a closed island. Notably, this gives a closed region for the fermion bilinear dimension Δ_r as well as for $\Delta_{\mathcal{M}_{1/2}}$. Our bootstrap island at $\Lambda = 31$ overlaps with previous lattice estimates for Δ_r and $\Delta_{\mathcal{M}_{1/2}}$ [41,43,59]. However, by computing lower bounds on the central charges c_J, c_J^t and c_T inside this island, we see that the lattice estimates of $(\Delta_{\mathcal{M}_{1/2}}, \Delta_r)$ require c_J and c_J^t to be significantly higher than their $1/N_f$ perturbative estimates, suggesting that this region is likely unphysical. In contrast, the lower bounds on the central charges agree with their $1/N_f$ perturbative results in the region with $\Delta_{\mathcal{M}_{1/2}} \in (1.0, 1.1)$, compatible with the $1/N_f$ estimate $\Delta_{\mathcal{M}_{1/2}} \simeq 1.022$. In fact, if we adopt the more restrictive assumption $\Delta_{\mathcal{M}_1} \leq 2.5$, then a linear extrapolation of the bootstrap island suggests that it shrinks to a small range with $\Delta_{\mathcal{M}_{1/2}} \in (1.02, 1.04)$, beautifully

compatible with the perturbative results for both the scaling dimension and central charge data.

The results we have laid out so far give a potentially bright outlook for the future of bootstrapping QED$_3$, and we see several concrete directions for future work. The islands we obtained in this work rely on inputting an assumption which places either $\Delta_{\mathcal{M}_1}$ or $\Delta_{\mathcal{M}_{1/2}}$ near its perturbative value. It is important to find ways to get rid of this condition. Moreover, in this work some of the gap assumptions we made are not fully justified, and we hope that bootstrap results for QED$_3$ can ultimately be established using a set of sufficiently general assumptions that are more firmly established. A key point to improving this situation is to find an even more restrictive bootstrap setup, and there are a number of concrete mixed-correlator setups that could be pursued.

The bounds on the scaling dimension of the lowest charge 1 monopole operator have an interesting wave structure, which explains why islands can be formed with interval positivity assumptions and generally provides strong constraints if one assumes that the lattice results [43] are reliable. This wave structure is reminiscent of a similar structure appearing in the bootstrap of the 3D Ising CFT, leading to the conjecture that the solution at the tip of the wave might be further isolated by bootstrapping mixed correlators of the monopoles $\mathcal{M}_{1/2}$ and $\mathcal{M}_1$. In this mixed correlator setup, we can get access to more representations of $SU(4) \times U(1)_t$ and further exploit the constraints from parity symmetry and gaps in the monopole spectrum (which reflect the underlying equations of motion), which have played crucial roles in generating the current bootstrap results. Besides the gaps explored in this work, there are likely to be other sectors which can also introduce strong constraints on the CFT data, especially the spin 1 sectors appearing in the $SO(12) \rightarrow SU(4) \times U(1)_t$ branching rules. We hope to provide a more systematic exploration of these directions in future work.

APPENDIX A: FURTHER DETAILS ON THE FERMION BILINEAR BOOTSTRAP

1. Conventions

In this appendix, we set the conventions to describe various operators in QED$_3$. We use the Minkowski metric in mostly plus signature $\eta_{\mu\nu} = \text{diag}(-1, 1, 1)$. We will denote a fermion in the fundamental representation and its dual with uppercase and lowercase indices, respectively, i.e. ψ^α and ψ_α—and similarly for the complex conjugate representation $\psi_{\dot\alpha}$ and its dual $\psi^{\dot\alpha}$. Between these representations, we have the relation $(\psi^\alpha)^\dagger = (\psi^\dagger)^{\dot\alpha}$ and we have the intertwining operator $\gamma^0_{\dot\alpha\alpha}$, so that $(\psi^\alpha)^\dagger \gamma^0_{\dot\alpha\beta}$ transforms as the dual fermion ψ_β. We will then define $\bar\psi_\alpha := (\psi^\beta)^\dagger \gamma^0_{\dot\beta\alpha}$, with which we can construct the invariant scalar $\bar\psi_\alpha \psi^\alpha$.[16] Whenever there is no room for confusion, we will suppress spinor indices.[17]

We use an explicit real representation of the γ^μ matrices, i.e.

$$\gamma^0 = \begin{pmatrix} 0 & 1 \\ -1 & 0 \end{pmatrix}, \quad \gamma^1 = \begin{pmatrix} 0 & 1 \\ 1 & 0 \end{pmatrix}, \quad \gamma^2 = \begin{pmatrix} 1 & 0 \\ 0 & -1 \end{pmatrix},$$

$$\text{(A1)}$$

with which the Lorentz generators acting on the Dirac spinors can be written as $\gamma_{\mu\nu} = \frac{i}{4}(\gamma_\mu\gamma_\nu - \gamma_\nu\gamma_\mu)$. We take the space parity transformation as the reflection $x^2 \rightarrow -x^2$, and we choose its action on the fermions as $\psi \rightarrow \gamma^2\psi$.[18] This means $\bar\psi \rightarrow -\bar\psi\gamma^2$, indicating that $\bar\psi\psi$ transforms as a parity-odd scalar.

We can also work out how space parity transformations act on the standard $|l, m\rangle$ basis from the theory of angular momentum. Its coordinate representation, the spherical harmonics $Y_{lm}(\theta, \phi)$, pick up a sign under our parity transformation: $Y_{lm}(\theta, \phi) \rightarrow (-1)^{l+m}Y_{lm}(\theta, \phi)$.[19] In the presence of a magnetic flux q with $l - |q| \geq 0$, we will

---

[16]For Majorana fermions, we can convert all dotted indices to undotted ones, with which $\gamma^0_{\alpha\beta}$ and ψ^a can be interpreted as the symplectic tensor and fundamental representation of $Sp(2, \mathbb{R})$ group, as was done in [83–86].

[17]In our conventions, (un)dotted indices are contracted from north(south)-west to south(north)-east.

[18]As the double cover of the rotation group (Pin group) acts on ψ, both $\pm\gamma^2\psi$ are valid choices. Since we will always consider operators containing an even number of fermions, this does not pose any ambiguity.

[19]We note that this is different from the standard formula $\mathcal{P}: Y_{lm}(\theta, \phi) \rightarrow (-1)^l Y_{lm}(\theta, \phi)$ because we took our parity transformation as the reflection $x^2 \rightarrow -x^2$ instead of the inversion $x^i \rightarrow -x^i$.

instead resort to the *scalar monopole spherical harmonics* introduced in [87,88]:

$$Y_{q,lm}(\theta, \phi) \equiv \Theta_{q,lm}(\cos\theta)e^{i(m+\kappa q)\phi},$$

$$\Theta_{q,lm}(x) \equiv 2^{m-1}\sqrt{\frac{(2\ell+1)(\ell-m)!(\ell+m)!}{\pi(\ell-q)!(\ell+q)!}}$$

$$\times \sqrt{\frac{(1+x)^{q-m}}{(1-x)^{q+m}}}P_{\ell+m}^{-q-m,q-m}(x), \tag{A2}$$

where $P_n^{\alpha,\beta}(x)$ is the Jacobi polynomial and the parameter $\kappa = \pm 1$.[20] In our conventions,

Space parity : $Y_{q,lm}(\theta, \phi) \to (-1)^{l+m}e^{2iq\phi}Y_{-q,lm}(\theta, \phi).$

$$\tag{A3}$$

Our conventions for the global $SU(N)$ symmetry is analogous: we write indices in the (anti)fundamental representations (downstairs)upstairs, i.e. $\mathcal{O}^i$ vs $\mathcal{O}_i$. However, unlike the spacetime representations, these ones are actually conjugate, hence we have $(\mathcal{O}^i)^\dagger = \mathcal{O}_i$. Similar to γ^0 for the Clifford algebra, we have the Levi-Civita tensor ϵ which acts an intertwining operator between these conjugate representations,[21] hence we choose[22]

$$A_{i_1\ldots i_n} = \frac{1}{\sqrt{n!\bar{n}!}}\epsilon_{i_1\ldots i_n j_1\ldots j_{\bar{n}}}B^{j_1\ldots j_{\bar{n}}},$$

$$C^{i_1\ldots i_m} = \frac{1}{\sqrt{m!\bar{m}!}}D_{j_1\ldots j_{\bar{m}}}\epsilon^{j_1\ldots j_{\bar{m}}i_1\ldots i_m}, \tag{A4}$$

for operators A, B, C, and D in representations $\mathfrak{m}_1$, $\mathfrak{m}_1^*$, $\mathfrak{m}_2$, and $\mathfrak{m}_2^*$, respectively. Here, we defined the shorthand notation

$$\bar{n} \equiv N - n \tag{A5}$$

and similarly for m. If $m = \bar{m} = n = \bar{n} = \frac{N}{2}$, then we can choose $B = C = \mathcal{O}$ and $A = D = \mathcal{O}^\dagger$, which gives the reality conditions

$$(\mathcal{O}^{i_1\ldots i_n})^\dagger = \frac{1}{n!}\epsilon_{i_1\ldots i_n j_1\ldots j_n}\mathcal{O}^{j_1\ldots j_n},$$

$$\mathcal{O}^{i_1\ldots i_n} = \frac{1}{n!}(\mathcal{O}^{j_1\ldots j_n})^\dagger\epsilon^{j_1\ldots j_n i_1\ldots i_n}. \tag{A6}$$

The generalization of our notation to mixed tensors of $SU(N)$ is straightforward. For notational brevity, we will take consecutive indices antisymmetrized, whereas groups of indices separated by lines are symmetrized; for instance, the Young diagram for the representation of $\mathcal{O}^{il|jm|k}$ reads as

$$\begin{array}{|c|c|c|}\hline i & j & k \\\hline \ell & m \\\cline{1-2}\end{array}.$$[23] Equation (A4) then generalizes as

$$A_{k_{11}\ldots k_{1n_1}|k_{21}\ldots k_{2n_2}|\cdots|k_{c1}\ldots k_{cn_c}} = \left(\prod_{a=1}^{c}\frac{\epsilon_{k_{a1}\ldots k_{an_a}l_{a1}\ldots l_{a\bar{n}_a}}}{\sqrt{n_a!\bar{n}_a!}}\right)$$

$$\times B^{l_{c1}\ldots l_{c\bar{n}_c}|\cdots|l_{21}\ldots l_{2\bar{n}_2}|l_{11}\ldots l_{1\bar{n}_1}}, \tag{A7}$$

where A transforms in the Young diagram of c columns, each column having n_c boxes (and B transforms as its dual). For instance, two operators A and B in the conjugate representations $(\mathsf{A\bar{S}})$ and $(\mathsf{S\bar{A}})$ of $SU(4)$ would be related as

$$(A^{k_{11}k_{12}k_{13}|k_{21}k_{22}k_{23}|k_{31}k_{32}})^\dagger = \frac{\epsilon_{k_{11}k_{12}k_{13}l_{11}}\epsilon_{k_{21}k_{22}k_{23}l_{21}}\epsilon_{k_{31}k_{32}l_{31}l_{32}}}{\sqrt{3!3!2!2!}}$$

$$\times B^{l_{31}l_{32}|l_{21}|l_{11}}. \tag{A8}$$

The final group that we should set our conventions for is the $SO(2)$ group under which the monopole operators transform in the fundamental representation, i.e. $M^{I;a}$ for $a = 1, 2$ [I denotes the collective indices for $SU(N)$]. We are interested in cases where the monopole operators are real, hence Eq. (A6) generalizes as[24]

$$(\mathcal{O}^{i_1\ldots i_n;b})^\dagger = \frac{1}{n!}\delta_{ab}\epsilon_{i_1\ldots i_n j_1\ldots j_n}\mathcal{O}^{j_1\ldots j_n;a},$$

$$\mathcal{O}^{i_1\ldots i_n;b} = \frac{1}{n!}\delta_{ab}(\mathcal{O}^{j_1\ldots j_n;a})^\dagger\epsilon^{j_1\ldots j_n i_1\ldots i_n}. \tag{A9}$$

---

[20]The value of κ depends on which coordinate chart we are using to describe $Y_{q,lm}$: if we choose the chart that includes the whole sphere minus the south (north) pole, then κ is 1 (−1). In the rest of the paper, we stick to $\kappa = 1$.

[21]Let an operator $\mathcal{O}^{i_1\ldots i_n}$ transform under the $SU(N)$ action as $\mathcal{O}^{i_1\ldots i_n} \to U^{i_1}_{j_1}\ldots U^{i_n}_{j_n}\mathcal{O}^{j_1\ldots j_n}$, or $\mathcal{O}^I \to U^I_J\mathcal{O}^J$ as a shorthand notation. We similarly have $\mathcal{O}_I \to \mathcal{O}_J(U^\dagger)^J_I$ for the conjugate operator. Due to the identity $\epsilon_{IK}U^K_J = (U^\dagger)^L_I\epsilon_{LJ}$, $(\epsilon_{IJ}\mathcal{O}^J)$ transforms as an operator in the conjugate representation, i.e. $(\epsilon_{KJ}\mathcal{O}^J)(U^\dagger)^K_I$—similarly, the relation $\epsilon^{IK}U^J_K = (U^\dagger)^I_L\epsilon^{LJ}$ implies the inverse, i.e. $(\mathcal{O}_K\epsilon^{KI}) \to U^I_J(\mathcal{O}_K\epsilon^{KJ})$. Note that the identity $\epsilon_{i_1\ldots i_n k_1\ldots k_{\bar{n}}}U^{k_1}_{j_1}\cdots U^{k_{\bar{n}}}_{j_{\bar{n}}} = (U^\dagger)^{l_1}_{i_1}\cdots(U^\dagger)^{l_n}_{i_n}\epsilon_{l_1\ldots l_n j_1\ldots j_{\bar{n}}}$ follows from $\det U = 1$ condition and hence is valid only for the special unitary group.

[22]Our choice of normalization follows from the useful identity $\epsilon_{i_1\ldots i_n j_1\ldots j_m}\epsilon^{k_1\ldots k_n j_1\ldots j_m} = n!m!\delta^{k_1}_{[i_1}\cdots\delta^{k_n}_{i_n]}.$

[23]We note that for the representation to correspond to a valid Young diagram, we have the constraint $l_1 \geq l_2 \geq \ldots \geq l_n$ for $\mathcal{O}^{k_{11}\ldots k_{1l_1}|k_{21}\ldots k_{2l_2}|\cdots|k_{n1}\ldots k_{nl_n}}$.

[24]As monopole operators have the Dynkin labels $[\bar{0}, 2|q|, \bar{0}]$ ($\bar{0}$ denoting the sequence of $\frac{N-2}{2}$ many 0s), they are pseudoreal if $2|q| + 1 \in 2\mathbb{N}^+$ and $N = 4n - 2$ for $n \in \mathbb{N}^+$ [89]. For such cases, one uses ϵ_{ab} instead of δ_{ab}.

2. Index free notation for $SU(N_f)$ tensors

One can represent arbitrary mixed representations of the $SU(N)$ group as polynomials of a set of commuting and anticommuting variables by constructing explicit projector operators in the basis of fundamental indices.[25] Instead of doing this, we will follow a similar approach to [92] and use a less systematic yet more practical approach by mixing fundamental and antifundamental indices.

Let us first consider operators of the form $\mathcal{O}^{k_1|k_2|\ldots|k_n}_{l_1|l_2\ldots|l_m}$.[26] We can construct this tensor with auxiliary bosonic vectors u^i and $\bar{u}_i$ and define $\mathcal{O}(u,\bar{u}) := (\prod_{i=1}^{m} u^{l_i})(\prod_{i=1}^{n} \bar{u}_{k_i}) \mathcal{O}^{k_1|k_2|\ldots|k_n}_{l_1|l_2\ldots|l_m}$. One can reconstruct the tensor as $\mathcal{O}^{k_1|k_2|\ldots|k_n}_{l_1|l_2\ldots|l_m} = \left[\left(\prod_{i=1}^{m} \frac{\partial}{\partial u^{l_i}}\right)\left(\prod_{i=1}^{n} \frac{\partial}{\partial \bar{u}_{k_i}}\right)\mathcal{O}(u,\bar{u}) - \text{traces}\right]$. As $u \cdot \bar{u}$ only contributes to the trace, we drop such terms in $\mathcal{O}(u,\bar{u})$.[27]
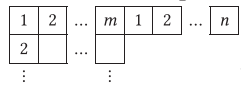
For more general tensors, we need to consider other auxiliary vectors and further constraints on the polynomial. For an operator of the most general form $\mathcal{O}^{k_1 k_2\ldots k_n|\ldots}_{l_1 l_2\ldots l_m|\ldots}$, we have the polynomial form $\mathcal{O}(u^{(1)},\ldots u^{(m)},\bar{u}^{(1)},\ldots\bar{u}^{(n)})$. Symmetrization of the indices are already satisfied as we are multiplying with the same vectors for indices in the same row; to satisfy antisymmetrization between indices in different rows, we impose the constraints

$$u^{(a)} \cdot \frac{\partial}{\partial u^{(b)}}\mathcal{O}(u^{(1)},\ldots u^{(m)},\bar{u}^{(1)},\ldots\bar{u}^{(n)}) = 0,$$
$$\bar{u}^{(a)} \cdot \frac{\partial}{\partial \bar{u}^{(b)}}\mathcal{O}(u^{(1)},\ldots u^{(m)},\bar{u}^{(1)},\ldots\bar{u}^{(n)}) = 0 \ \text{ for } a \neq b.$$
$$(A10)$$

By using these constraints alongside $u^{(a)} \cdot \bar{u}^{(b)} = 0$ for any a and b, we can construct correlation functions as polynomials of auxiliary vectors.[28]

We can illustrate this with the trivial case of the two-point function of the adjoint operators:

---

[25]Interested readers can consult [90,91] for examples of such projectors and the related illustrative birdtrack notation.
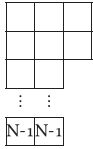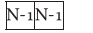[26]These correspond to representations with the Young diagram

, where the adjoint operator is the special case with $m = n = 1$.
[27]More precisely, $\mathcal{O}(u,\bar{u})$ is only defined modulo the ideal of functions proportional to $u \cdot \bar{u}$, hence we can restrict $\mathcal{O}(u,\bar{u})$ to the locus $u \cdot \bar{u} = 0$. For similar index-free techniques, see [93–95].
[28]One can always can get back the explicit tensorial form by differentiating and subtracting the indices, however we actually do not need tensor forms for practical purposes.

$$\left\langle \mathcal{O}_{\text{Adj}}\left(u_1^{(1)},\bar{u}_1^{(1)}\right)\mathcal{O}_{\text{Adj}}(u_2^{(1)},\bar{u}_2^{(1)})\right\rangle \propto u_1^{(1)} \cdot \bar{u}_2^{(1)} u_2^{(1)} \cdot \bar{u}_1^{(1)}.$$
$$(A11)$$

As a more detailed example, let us consider the two-point function of $(A\bar{S})$ and $(S\bar{A})$ operators. These operators are dual of each other and have the Young diagrams

and

, respectively. The two-point function then reads as

$$\left\langle \mathcal{O}_{(A\bar{S})}(u_1^{(1)},u_1^{(2)},\bar{u}_1^{(1)})\mathcal{O}_{(S\bar{A})}(\bar{u}_2^{(1)},\bar{u}_2^{(2)},u_2^{(1)})\right\rangle$$
$$\propto \left(u_1^{(1)} \cdot \bar{u}_2^{(1)} u_1^{(2)} \cdot \bar{u}_2^{(2)} - u_1^{(1)} \cdot \bar{u}_2^{(2)} u_1^{(2)} \cdot \bar{u}_2^{(1)}\right)\left(\bar{u}_1^{(1)} \cdot u_2^{(1)}\right)^2,$$
$$(A12)$$

which is the only combination that
  (i) has the correct order in each term,
  (ii) is free of $u_i \cdot \bar{u}_i$,
  (iii) satisfies the necessary conditions

$$u_i^{(a)} \cdot \frac{\partial}{\partial u_i^{(b)}}\left\langle \mathcal{O}_{(A\bar{S})}\left(\bar{u}_1^{(1)},\bar{u}_1^{(2)}\right)\mathcal{O}_{(S\bar{A})}\left(u_2^{(1)},u_2^{(2)}\right)\right\rangle = 0$$
$$\bar{u}_i^{(a)} \cdot \frac{\partial}{\partial \bar{u}_i^{(b)}}\left\langle \mathcal{O}_{(A\bar{S})}\left(\bar{u}_1^{(1)},\bar{u}_1^{(2)}\right)\mathcal{O}_{(S\bar{A})}\left(u_2^{(1)},u_2^{(2)}\right)\right\rangle = 0$$

$$\text{for } a \neq b = 1,2 \text{ and } i = 1,2.$$
$$(A13)$$

We can similarly write down three-point functions of two external adjoint operators as follows:

$$\langle\mathcal{O}_{\text{Adj}}\mathcal{O}_{\text{Adj}}\mathcal{O}_{S\bar{A}}\rangle \propto (U_{31}U_{32})V^{1112}_{1323}, \quad (A14a)$$

$$\langle\mathcal{O}_{\text{Adj}}\mathcal{O}_{\text{Adj}}\mathcal{O}_{A\bar{S}}\rangle \propto (U_{31}U_{32})^*(V^{1112}_{1323})^*, \quad (A14b)$$

$$\langle\mathcal{O}_{\text{Adj}}\mathcal{O}_{\text{Adj}}\mathcal{O}_{S\bar{S}}\rangle \propto (U_{13}U_{23})(U_{13}U_{23})^*, \quad (A14c)$$

$$\langle\mathcal{O}_{\text{Adj}}\mathcal{O}_{\text{Adj}}\mathcal{O}_{A\bar{A}}\rangle \propto V^{1112}_{1323}(V^{1112}_{1323})^*, \quad (A14d)$$

$$\langle\mathcal{O}_{\text{Adj}}\mathcal{O}_{\text{Adj}}\mathcal{O}_{\text{Adj}}\rangle \propto (U_{12}U_{23}U_{31}) \pm (U_{12}U_{23}U_{31})^*, \quad (A14e)$$

$$\langle\mathcal{O}_{\text{Adj}}\mathcal{O}_{\text{Adj}}\mathcal{O}_{\text{Singlet}}\rangle \propto U_{12}U^*_{12}, \quad (A14f)$$

where

$$V_{ijkl}^{abcd} := U_{ij}^{ab} U_{kl}^{cd} - U_{il}^{ad} U_{kj}^{cb} \qquad \text{(A15)}$$

for

$$U_{ij}^{ab} := u_i^{(a)} \cdot \bar{u}_j^{(b)}, \quad (U_{ij}^{ab})^* := \bar{u}_i^{(a)} \cdot u_j^{(b)} \qquad \text{(A16)}$$

with the shorthand notation $U_{ij} \equiv U_{ij}^{11}$. We observe that there are two structures for three adjoint operators (self-dual and anti-self-dual) and that the structures for A$\bar{\text{S}}$ and S$\bar{\text{A}}$ are dual of each other. All the other structures are evidently self-dual.

Once we include monopole operators, the number of auxiliary variables depend on N, hence we will focus on $N = 4$ below. For external $\mathcal{O}_\mathsf{M}$ and $\mathcal{O}_{\mathcal{M}^\dagger}$, we have

$$\langle \mathcal{O}_\mathsf{M} \mathcal{O}_{\mathsf{M}^\dagger} \mathcal{O}_\mathsf{Singlet} \rangle \propto V_{1212}^{1122},$$
$$\langle \mathcal{O}_\mathsf{M} \mathcal{O}_{\mathsf{M}^\dagger} \mathcal{O}_\mathsf{Adj} \rangle \propto U_{32}^{11} V_{1312}^{1122} - U_{32}^{12} V_{1312}^{1121},$$
$$\langle \mathcal{O}_\mathsf{M} \mathcal{O}_{\mathsf{M}^\dagger} \mathcal{O}_\mathsf{A\bar{A}} \rangle \propto V_{1313}^{1122} (V_{2323}^{1122})^*, \qquad \text{(A17)}$$

which satisfy all the necessary conditions stated above. In addition, we can explicitly check that the structures are invariant under the combined action of conjugation with permutation of first two external operators, i.e. under $U_{ab}^{ij} \to (U_{ab}^{ij})^* \big|_{\substack{u_1^{(a)} \leftrightarrow u_2^{(a)} \\ \bar{u}_1^{(a)} \leftrightarrow \bar{u}_2^{(a)}}}$.[29]

A basis of four-point functions can also be constructed as polynomials of auxiliary vectors; for instance, for four external adjoint operators, there are nine such structures:

$$T_{13} T_{24}, \quad T_{12} T_{34} \pm T_{14} T_{23}, \quad T_{1234} \pm T_{1423},$$
$$T_{1243} \pm T_{1324}, \quad T_{1342} \pm T_{1432} \qquad \text{(A18)}$$

for

$$T_{i_1 i_2 \dots i_n} := U_{i_1 i_2} U_{i_2 i_3} \cdots U_{i_n i_1}, \qquad \text{(A19)}$$

where we choose combinations that are invariant under $1 \leftrightarrow 3$ exchange modulo a sign.

3. Setup of the crossing equations

Let us consider a four-point function $\langle A_{1m} B_{2n} C_{3r} D_{4p} \rangle$, where $\mathcal{O}_{im} \equiv \mathcal{O}_m(x_i)$ for the collective global symmetry index m. We also assume in this section that an operator A is in the representation a of the global group.

In this notation, we have the conformal block decomposition

---

[29]For instance, one can show that $(V_{1212}^{1122})^* = V_{2121}^{1122}$ hence V_{1212}^{1122} is indeed invariant after conjugation followed by $1 \leftrightarrow 2$ in the lower-stair indices. To show the invariance of such structures, the identities $(V_{ijkl}^{abcd})^* = V_{lkji}^{dcba}$, $V_{ijkl}^{abcd} = -V_{ilkj}^{adcb} = -V_{kjil}^{cbad}$ become useful.

$$\langle A_{1m} B_{2n} C_{4r} \rangle = \frac{1}{x_{12}^{\Delta_A + \Delta_B} x_{34}^{\Delta_C + \Delta_D}} \left(\frac{x_{24}}{x_{14}} \right)^{\Delta_{AB}} \left(\frac{x_{14}}{x_{13}} \right)^{\Delta_{CD}}$$
$$\times \sum_{\substack{O \in A \times B \\ O^\dagger \in C \times D \\ i,j}} (-1)^{l_\mathcal{O}} \lambda_{ABO}^{(i)} \lambda_{CDO^\dagger}^{(j)}$$
$$\times (T_o^{abcd})_{mnpr}^{(ij)} g_O^{ABCD}(u, v), \qquad \text{(A20)}$$

where T is the global symmetry four-point tensor structure. The summation i, j is over the multiplicity of the representation $o, \bar{o}$.

For bosonic operators, we can go to a kinematic regime where $\langle A_{1m} B_{2n} C_{3p} D_{4r} \rangle = \langle C_{3p} B_{2n} A_{1m} D_{4r} \rangle$ by fixing the conformal frame as

$$x_1 = (0, 0, \vec{0}), \quad x_2 = \left(\frac{z - \bar{z}}{2i}, \frac{z + \bar{z}}{2}, \vec{0} \right),$$
$$x_3 = (0, 1, \vec{0}), \quad x_4 = (0, \infty, \vec{0}) \qquad \text{(A21)}$$

with $u = z\bar{z}$ and $v = (1 - z)(1 - \bar{z})$[30]; this leads to

$$\sum_{\substack{O \in A \times B \\ O^\dagger \in C \times D \\ i,j}} (-1)^{l_\mathcal{O}} \lambda_{ABO}^{(i)} \lambda_{CDO^\dagger}^{(j)} (T_o^{abcd})_{mnpr}^{(ij)} F_{\pm,O}^{ABCD}(u, v)$$
$$\mp \sum_{\substack{O \in C \times B \\ O^\dagger \in A \times D \\ i,j}} (-1)^{l_\mathcal{O}} \lambda_{CBO}^{(i)} \lambda_{ADO^\dagger}^{(j)} (T_o^{cbad})_{pnmr}^{(ij)} F_{\pm,O}^{CBAD}(u, v) = 0,$$
$$\text{(A22)}$$

where we added/subtracted $(u \leftrightarrow v)$ from the original equation. We also defined

$$F_{\pm,O}^{ABCD}(u, v) \equiv v^{\frac{\Delta_B + \Delta_C}{2}} g_O^{ABCD}(u, v) \pm u^{\frac{\Delta_B + \Delta_C}{2}} g_O^{ABCD}(v, u).$$
$$\text{(A23)}$$

The crossing equation simplifies for certain correlators; for instance, for $\langle ABAB \rangle$, it reads as

$$\sum_{\substack{O, O^\dagger \in A \times B \\ i,j}} (-1)^{l_\mathcal{O}} \lambda_{ABO}^{(i)} \lambda_{ABO^\dagger}^{(j)} ((T_o^{abab})_{mnpr}^{(ij)}$$
$$\mp (T_o^{abab})_{pnmr}^{(ij)}) F_{\pm,O}^{ABAB}(u, v) = 0. \qquad \text{(A24)}$$

The global symmetry tensor structure T can be fixed once the three-point structures are chosen. To set this convention, we can define the OPE expansion as

$$A_{1m} B_{2n} = \sum_{\substack{O \in A \times B \\ o \in a \times b \\ i}} \lambda_{ABO}^{(i)} (t_o^{ab})_{mn}^{(i)s} c_{ABO}(x_1, x_2, \partial_5) O_{5s}, \qquad \text{(A25)}$$

---

[30]An operator at infinity is defined as $\mathcal{O}_4 \equiv \mathcal{O}(x_4) = \lim_{L \to \infty} L^{2\Delta_\mathcal{O}} \mathcal{O}(0, L, \vec{0})$.

where $(t_o^{ab})_{mn}^{(i)s}$ are three-point structures of the global group and $c(x_1, x_2, \partial_5)$ is a differential operator containing the information of the descendants of O.[31] If we apply this OPE inside a three-point function, then we see that

$$\langle A_{1m}B_{2n}O_{3t}^\dagger\rangle = \sum_i \lambda_{ABO}^{(i)}(t_o^{ab})_{mn}^{(i)s}(\delta^{o\bar{o}})_{st}\langle A_1 B_2 O_3^\dagger\rangle, \quad (A26)$$

where $\langle A_1 B_2 O_3^\dagger\rangle \equiv c_{ABO}(x_1, x_2, \partial_5)\langle O_5 O_3^\dagger\rangle$ is the standard three-point structure of the conformal group with global symmetry dependence stripped off.[32] This structure has the symmetry $\langle A_1 B_2 O_3^\dagger\rangle = (-1)^l \langle B_2 A_1 O_3^\dagger\rangle$; as we also have $\langle A_{1m}B_{2n}O_{3t}^\dagger\rangle = \langle B_{2n}A_{1m}O_{3t}^\dagger\rangle$ for bosonic operators A and B, we conclude

$$\sum_i \lambda_{ABO}^{(i)}(t_o^{ab})_{mn}^{(i)s} = (-1)^l \sum_i \lambda_{BAO}^{(i)}(t_o^{ba})_{nm}^{(i)s}. \quad (A27)$$

By applying the OPE twice in a four-point function, we find the relations

$$c_{ABO}(x_1, x_2, \partial_5)c_{CDO^\dagger}(x_3, x_4, \partial_5)\langle O_5 O_5^\dagger\rangle$$
$$= \frac{(-1)^{l_O}}{x_{12}^{\Delta_A+\Delta_B}x_{34}^{\Delta_C+\Delta_D}}\left(\frac{x_{24}}{x_{14}}\right)^{\Delta_{AB}}\left(\frac{x_{14}}{x_{13}}\right)^{\Delta_{CD}} g_O^{ABCD}(u, v), \quad (A28)$$

and

$$(T_o^{abcd})_{mnpr}^{(ij)} = (t_o^{ab})_{mn}^{(i)s}(t_o^{cd})_{pr}^{(j)t}(\delta^{o\bar{o}})_{st}. \quad (A29)$$

With Eq. (A27), one can use the latter equation to obtain several relations.[33]

With all the conventions set up, we can finally choose our conformal block normalization. For this,

---

[31]We are suppressing the contracted spacetime indices of the operator $\mathcal{O}$ and the structure c_{ABO}.

[32]For 3D CFTs, we can write it down as $\frac{\langle S_3 X_1 X_2 S_3\rangle^l}{(X_1 \cdot X_2)^\# (X_2 \cdot X_3)^\# (X_3 \cdot X_1)^\#}$ up to an overall factor in the embedding space formalism, where X and S are the position vector and auxiliary spinor, respectively.

[33]One can immediately write down

$$\sum_i \lambda_{ABO}^{(i)}(T_o^{abcd})_{mnpr}^{(ij)} = (-1)^{l_O}\sum_i \lambda_{BAO}^{(i)}(T_o^{bacd})_{nmpr}^{(ij)}, \quad (A30a)$$

$$\sum_j \lambda_{CDO}^{(j)}(T_o^{abcd})_{mnpr}^{(ij)} = (-1)^{l_O}\sum_j \lambda_{DCO}^{(j)}(T_o^{abdc})_{mnrp}^{(ij)}. \quad (A30b)$$

By using this, we can also obtain further relations; for instance,

$$\sum_{i,j}\lambda_{AAO}^{(i)}\lambda_{BBO^\dagger}^{(j)}(T_o^{aabb})_{mnpr}^{(ij)} = \sum_{\substack{i,j \\ \text{even}\,l}}\lambda_{AAO}^{(i)}\lambda_{BBO^\dagger}^{(j)}(T_o^{aabb})_{\{mn\}\{pr\}}^{(ij)}$$
$$+ \sum_{\substack{i,j \\ \text{odd}\,l}}\lambda_{AAO}^{(i)}\lambda_{BBO^\dagger}^{(j)}(T_o^{aabb})_{[mn][pr]}^{(ij)} \quad (A31)$$

for $O_{\{ab\}} \equiv \frac{1}{2}(O_{ab} + O_{ba})$ and $O_{[ab]} \equiv \frac{1}{2}(O_{ab} - O_{ba})$.

we consider the normalization of the differential operator $c_{ABO}(x_1, x_2, \partial_5)$. In the OPE limit, we choose it such that[34]

$$c_{ABO}(x_1, x_2, \partial_3) \sim \sqrt{\frac{2^l \Gamma(l + \frac{1}{2})}{\sqrt{\pi}\Gamma(l+1)}}x_{12}^{\Delta_O - \Delta_A - \Delta_B},$$
$$|x_{12}| \ll |x_{13}|, |x_{23}|. \quad (A32)$$

With Eq. (A28), this fixes the normalization of the conformal block as in the second row of Table 1 of [50], i.e. $g(z, \bar{z}) \sim \frac{\Gamma(l+\frac{1}{2})}{\sqrt{\pi}\Gamma(l+1)}z^h\bar{z}^{\bar{h}}$ for $0 < z \ll \bar{z} \ll 1$.[35]

The global symmetry structures $(t_o^{ab})_{mn}^{(i)s}$ in Eq. (A26) can be computed in various ways; for instance, one can compute them as explicit tensors [72], or one can use index-free formalism to write them down as we did in Eq. (A14). We will not dwell on the details here, but only present how reflection positivity fixes the overall signs of certain structures in our conventions. For this, we look at a reflection positive configuration of Hermitian operators A and B; Eq. (A20) becomes

$$\langle A_{1m}B_{2n}B_{3p}A_{4r}\rangle \propto \sum_{\substack{O \in A \times B \\ O^\dagger \in B \times A \\ i,j}} (-1)^{l_O}\lambda_{ABO}^{(i)}\lambda_{BAO^\dagger}^{(j)}$$
$$\times (T_o^{abba})_{mnpr}^{(ij)}g_O^{ABBA}(u, v) \quad (A33)$$

up to a positive proportionality constant. Via Eq. (A30), this indicates

$$\langle A_{1m}B_{2n}|\mathcal{O}|B_{3p}A_{4r}\rangle \propto \sum_{i,j}\lambda_{ABO}^{(i)}\lambda_{ABO^\dagger}^{(j)}$$
$$\times (T_o^{abab})_{mnrp}^{(ij)}g_O^{ABBA}(u, v). \quad (A34)$$

For $A_{1m} = (A_{4r})^\dagger$ and $B_{2n} = (B_{3p})^\dagger$, the left-hand side can be interpreted as the norm of a state in radial quantization, hence needs to be positive. We then conclude[36] $\sum_{i,j}\lambda_{ABO}^{(i)}\lambda_{ABO^\dagger}^{(j)}(T_o^{abab})_{mnrp}^{(ij)} \geq 0$, or rather

$$\begin{pmatrix} (T_o^{abab})_{mnrp}^{(11)} & (T_o^{abab})_{mnrp}^{(12)} \\ (T_o^{abab})_{mnrp}^{(21)} & (T_o^{abab})_{mnrp}^{(22)} \\ & & \ddots \end{pmatrix} \succeq 0,$$

$$\text{for } A_{1m} = (A_{4r})^\dagger, \quad B_{2n} = (B_{3p})^\dagger \quad (A35)$$

for real λ, which is the case for real scalars.

---

[34]This form is schematic in that it only determines the overall scaling while suppressing the spacetime tensor structure.

[35]For further details on the relation between c_{ABO} and the conformal block normalization, one can refer to [96].

[36]Note that this relies on our choice that the conformal block is normalized to be positive.

4. Direct computation of the correlators in mean field theory limit

In Sec. III, we discussed the importance of fermion bilinears in the exploration of QED$_3$ via nonperturbative methods. On the other hand, explicit computations in the mixed conformal bootstrap setup can be computationally demanding. One regime where computations can actually be done in a relatively straightforward manner is the mean field theory limit, where correlators can be computed via Wick contractions. Although such a MFT is expected to be rather unrelated to the physical QED$_3$, a better grasp of its correlators can nevertheless be useful. This is particularly true in the large spin limit, where the spectrum of any CFT approaches asymptotically to that of the MFT.

We start by considering the operators

$$
\mathcal{O}_i^m = \bar{\psi}^m \psi_i - \frac{1}{N} \delta_i^m \bar{\psi}^k \psi_k,
$$

$$
\mathcal{O}_i'^m = \frac{1}{\sqrt{N}} \left[(\bar{\psi}^{[m} \psi_{[k]})(\bar{\psi}^{k]} \psi_{i]}) - \frac{\delta_i^m}{N} (\bar{\psi}^{[l} \psi_{[k]})(\bar{\psi}^{k]} \psi_{l]}) \right],
$$

$$
\mathcal{O}_i''^m = \frac{1}{\sqrt{N}} (\bar{\psi}^k \psi_k) \mathcal{O}_i^m, \tag{A36}
$$

where ψ is a Dirac fermion in the conventions of Sec. A 1.[37] We now define the following operators

$$
A_i^m = \frac{i}{\sqrt{2}} \mathcal{O}_i^m,
$$

$$
B_i^m = -\frac{i}{\sqrt{2}} \sqrt{\frac{N}{N-1}} \mathcal{O}_i''^m,
$$

$$
C_i^m = -\sqrt{\frac{4(N-1)N}{3(N-2)(N+2)}} \left(\mathcal{O}_i'^m - i \frac{3(N-2)}{2\sqrt{2}(N-1)} \mathcal{O}_i''^m \right), \tag{A38}
$$

which are orthonormal in the sense that

$$
\langle A_1 A_2 \rangle = \frac{U_{12}}{x_{12}^{4\Delta}}, \quad \langle B_1 B_2 \rangle = \frac{U_{12}}{x_{12}^{8\Delta}}, \quad \langle C_1 C_2 \rangle = \frac{U_{12}}{x_{12}^{8\Delta}},
$$

$$
\langle X_1 Y_2 \rangle = 0 \quad \text{if } X \neq Y, \tag{A39}
$$

[37]These operators are also studied in [65], except they work with

$$
\tilde{\mathcal{O}}_i^m = \frac{1}{\sqrt{N}} \sum_{k=3}^N (\psi_{(\alpha_1)[i} (\psi_{\alpha_2})_{k]}) (\bar{\psi}^{(\alpha_1)[m} (\bar{\psi}^{\alpha_2})^{k]}) - SU(N) \text{ traces}
$$

(A37)

instead of $\mathcal{O}_i'^m$. These two operators are equal if the summation range above is extended down to $k = 1$.

where we are using the index-free notation introduced in Sec. A 2.[38]

We can now treat A_i^m as the lightest parity-odd adjoint bilinear scalar, whereas B_i^m and C_i^m are the lightest parity-even adjoint bilinear scalars. Therefore, we can consider various correlators such as $\langle AAB \rangle$ or $\langle BBB \rangle$ and extract the OPE coefficients in the MFT limit. Performing the explicit computation, we find

$$
\langle A_1 A_2 X_3^{(1)} \rangle = \lambda_{AAX} \frac{T_{123} + T_{213}}{v^{2\Delta}},
$$

$$
\langle X_1^{(1)} X_2^{(2)} X_3^{(3)} \rangle = \lambda_{X^{(1)} X^{(2)} X^{(3)}} \frac{T_{123} + T_{213}}{u^{2\Delta} v^{2\Delta}}, \quad \text{for } X^{(i)} = B, C, \tag{A41}
$$

where $T_{i_1 i_2 \ldots i_n}$ are defined in Eq. (A19) and the operators are in the conformal frame of Eq. (A21). The OPE coefficients read as

$$
\lambda_{AAB} = \frac{1}{2\sqrt{N-1}}, \quad \lambda_{AAC} = \frac{\sqrt{3}N}{2\sqrt{(N-2)(N-1)(N+2)}},
$$

$$
\lambda_{BBB} = \frac{3N-4}{2(N-1)^{3/2}}, \quad \lambda_{BBC} = \frac{\sqrt{3}N\sqrt{\frac{N-2}{N^2+N-2}}}{2(N-1)},
$$

$$
\lambda_{BCC} = \frac{N^3 - 12N + 8}{2(N-2)(N-1)^{3/2}(N+2)},
$$

$$
\lambda_{CCC} = \frac{(N-4)(3N^3 + 10N^2 + 28N - 32)}{6\sqrt{3}(N-2)^{3/2}(N-1)^{3/2}(N+2)^{3/2}}. \tag{A42}
$$

For $N = 4$, they become

$$
\lambda_{AAB} = \frac{1}{2\sqrt{3}}, \quad \lambda_{AAC} = \frac{1}{\sqrt{3}}, \quad \lambda_{BBB} = \frac{4}{3\sqrt{3}},
$$

$$
\lambda_{BBC} = \frac{2}{3\sqrt{3}}, \quad \lambda_{BCC} = \frac{1}{3\sqrt{3}}, \quad \lambda_{CCC} = 0. \tag{A43}
$$

By using Wick contractions, we can also compute the four-point correlators and then compare them with the conformal block expansion in Eq. (A20) to extract $F_{\pm,\mathcal{O}}^{ABCD}(u, v)$ as defined in Eq. (A23). For instance, for $\langle AAAA \rangle$, if we define

[38]These equations follow from the normalization of the Dirac field ψ such that its real and imaginary parts are normalized as two independent Majorana fermions ξ and χ:

$$
\langle \chi^{\alpha,m}(x_1) \chi_{\beta,i}(x_2) \rangle = \langle \xi^{\alpha,m}(x_1) \xi_{\beta,i}(x_2) \rangle = \frac{i}{2} \frac{(x_{12})_\beta^\alpha}{x_{12}^{2\Delta+1}} \delta_i^m,
$$

$$
\langle \xi^{\alpha,m}(x_1) \chi_{\beta,i}(x_2) \rangle = 0. \tag{A40}
$$

$$\langle A_i^m A_j^n A_k^p A_l^r \rangle = \sum_\alpha f_\alpha^{AAAA}(x_1, x_2, x_3, x_4)(\mathsf{t}_\alpha)_{ijkl}^{mnpr} \quad (A44)$$

for various four-point tensor structures $(\mathsf{t}_\alpha)_{ijkl}^{mnpr}$, we can extract $F_{\pm,O}^{AAAA}(u, v)$ from the equation

$$\left[\sum_\alpha (uv)^{2\Delta} f_\alpha^{AAAA}(u, v)(\mathsf{t}_\alpha)_{mnpr}\right] \pm [u \leftrightarrow v]$$
$$= \sum_{\substack{O, O^\dagger \in A \times A \\ i, j}} (-1)^{l_O} \lambda_{AAO}^{(i)} \lambda_{AAO}^{(j)} (T_o^{aaaa})_{mnpr}^{(ij)} F_{\pm,O}^{AAAA}(u, v) \quad (A45)$$

by matching the structures $(\mathsf{t}_\alpha)_{ijkl}^{mnpr}$ with different pieces of $(T_o^{aaaa})_{mnpr}^{(ij)}$.[39]

In this convention, we can explicitly compute that

$$\langle A_1 A_2 A_3 A_4 \rangle = T_{13}T_{24} + \frac{1}{u^{2\Delta}} T_{12}T_{34} + \frac{1}{v^{2\Delta}} T_{14}T_{23}$$
$$- \frac{u + v - 1}{4u^{\Delta+\frac{1}{2}} v^{\Delta+\frac{1}{2}}}(T_{1234} + T_{1432})$$
$$- \frac{1 + u - v}{4u^{\Delta+\frac{1}{2}}}(T_{1243} + T_{1342})$$
$$- \frac{1 - u + v}{4v^{\Delta+\frac{1}{2}}}(T_{1324} + T_{1423}), \quad (A46)$$

where $T_{i_1 i_2 \dots i_n}$ are defined in Eq. (A19). We can now use Eq. (A45) and explicitly compute $\mathcal{F}_{\pm,O}^{ij} \equiv (-1)^{l_O} \lambda_{AAO}^{(i)} \lambda_{AAO}^{(j)} F_{\pm,O}^{AAAA}(u, v)$ as

$$\mathcal{F}_{-,\mathsf{Adj}^+}^{11} = \frac{Nu^\Delta(N(u-1)u^\Delta v^\Delta + N\sqrt{u}v^{2\Delta+\frac{1}{2}} + 8\sqrt{v}u^\Delta)}{16(N^2 - 4)\sqrt{v}}$$
$$- (u \leftrightarrow v), \quad (A47a)$$

$$\mathcal{F}_{-,\mathsf{Adj}^-}^{22} = \frac{1}{16} u^\Delta \left(-\frac{8u^\Delta}{N} + (u-1)u^\Delta v^{\Delta-\frac{1}{2}} + \sqrt{u}v^{2\Delta}\right)$$
$$- (u \leftrightarrow v), \quad (A47b)$$

$$\mathcal{F}_{-,\mathsf{Singlet}}^{11}$$
$$= \frac{u^\Delta(-4(N^2-2)\sqrt{v}u^\Delta + N(u-1)u^\Delta v^\Delta + N\sqrt{u}v^{2\Delta+\frac{1}{2}})}{4(N^2-1)\sqrt{v}}$$
$$- (u \leftrightarrow v), \quad (A47c)$$

$$\mathcal{F}_{-,\mathsf{S\bar{S}}}^{11} = \frac{1}{16} u^\Delta \left(4u^\Delta - (u-1)u^\Delta v^{\Delta-\frac{1}{2}} - \sqrt{u}v^{2\Delta}\right)$$
$$- (u \leftrightarrow v), \quad (A47d)$$

$$\mathcal{F}_{-,\mathsf{ReA\bar{S}}}^{11} = -\frac{u^{2\Delta}}{2} - (u \leftrightarrow v), \quad (A47e)$$

$$\mathcal{F}_{-,\mathsf{A\bar{A}}}^{11} = \frac{1}{16} u^\Delta \left(4u^\Delta + (u-1)u^\Delta v^{\Delta-\frac{1}{2}} + \sqrt{u}v^{2\Delta}\right)$$
$$- (u \leftrightarrow v), \quad (A47f)$$

$$\mathcal{F}_{+,\mathsf{Adj}^+}^{11} = \frac{Nu^{2\Delta}}{2(N^2-4)} + \left(\frac{1}{16 - 4N^2} + \frac{1}{16}\right) u^{2\Delta} v^{\Delta-\frac{1}{2}}$$
$$+ \left(\frac{1}{4(N^2-4)} - \frac{1}{16}\right) u^{2\Delta+1} v^{\Delta-\frac{1}{2}} + \frac{Nu^{2\Delta} v^{2\Delta}}{2(N^2-4)}$$
$$+ \left(\frac{1}{16 - 4N^2} + \frac{1}{16}\right) u^{\Delta+\frac{1}{2}} v^{2\Delta} - \frac{1}{16} u^{\Delta-\frac{1}{2}} v^{\Delta-\frac{1}{2}}$$
$$+ \frac{1}{8} u^{\Delta+\frac{1}{2}} v^{\Delta-\frac{1}{2}} + (u \leftrightarrow v), \quad (A47g)$$

$$\mathcal{F}_{+,\mathsf{Adj}^-}^{22} = -\frac{u^{2\Delta}}{2N} + \frac{u^{2\Delta} v^{2\Delta}}{2N} + \frac{1}{16} u^{\Delta-\frac{1}{2}} v^{\Delta-\frac{1}{2}} + \frac{1}{16} u^{2\Delta} v^{\Delta-\frac{1}{2}}$$
$$- \frac{1}{8} u^{\Delta+\frac{1}{2}} v^{\Delta-\frac{1}{2}} - \frac{1}{16} u^{2\Delta+1} v^{\Delta-\frac{1}{2}}$$
$$+ \frac{1}{16} u^{\Delta+\frac{1}{2}} v^{2\Delta} + (u \leftrightarrow v), \quad (A47h)$$

$$\mathcal{F}_{+,\mathsf{Singlet}}^{11} = \frac{N^2 u^{2\Delta}}{N^2 - 1} + \frac{(2-N^2)u^{2\Delta} v^{\Delta-\frac{1}{2}}}{4N - 4N^3}$$
$$- \frac{(2-N^2)u^{2\Delta+1} v^{\Delta-\frac{1}{2}}}{4N - 4N^3} + \frac{u^{2\Delta} v^{2\Delta}}{N^2 - 1}$$
$$+ \frac{(2-N^2)u^{\Delta+\frac{1}{2}} v^{2\Delta}}{4N - 4N^3} - \frac{u^{\Delta-\frac{1}{2}} v^{\Delta-\frac{1}{2}}}{4N}$$
$$+ \frac{u^{\Delta+\frac{1}{2}} v^{\Delta-\frac{1}{2}}}{2N} + (u \leftrightarrow v), \quad (A47i)$$

$$\mathcal{F}_{+,\mathsf{S\bar{S}}}^{11} = \frac{u^{2\Delta}}{4} + \frac{1}{16} u^{2\Delta} v^{\Delta-\frac{1}{2}} - \frac{1}{16} u^{2\Delta+1} v^{\Delta-\frac{1}{2}} + \frac{1}{4} u^{2\Delta} v^{2\Delta}$$
$$+ \frac{1}{16} u^{\Delta+\frac{1}{2}} v^{2\Delta} + (u \leftrightarrow v), \quad (A47j)$$

$$\mathcal{F}_{+,\mathsf{ReA\bar{S}}}^{11} = \frac{1}{2} u^{2\Delta} v^{2\Delta} - \frac{u^{2\Delta}}{2} + (u \leftrightarrow v), \quad (A47k)$$

$$\mathcal{F}_{+,\mathsf{A\bar{A}}}^{11} = \frac{u^{2\Delta}}{4} - \frac{1}{16} u^{2\Delta} v^{\Delta-\frac{1}{2}} + \frac{1}{16} u^{2\Delta+1} v^{\Delta-\frac{1}{2}} + \frac{1}{4} u^{2\Delta} v^{2\Delta}$$
$$- \frac{1}{16} u^{\Delta+\frac{1}{2}} v^{2\Delta} + (u \leftrightarrow v), \quad (A47l)$$

where the representations $\mathsf{Adj}^\pm$ are those that come with the structures in Eq. (A14) with the relative sign $\pm$.

---

[39] Equation (A45) generalizes to other correlators with the single modification that $(uv)^{2\Delta}$ is replaced by $(uv)^{4\Delta}$, $u^{2\Delta} v^{3\Delta}$, $(uv)^{3\Delta}$, and $u^{3\Delta} v^{2\Delta}$ for the correlators $\langle BBBB \rangle$, $\langle AABB \rangle$, $\langle ABAB \rangle$, and $\langle BAAB \rangle$, respectively (or any correlator with C instead of B).

The computation can straightforwardly be extended to other correlators as explained above; however, we will not be providing explicit results as they are relatively lengthy.

The explicit forms in Eq. (A47) can be used to check the consistency of the crossing equations. Furthermore, one can use them to fix the overall signs of the global symmetry tensor structures $(T_o^{abcd})_{mnpr}^{(ij)}$ which cannot be fixed by group theory arguments. This is especially useful as the reflection positivity constraint in Eq. (A35) is insufficient to fix the signs of *all* tensor structures.

APPENDIX B: MIXED CORRELATOR BOOTSTRAP OF $SU(4)$ ADJOINT SCALARS WITH OPPOSITE PARITY CHARGES

In Fig. 2 we presented the fermion bilinear single correlator bootstrap results, which show interesting kinks in different channels after imposing gaps inspired by the perturbative QED$_3$ spectrum. One may expect to obtain stronger bootstrap results and even restrict the CFT data into a closed island by bootstrapping mixed correlators, reminiscent to the remarkable success in [92]. In addition to mixing with monopole operators, another simple candidate for the mixed correlator bootstrap study is the lowest scalar R in the parity even $SU(4)$ adjoint representation. There are yet other interesting candidates for the mixed correlator bootstrap studies, such as the lowest scalar in the (422) representation of $SU(4)$ and the lowest spin 1 operator in the real combination of $((310) + (332))^-$ representation. Nevertheless, their mixed correlator bootstrap implementations are much more challenging.

The results of our preliminary exploration of the mixed correlator bootstrap with external scalars r and R are shown in Fig. 14. By introducing a gap 4.0 for the second lowest scalar in the (2, 1, 1) sector, there is a mild lower bound on the scaling dimension Δ_R from the single correlator bootstrap, which becomes stronger in the mixed correlator bootstrap results. This suggests the mixed correlator bootstrap indeed can help to generate a stronger bound. However, the lower bound on Δ_R obtained from the mixed correlator bootstrap is not close to the kink in the upper bound or the large N_f perturbative result. The results suggest it is hard to further isolate the kinks in the single correlator bootstrap bound into a closed region using this mixed correlator bootstrap. This may not be surprising. As mentioned in our discussion for the bootstrap results in Fig. 3, it is hard to distinguish conformal QED$_3$ from QCD$_3$ in the bootstrap bounds on the scaling dimensions of fermion bilinear and 4-fermion operators, as both of them share a similar low-lying spectrum. However, they have significantly different central charges. It might be interesting to further explore the roles of conserved currents and their associated central charges in the bootstrap studies
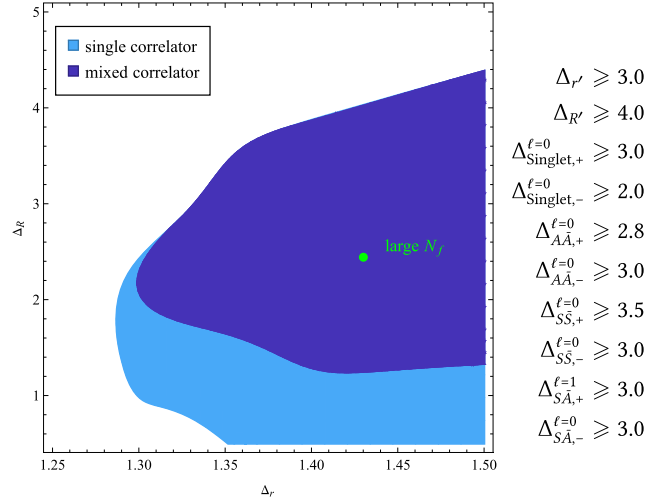

FIG. 14. Bootstrap bounds on the scaling dimensions of the fermion bilinear scalar r and the lowest parity even $SU(4)$ adjoint scalar R appearing in the $r \times r$ OPE. The light shaded region represents the bound from the single correlator bootstrap with an external scalar r at $\Lambda = 19$, and the dark shaded region denotes the bound from the mixed correlator bootstrap with external scalars r and R.

of conformal QED$_3$ in mixed correlator bootstraps involving 4-fermion operators.

APPENDIX C: MORE DETAILS ON THE LARGE N_f MODE CONSTRUCTION

In this section we give more details on the computations of the spectrum at large N_f, primarily following [52,69].

1. Monopole harmonics

First, we review the spinor monopole spherical harmonics described in [69]. In terms of the scalar monopole spherical harmonics $Y_{q,lm}$ used in Eq. (A2), they read as

$$
\begin{aligned}
T_{q,lm}(\theta, \phi) &\equiv \begin{pmatrix} \sqrt{\frac{\ell+m+1}{2\ell+1}} Y_{q,lm}(\theta,\phi) \\ \sqrt{\frac{\ell-m}{2\ell+1}} Y_{q,l(m+1)}(\theta,\phi) \end{pmatrix}, \\
S_{q,lm}(\theta, \phi) &\equiv \begin{pmatrix} -\sqrt{\frac{\ell-m}{2\ell+1}} Y_{q,lm}(\theta,\phi) \\ \sqrt{\frac{\ell+m+1}{2\ell+1}} Y_{q,l(m+1)}(\theta,\phi) \end{pmatrix}.
\end{aligned} \tag{C1}
$$

The wave functions in Eq. (2.10) are defined as

$$A_{qlm} = \frac{qT_{q,lm} + (\lambda_l + l + 1/2)S_{q,lm}}{\sqrt{(2l+1)(l+1/2+\lambda_l)}},$$

$$B_{qlm} = \frac{qT_{q,lm} + (\lambda_l - l - 1/2)S_{q,lm}}{\sqrt{(2l+1)(l+1/2-\lambda_l)}},$$

$$C_{q,q-1/2,m} = S_{q,q-1/2,m}. \tag{C2}$$

The equation above along with Eq. (C3) indicates that A_{qlm} and B_{qlm} does not transform nicely under space parity unless $q = 0$. For $q = 0$, we have[40]

Space parity : $X_{0lm}(\theta, \phi) \to (-1)^{l+m} X_{0lm}(\theta, \phi)$

for $X = A, B$. (C4)

Therefore, we can implement the parity transformation in the Hilbert space in a straightforward fashion for the $q = 0$ sector. If we define

$$\mathcal{P}\psi(x^0, x^1, x^2)\mathcal{P}^{-1} = \gamma^2\psi(x^0, x^1, -x^2), \tag{C5}$$

then we conclude via Eqs. (2.10) and (C4) that, for the $q = 0$ sector,

$$\mathcal{P}a_{lm}^{i,\dagger}\mathcal{P}^{-1} = (-1)^{\ell+m}a_{lm}^{i,\dagger},$$
$$\mathcal{P}b_{lm}^i\mathcal{P}^{-1} = (-1)^{\ell+m}b_{lm}^i, \tag{C6}$$

where $c_{q-1/2,m}^{i,\dagger}$ does not show up in $q = 0$ sectors.

2. Construction of the large N_f states

Now we discuss how to construct the large N_f states from the oscillator modes in (2.10). Schematically, this takes three steps:

(1) Take all possible combinations of creation operators $a_{jm}^{i,\dagger}$, $b_{jm,i}^\dagger$, and $c_{q-1/2,m}^{i,\dagger}$ below a certain energy $E_{\max}$ that are charge neutral.

(2) For each string of creation operators, construct all $SU(N_f)$ and $SO(3)$ reps in the product of reps of individual operators.

(3) For each representation, try antisymmetrizing the identical fermion creation operators.

a. Selection of operators

The first step is straightforward. The $c^\dagger$ operator has zero energy so there is always a ground state populated by $c^\dagger$ only. The operators $a_{jm}^{i,\dagger}$ and $b_{jm,i}^\dagger$ have energy

$$\lambda_j = \sqrt{(j+1/2)^2 - q^2}. \tag{C7}$$

Since their spin is bounded from below $j \ge q + 1/2$, the lowest energy of a single oscillator is $\lambda_{q+1/2} = \sqrt{2q+1}$, which sets an upper bound on the total number of $a_{jm}^{i,\dagger}$ and $b_{jm,i}^\dagger$

$$n_a + n_b \le \frac{E_{\max}}{\sqrt{2q+1}}. \tag{C8}$$

After this, the gauge charge neutrality and $n_b \ge 0$ requires

$$n_a \le \min\left\{n_a + n_b, -q\left(k - \frac{N}{2}\right) + \frac{n_a + n_b}{2}\right\}. \tag{C9}$$

Finally, the largest spin of each operator $a_{jm}^{i,\dagger}$ and $b_{jm,i}^\dagger$ is bounded by $E_{\max}$

$$j \le \sqrt{E_{\max}^2 + q^2} - \frac{1}{2}. \tag{C10}$$

These constraints leave us finitely many possible combinations. We can exhaust these possibilities and select those below $E_{\max}$.

b. Constructing $SU(N_f)$ and $SO(3)$ reps

In this step we focus on the $SU(N_f)$ and $SO(3)$ states separately, and treat for now each creation operator as a distinct particle. An $SU(N_f)$ state corresponds to a tensor

$$|T\rangle \equiv T_{i_1,i_2,\ldots,i_{n_a}}^{k_1,k_2,\ldots,k_{n_b}} a^{i_1,\dagger}a^{i_2,\dagger}\cdots a^{i_{n_a},\dagger} b_{k_1}^\dagger b_{k_2}^\dagger \cdots b_{k_{n_b}}^\dagger |M_{\text{bare}}\rangle, \tag{C11}$$

where the spin indices are suppressed. To project to a certain representation, we diagonalize the quadratic Casimir operator

$$C_2|T, r\rangle = c_2(r)|T, r\rangle. \tag{C12}$$

Similarly, we associate each $SO(3)$ state to a tensor

$$|U\rangle \equiv U^{m_1, m_2, \ldots, m_n}|j_1, m_1\rangle \otimes |j_2, m_2\rangle \otimes \cdots \otimes |j_n, m_n\rangle, \tag{C13}$$

where $-j_i \le m_i \le j_i$, and again diagonalize the $SO(3)$ quadratic Casimir

$$L^2|U, j\rangle = j(j+1)|U, j\rangle. \tag{C14}$$

We collect all eigenstates for the next step.

---

[40]The general relation reads as

Space parity : $X_{q,lm}(\theta, \phi) \to (-1)^{l+m} e^{2iq\phi} X_{-q,lm}(\theta, \phi)$

for $X = T, S$, (C3)

which follows from the application of Eq. (A3) for the spinor monopole spherical harmonics $T_{q,lm}^\alpha(x)$ and $S_{q,lm}^\alpha(x)$ defined in [69].

c. Antisymmetrization

Potentially, a state $|\Psi_{j,r}\rangle$ of spin j transforming in an $SU(N)$ rep r live in the linear space

$$|\Psi_{j,r}\rangle \in \text{span}\{|U_k, j\rangle \otimes |T_\ell, r\rangle\}, \qquad (C15)$$

and we fully antisymmetrize it to make it fermionic. If all creation operators $a_{jm}^{i,\dagger}$, $b_{jm,i}^{\dagger}$, and $c_{q-1/2,m}^{i,\dagger}$ have distinct quantum numbers, then the antisymmetrization is trivial. However, if there are two or more operators of the same type a, b, or c having the same spin, we need to check if there is at least a state in the above space that is antisymmetric under the permutation between those operators. We take as an example the states created by four identical $c^\dagger$ operators to explain the procedure to determine whether certain reps can show up.

Example: $q = 1$ sector ground state representation

$$|\Psi\rangle \sim (c_{1/2,m}^\dagger)^4 |M_{\text{bare}}\rangle. \qquad (C16)$$

This is also the ground state of the $q = 1$ sector in the $N_f = 4$ case. After brute-force diagonalizing the Casimir matrix, we obtain some number of eigenvectors in the reps listed below:

$c_2(r)$	0	4	6	8
dimension	1	45	40	135

j	0	1	2
dimension	2	9	5

$$(C17)$$

Note that the dimension of the eigenvector space is multiple times the dimension of the rep. This is because we may construct the same rep from a different tensor contraction, and they mix when we permute the particles. We would like to study how the $c^\dagger$s' permutation group acts on the states. The generators of permutation group $\mathbb{Z}_n$ of n particles are $(n-1)$ subsequent permutations, in our case R_{12}, R_{23}, and R_{34}. The matrix representation of these generators are, for example for R_{12}

$$\left(R_{12}^{(r)}\right)_{ik} \equiv \left\langle T_i^{(2134)}, r | T_k^{(1234)}, r \right\rangle, \qquad (C18)$$

$$\left(R_{12}^{(j)}\right)_{ik} \equiv \left\langle U_i^{(2134)}, j | U_k^{(1234)}, j \right\rangle. \qquad (C19)$$

To show that an antisymmetric state exists, we just need to find a common eigenvector of eigenvalue (-1) for all three product matrices: $R_{12}^{(r)} \otimes R_{12}^{(j)}$, $R_{23}^{(r)} \otimes R_{23}^{(j)}$, and $R_{34}^{(r)} \otimes R_{34}^{(j)}$. Because R_{12} and R_{23} do not commute, generically we cannot simultaneously diagonalize them both, but the all-minus and all-plus sectors can be simultaneously diagonalized.

It may be tempting to try reducing this problem to individual matrices $R_{\alpha\beta}^{(r)}$ and $R_{\alpha\beta}^{(j)}$. The argument would sound like the following: the eigenvalue of the Kronecker product matrix $R_{\alpha\beta}^{(r)} \otimes R_{\alpha\beta}^{(j)}$ is the product of constituents, thus the eigenvalues of $R_{\alpha\beta}^{(r)}$ and $R_{\alpha\beta}^{(j)}$ individually must be either $(+1, -1)$ or $(-1, +1)$. But this implies that each eigenvector we find would be an eigenvector of all six matrices, which is in tension with the fact that the permutation operators do not commute. Indeed a straightforward check shows that this is not the case. What is wrong? The issue is that an eigenvector of the Kronecker product matrix does not necessarily factorize into a Kronecker product, so our target state may not have definitive permutation parity if projected to either $|T\rangle$ space or $|U\rangle$ space, but it is antisymmetric in the space of the product group representation. This makes the problem much harder because we are forced to run an eigenvalue problem on Kronecker product matrices which have huge dimension.

To speed up the computation, we use the Lanczos method [97] to find the eigenvectors of eigenvalue (-1). Lanczos method is a variational ansatz that aims at minimizing the expectation value of a matrix. Schematically, to diagonalize a Hermitian matrix H, we project H to a basis spanned by

$$\{\Psi, H\Psi, H^2\Psi, \cdots\}, \qquad (C20)$$

where Ψ is the initial condition, and diagonalize the submatrix. The lowest eigenvalue of the submatrix is an approximation of the lowest eigenvalue of the whole matrix. If H has big sparsity, which is the case in our example, then the approximation will converge with a much smaller dimensional basis than the full dimension of H. Since we would like to find a state with eigenvalue (-1) of all three matrices, we define

$$H\Psi \equiv \left(\frac{3}{5} R_{12}^{(r)} \otimes R_{12}^{(j)} + \frac{5}{7} R_{23}^{(r)} \otimes R_{23}^{(j)} + \frac{7}{11} R_{34}^{(r)} \otimes R_{34}^{(j)}\right)\Psi, \qquad (C21)$$

where Ψ has dimension $(\dim_k\{|U_k, j\rangle\} \times \dim_\ell\{|T_\ell, r\rangle\})$. We use the Lanczos method to find the lowest eigenvalue of H. The three matrices will have eigenvalue (-1) if and only if the eigenvalue of H is $-\frac{3}{5} - \frac{5}{7} - \frac{7}{11} \approx -1.95065$, and that all other eigenvalues of H are larger. If the eigenvalue converges to -1.95065, then we conclude that an antisymmetric state exists. Otherwise, the eigenvalue will converge to a greater value, and we conclude that a fermionic state that is constructed from four identical $c^\dagger$s and transforms in reps (r, j) does not exist.

Using this method, we check the existence of antisymmetric states in each pair of reps in (C17). The result is the following:

	$j=0$	$j=1$	$j=2$
$c_2=0$	No	No	Yes
$c_2=4$	No	Yes	No
$c_2=6$	Yes	No	No
$c_2=8$	No	No	No

$$\text{(C22)}$$

The lowest $q=1$ scalar monopole is indeed in the $SU(4)$ rep $A\bar{A}$ which has $c_2=6$.

3. Implications of the parity symmetry for uncharged sectors

In Sec. C 1, we discussed that the creation operators transform irreducibly under the space parity transformation in the $q=0$ sector. Indeed, $c_{q-1/2,m}^{i,\dagger}$ does not show up in this sector and $a_{jm}^{i,\dagger}$ and $b_{jm,i}^{\dagger}$ simply get a sign $(-1)^{j+m}$ under reflection. For an operator made of several $a^{\dagger}$s and $b^{\dagger}$s, $\mathcal{O} \sim a_{j_1 m_1}^{\dagger} \cdots b_{j_n m_n}^{\dagger}$, the internal parity is the product of the signs of each constituents, factoring out the total $(-1)^{j_{\mathcal{O}}+m_{\mathcal{O}}}$; thus,

$$\text{internal parity of } \mathcal{O} = (-1)^{(\sum_i j_i)-j_{\mathcal{O}}}. \quad \text{(C23)}$$

We can check this explicitly for several low-dimension operators. For instance, we know that $\bar{\psi}\psi$ and $\bar{\psi}\gamma^{\mu}\overleftrightarrow{\partial}\psi$ are parity-odd whereas $\bar{\psi}\gamma^{\mu}\psi$, $\bar{\psi}\overleftrightarrow{\partial}\psi$, and $\bar{\psi}\overleftrightarrow{\partial}\gamma^{\mu}\overleftrightarrow{\partial}\psi$ are parity even.[41] In the large N_f limit, $\Delta_{\psi}=1$ and the operators have their engineering dimensions. The first two operators $\bar{\psi}\psi$ and $\bar{\psi}\gamma^{\mu}\psi$ have a dimension of 2, so they must be made of a pair of lowest spin creation operators, $a_{1/2}^{\dagger}b_{1/2}^{\dagger}$. Using (C23) we determine that the scalar is parity odd and vector is parity even. Next we have two dimension-3 operators. In our construction the dimension-3 scalar does not exist, and the vector is made of $a_{3/2}^{\dagger}b_{1/2}^{\dagger}$ or $a_{1/2}^{\dagger}b_{3/2}^{\dagger}$. In either case, the parity is odd. Finally, the dimension-4 vector is made of $a_{3/2}^{\dagger}b_{3/2}^{\dagger}$ and has even parity.

Combining the parity rule with the large N_f state construction discussed in the last subsection, we can write a summary of the $q=0$ sector as the table (up to 6 particles and energy level 6)

	singlet	Adj	$A\bar{A}$	$S\bar{A}$	$S\bar{S}$
$j=0$	$0^+,2^-,4^{\pm},5^-,6^{\pm}$	$2^-,4^{\pm},5^-,6^{\pm}$	$4^+,5^-,6^{\pm}$	$5^-,6^{\pm}$	$4^+,6^{\pm}$
$j=1$	$2^+,3^-,4^{\pm},5^{\pm},6^{\pm}$	$2^+,3^-,4^{\pm},5^{\pm},6^{\pm}$	$4^-,5^+,6^{\pm}$	$4^-,5^+,6^{\pm}$	$5^+,6^{\pm}$
$j=2$	$3^+,4^{\pm},5^{\pm},6^{\pm}$	$3^+,4^{\pm},5^{\pm},6^{\pm}$	$4^+,5^-,6^{\pm}$	$5^-,6^{\pm}$	$5^-,6^+$
$j=3$	$4^+,5^{\pm},6^{\pm}$	$4^+,5^{\pm},6^{\pm}$	$5^+,6^-$	$5^+,6^-$	$5^+,6^-$

$$\text{(C24)}$$

where the number and superscript sign are the dimension and parity of the corresponding operator, respectively, and $\pm$ means both parity odd and even operators can be found at this dimension. The parity even operators appear in the S sector of $M \times M$ OPE, and the parity odd operators appear in the A sector.

APPENDIX D: MIXED CROSSING EQUATIONS BETWEEN THE LOWEST MONOPOLE $\mathcal{M}_{1/2}$ AND THE FERMION BILINEAR r

We study the mixed correlator system of the lowest monopole $M \equiv \mathcal{M}_{1/2}$ and the lowest parity odd adjoint scalar r. In addition to the $\langle rrrr \rangle$ correlator discussed in (3.1) and the $\langle MMMM \rangle$ correlator discussed in (4.3) and (4.4), we further have the mixed correlators $\langle MMrr \rangle$, $\langle MrrM \rangle$ and $\langle MrMr \rangle$. In the language of $SO(2)$ and $SU(4)$ representations, M is in the $V,(110)$ representation and r is in the $S,(211)$ representation. The additional tensor product of representation we have in the system is that of $r \times M$,

$$SU(4): (110) \otimes (211) = (110) \oplus (200) \oplus (321),$$
$$SO(2): V \otimes S = V. \quad \text{(D1)}$$

The full crossing equation system from all correlators is thus

$$0 = \vec{V}_{\mathbb{1}} + \sum_{\mathcal{O},i^+} \begin{pmatrix} \lambda_{MM\mathcal{O}} & \lambda_{rr\mathcal{O}} \end{pmatrix} \vec{V}_{\Delta,\ell}^{S,i^+} \begin{pmatrix} \lambda_{MM\mathcal{O}} \\ \lambda_{rr\mathcal{O}} \end{pmatrix}$$
$$+ \lambda_{MMr}^2 \vec{V}_{MMr} + \sum_{\mathcal{O},j} \lambda_{rr\mathcal{O}}^2 \vec{V}_{\Delta,\ell}^{S,j} + \sum_{\mathcal{O},i^-} \lambda_{MM\mathcal{O}}^2 \vec{V}_{\Delta,\ell}^{A,i^-}$$
$$+ \sum_{\mathcal{O},i^+} \lambda_{MM\mathcal{O}}^2 \vec{V}_{\Delta,\ell}^{T,i^+} + \sum_{\mathcal{O},k} \lambda_{rM\mathcal{O}}^2 \vec{V}_{\Delta,\ell}^{V,k}, \quad \text{(D2)}$$

where $i^{\pm}=(000)^{\pm},(211)^{\mp},(220)^{\pm},j=(211)^+,(310)_R^-,(422)^+,$ $k=(110),(200),(321)$ are the sets of representations and

---

[41]One can explicitly check this using $\psi \to \gamma^2\psi$ and $\bar{\psi} \to -\bar{\psi}\gamma^2$ along with some gamma algebra identities; however, we can see this more simply by group-theoretical arguments. Under the Pin$(2,1)$ group, we label the representations as j^p where j is the usual spin and p is the parity of the representation. We then have the branching $j_1^{p_1} \otimes j_2^{p_2} = (j_1 + j_2)^{p_1 p_2} \oplus (j_1 + j_2 - 1)^{-p_1 p_2} \oplus \cdots \oplus |j_1 - j_2|^{\pm}$ where parities alternate between representations. If we choose the fermions to have positive parity (this does not affect anything for operators containing an even number of fermions), then we see that $\frac{1}{2}^+ \otimes \frac{1}{2}^+ = 1^+ \otimes 0^-$; hence, the scalar $\bar{\psi}\psi$ has odd parity whereas the vector $\bar{\psi}\gamma^{\mu}\psi$ has even parity.

TABLE VI. A summary of the conformal blocks and the OPE coefficients in the $SU(4)$ mixed monopole-fermion-bilinear correlators.

$SU(4)$ name	Young tableaux	$SO(2)$ rep	Spin	OPE
Singlet(000)	•	S	Even	$\lambda_{rrO}, \lambda_{MMO}$
		A	Odd	λ_{MMO}
		T	Even	λ_{MMO}
Adj(211)	⊞	S	Odd	$\lambda_{rrO}, \lambda_{MMO}$
		S	Even	λ_{rrO}
		A	Even	λ_{MMO}
		T	Odd	λ_{MMO}
AA (220)	⊞	S	Even	$\lambda_{rrO}, \lambda_{MMO}$
		A	Odd	λ_{MMO}
		T	Even	λ_{MMO}
SĀ $(310)_R$	⊞	S	Odd	λ_{rrO}
SS̄ (422)	⊞	S	Even	λ_{rrO}
Anti(110)	⊞	V	Both	λ_{rMO}
Sym (200)	⊞	V	Both	λ_{rMO}
AAdj (321)	⊞	V	Both	λ_{rMO}

spins appearing in the summation. The $+(-)$ in the superscript of each representation means only even(odd) spins appear in the sum. The operators in representations $SO(2)$ V, $SU(4)$ k can have any spin. The explicit forms of the vector blocks $\vec{V}_{\mathbb{1}}$, $\vec{V}_{MMr}$, $\vec{V}_{\Delta,\ell}^{S,i+}$, etc., are given in the attached *Mathematica* notebook. There are in total 18

different channels and 24 crossing equations. Various selection rules from global symmetry representations, parity, and spin control the possible contributions to the OPE in each channel. We summarize these selection rules in Table VI.

The OPE coefficients of the stress tensor $T^{\mu\nu}$, $SU(4)$ conserved current $J^{f\mu}$ and the topological $U(1)$ conserved current $J^{t\mu}$ are constrained by Ward identities in terms of the two-point coefficients c_T, c_J, and c_J^t, respectively. In our conventions, we have

$$c_T = \frac{9\Delta_M^2}{4\lambda_{MMT}^2} = \frac{9\Delta_r^2}{4\lambda_{rrT}^2}, \quad \begin{pmatrix} \lambda_{MMJ}^{\text{mix}} \\ \lambda_{rrJ}^{\text{mix}} \end{pmatrix} = \frac{1}{\sqrt{c_J}} \begin{pmatrix} \sqrt{30} \\ -\sqrt{60} \end{pmatrix},$$

$$\lambda_{MMJ^t}^{\text{mix}\,2} = \frac{6}{c_J^t}. \tag{D3}$$

APPENDIX E: NUMERICAL SETUP AND IMPLEMENTATION

Our bootstrap computations are run with SDBP [98,99] and set up using the packages found in [100–102]. We also used `autoboot` to cross check the r and $\mathcal{M}_{1/2}$ mixed correlator crossing equation [103].

The *interval positivity* condition plays an important role in our bootstrap study, which assumes the spectrum in the bootstrap equations satisfies the constraint:

$$\Delta_0 < \Delta \le \Delta_1 \quad \text{or} \quad \Delta \ge \Delta_2, \quad (\Delta_2 > \Delta_1).$$

It is less straightforward in SDPB to impose the positivity condition for the interval range of the scaling dimension $\Delta_0 < \Delta \le \Delta_1$. To do this requires a coordinate transformation to map the interval range to $(0, \infty)$, e.g.

TABLE VII. Parameters for the paper's computations. The sets $S_{19,27,31,39}$ are defined in (E1).

	$\Lambda = 19$	$\Lambda = 27$	$\Lambda = 31$	$\Lambda = 39$
keptPoleOrder	14	20	32	40
order	60	60	80	90
spins	S_{19}	S_{27}	S_{31}	S_{39}
precision	640	640	768	1024
dualityGapThreshold	10^{-30}	10^{-30}	10^{-30}	10^{-30}
primalErrorThreshold	10^{-200}	10^{-200}	10^{-200}	10^{-200}
dualErrorThreshold	10^{-200}	10^{-200}	10^{-200}	10^{-200}
findPrimalFeasible	False	False	False	False
findDualFeasible	False	False	False	False
detectPrimalFeasibleJump	True	True	True	True
detectDualFeasibleJump	True	True	True	True
initialMatrixScalePrimal	10^{40}	10^{50}	10^{50}	10^{60}
initialMatrixScaleDual	10^{40}	10^{50}	10^{50}	10^{60}
feasibleCenteringParameter	0.1	0.1	0.1	0.1
infeasibleCenteringParameter	0.3	0.3	0.3	0.3
stepLengthReduction	0.7	0.7	0.7	0.7
maxComplementarity	10^{100}	10^{130}	10^{160}	10^{200}

$$\Delta = \Delta_0 + \frac{x}{1+x}(\Delta_1 - \Delta_0),$$

based on which the interval $\Delta \in (\Delta_0, \Delta_1)$ is mapped to $x > 0$. Then the positivity constraint in the whole range $x \in (0, \infty)$ can be effectively studied using SDPB.

An alternative setup for the interval positivity constraints is to simply sample the interval (Δ_0, Δ_1) with many isolated points, and refine the sampling until the bounds are well converged. We have done computations where we sample the interval range with step $\delta = 0.005$, and find results consistent with the continuous formulation.

For the SDPB calculations, we provide a summary of the numerical parameters in Table VII.[42]

The spins used in the computations are

$$
\begin{aligned}
S_{19} &= \{0, \ldots, 26\} \cup \{49, 50\}, \\
S_{27} &= \{0, \ldots, 26\} \cup \{29, 30, 33, 34, 37, 38, 41, 42, 45, 46, 49, 50\}, \\
S_{31} &= \{0, \ldots, 44\} \cup \{47, 48, 51, 52, 55, 56, 59, 60, 63, 64, 67, 68\}, \\
S_{39} &= \{0, \ldots, 64\} \cup \{67, 68, 71, 72, 75, 76, 79, 80, 83, 84, 87, 88\}.
\end{aligned}
\tag{E1}
$$

---

[42]The code used to run these calculations can be found so the reader may run these calculations themselves at the following link and commit: https://gitlab.com/rajeev.erramilli/hyperion-projects/-/tree/fbcdd70673cf17cccc44f205a649fcfa8676130c.

---

[1] T. Appelquist, D. Nash, and L. C. R. Wijewardhana, Critical Behavior in $(2+1)$-Dimensional QED, Phys. Rev. Lett. **60**, 2575 (1988).

[2] D. Nash, Higher Order Corrections in $(2+1)$-Dimensional QED, Phys. Rev. Lett. **62**, 3024 (1989).

[3] A. M. Polyakov, Compact gauge fields and the infrared catastrophe, Phys. Lett. **59B**, 82 (1975).

[4] A. M. Polyakov, Quark confinement and topology of gauge groups, Nucl. Phys. **B120**, 429 (1977).

[5] R. D. Pisarski, Chiral-symmetry breaking in three-dimensional electrodynamics, Phys. Rev. D **29**, 2423 (1984).

[6] T. W. Appelquist, M. J. Bowick, D. Karabali, and L. C. R. Wijewardhana, Spontaneous chiral symmetry breaking in three-dimensional QED, Phys. Rev. D **33**, 3704 (1986).

[7] E. Dagotto, A. Kocic, and J. B. Kogut, Chiral symmetry breaking in three-dimensional QED with $N(f)$ flavors, Nucl. Phys. **B334**, 279 (1990).

[8] W. Rantner and X.-G. Wen, Electron Spectral Function and Algebraic Spin Liquid for the Normal State of Underdoped High T_c Superconductors, Phys. Rev. Lett. **86**, 3871 (2001).

[9] W. Rantner and X.-G. Wen, Spin correlations in the algebraic spin liquid: Implications for high-Tc superconductors, Phys. Rev. B **66**, 144501 (2002).

[10] I. F. Herbut, QED(3) theory of underdoped high temperature superconductors, Phys. Rev. B **66**, 094504 (2002).

[11] M. Franz, Z. Tesanovic, and O. Vafek, QED(3) theory of pairing pseudogap in cuprates. 1. From D wave superconductor to antiferromagnet via 'algebraic' Fermi liquid, Phys. Rev. B **66**, 054535 (2002).

[12] M. Hermele, T. Senthil, and M. P. A. Fisher, Algebraic spin liquid as the mother of many competing orders, Phys. Rev. B **72**, 104404 (2005).

[13] M. Hermele, Y. Ran, P. A. Lee, and X.-G. Wen, Properties of an algebraic spin liquid on the kagome lattice, Phys. Rev. B **77**, 224413 (2008).

[14] T. Senthil, D. T. Son, C. Wang, and C. Xu, Duality between $(2+1)$d quantum critical points, Phys. Rep. **827**, 1 (2019).

[15] P. Maris, The influence of the full vertex and vacuum polarization on the fermion propagator in QED in three-dimensions, Phys. Rev. D **54**, 4049 (1996).

[16] I. J. R. Aitchison, N. E. Mavromatos, and D. McNeill, Inverse Landau-Khalatnikov transformation and infrared critical exponents of $(2+1)$-dimensional quantum electrodynamics, Phys. Lett. B **402**, 154 (1997).

[17] T. Appelquist, A. G. Cohen, and M. Schmaltz, A new constraint on strongly coupled gauge theories, Phys. Rev. D **60**, 045003 (1999).

[18] K.-i. Kubota and H. Terao, Dynamical symmetry breaking in QED(3) from the Wilson RG point of view, Prog. Theor. Phys. **105**, 809 (2001).

[19] T. Appelquist and L. C. R. Wijewardhana, Phase structure of noncompact QED3 and the Abelian Higgs model, in *Proceedings of the 3rd International Symposium on Quantum Theory and Symmetries* (2004), pp. 177–191, 10.1142/9789812702340_0022.

[20] M. Franz, T. Pereg-Barnea, D. E. Sheehy, and Z. Tešanović, Gauge-invariant response functions in algebraic fermi liquids, Phys. Rev. B **68**, 024508 (2003).

[21] C. S. Fischer, R. Alkofer, T. Dahm, and P. Maris, Dynamical chiral symmetry breaking in unquenched QED(3), Phys. Rev. D **70**, 073007 (2004).

[22] A. V. Kotikov, V. I. Shilin, and S. Teber, Critical behavior of $(2 + 1)$-dimensional QED: $1/N_f$ corrections in the Landau gauge, Phys. Rev. D **94**, 056009 (2016); **99**, 119901(E) (2019).

[23] K. Kaveh and I. F. Herbut, Chiral symmetry breaking in three-dimensional quantum electrodynamics in the presence of irrelevant interactions: A renormalization group study, Phys. Rev. B **71**, 184519 (2005).

[24] S. Giombi, I. R. Klebanov, and G. Tarnopolsky, Conformal QED$_d$, F-theorem and the ϵ expansion, J. Phys. A **49**, 135403 (2016).

[25] L. Di Pietro, Z. Komargodski, I. Shamir, and E. Stamou, Quantum Electrodynamics in $d = 3$ from the ε Expansion, Phys. Rev. Lett. **116**, 131601 (2016).

[26] S. Giombi, G. Tarnopolsky, and I. R. Klebanov, On C_J and C_T in conformal QED, J. High Energy Phys. 08 (2016) 156.

[27] L. Di Pietro and E. Stamou, Scaling dimensions in QED$_3$ from the ϵ-expansion, J. High Energy Phys. 12 (2017) 054.

[28] N. Zerf, P. Marquard, R. Boyack, and J. Maciejko, Critical behavior of the QED$_3$-Gross-Neveu-Yukawa model at four loops, Phys. Rev. B **98**, 165125 (2018).

[29] I. F. Herbut, Chiral symmetry breaking in three-dimensional quantum electrodynamics as fixed point annihilation, Phys. Rev. D **94**, 025036 (2016).

[30] V. P. Gusynin and P. K. Pyatkovskiy, Critical number of fermions in three-dimensional QED, Phys. Rev. D **94**, 125009 (2016).

[31] S. Benvenuti and H. Khachatryan, QED's in $2 + 1$ dimensions: Complex fixed points and dualities, arXiv:1812.01544.

[32] S. Christofi, S. Hands, and C. Strouthos, Critical flavor number in the three dimensional Thirring model, Phys. Rev. D **75**, 101701 (2007).

[33] L. Janssen and H. Gies, Critical behavior of the $(2 + 1)$-dimensional Thirring model, Phys. Rev. D **86**, 105007 (2012).

[34] S. Hands, M. Mesiti, and J. Worthy, Critical behavior in the single flavor Thirring model in $2 + 1D$, Phys. Rev. D **102**, 094502 (2020).

[35] J. Braun, H. Gies, L. Janssen, and D. Roscher, Phase structure of many-flavor QED$_3$, Phys. Rev. D **90**, 036002 (2014).

[36] S. Gukov, RG flows and bifurcations, Nucl. Phys. **B919**, 583 (2017).

[37] S. J. Hands, J. B. Kogut, L. Scorzato, and C. G. Strouthos, The chiral limit of noncompact QED in three-dimensions, Nucl. Phys. B, Proc. Suppl. **119**, 974 (2003).

[38] S. J. Hands, J. B. Kogut, and C. G. Strouthos, Noncompact QED(3) with N(f) greater than or equal to 2, Nucl. Phys. **B645**, 321 (2002).

[39] S. J. Hands, J. B. Kogut, L. Scorzato, and C. G. Strouthos, Non-compact QED(3) with $N_f = 1$ and $N_f = 4$, Phys. Rev. B **70**, 104501 (2004).

[40] C. Strouthos and J. B. Kogut, The phases of non-compact QED(3), Proc. Sci. LATTICE2007 (**2007**) 278 [arXiv:0804.0300].

[41] N. Karthik and R. Narayanan, No evidence for bilinear condensate in parity-invariant three-dimensional QED with massless fermions, Phys. Rev. D **93**, 045020 (2016).

[42] N. Karthik and R. Narayanan, Scale-invariance of parity-invariant three-dimensional QED, Phys. Rev. D **94**, 065026 (2016).

[43] N. Karthik and R. Narayanan, Numerical determination of monopole scaling dimension in parity-invariant three-dimensional noncompact QED, Phys. Rev. D **100**, 054514 (2019).

[44] N. Karthik and R. Narayanan, QED$_3$-Inspired Three-Dimensional Conformal Lattice Gauge Theory without Fine-Tuning, Phys. Rev. Lett. **125**, 261601 (2020).

[45] Z. Li, On conformality and self-duality of $N_f = 2$ QED$_3$, arXiv:2107.09020.

[46] H. Gies and J. Jaeckel, Chiral phase structure of QCD with many flavors, Eur. Phys. J. C **46**, 433 (2006).

[47] D. B. Kaplan, J.-W. Lee, D. T. Son, and M. A. Stephanov, Conformality lost, Phys. Rev. D **80**, 125005 (2009).

[48] V. Gorbenko, S. Rychkov, and B. Zan, Walking, Weak first-order transitions, and Complex CFTs, J. High Energy Phys. 10 (2018) 108.

[49] R. Rattazzi, V. S. Rychkov, E. Tonni, and A. Vichi, Bounding scalar operator dimensions in 4D CFT, J. High Energy Phys. 12 (2008) 031.

[50] D. Poland, S. Rychkov, and A. Vichi, The conformal Bootstrap: Theory, numerical techniques, and applications, Rev. Mod. Phys. **91**, 015002 (2019).

[51] S. M. Chester and S. S. Pufu, Towards bootstrapping QED$_3$, J. High Energy Phys. 08 (2016) 019.

[52] S. M. Chester, L. V. Iliesiu, M. Mezei, and S. S. Pufu, Monopole operators in $U(1)$ Chern-Simons-Matter theories, J. High Energy Phys. 05 (2018) 157.

[53] Z. Li, Solving QED$_3$ with conformal bootstrap, arXiv:1812.09281.

[54] Z. Li and D. Poland, Searching for gauge theories with the conformal bootstrap, J. High Energy Phys. 03 (2021) 172.

[55] Z. Li, Symmetries of conformal correlation functions, arXiv:2006.05119.

[56] Y.-C. He, J. Rong, and N. Su, A roadmap for bootstrapping critical gauge theories: Decoupling operators of conformal field theories in $d > 2$ dimensions, SciPost Phys. **11**, 111 (2021).

[57] A. Manenti and A. Vichi, Exploring $SU(N)$ adjoint correlators in 3d, arXiv:2101.07318.

[58] Y.-C. He, J. Rong, and N. Su, Conformal bootstrap bounds for the $U(1)$ Dirac spin liquid and $N = 7$ Stiefel liquid, arXiv:2107.14637.

[59] X. Y. Xu, Y. Qi, L. Zhang, F. F. Assaad, C. Xu, and Z. Y. Meng, Monte Carlo Study of Lattice Compact Quantum Electrodynamics with Fermionic Matter: The Parent State of Quantum Phases, Phys. Rev. X **9**, 021022 (2019).

[60] J. A. Gracey, Computation of critical exponent η at $O(1/N_f^2)$ in quantum electrodynamics in arbitrary dimensions, Nucl. Phys. **B414**, 614 (1994).

[61] J. A. Gracey, Electron mass anomalous dimension at $O(1/(Nf(2)))$ in quantum electrodynamics, Phys. Lett. B **317**, 415 (1993).

[62] W. Rantner and X.-G. Wen, Spin correlations in the algebraic spin liquid: Implications for high-tcsuperconductors, Phys. Rev. B **66**, 144501 (2002).

[63] C. Xu, Renormalization group studies on four-fermion interaction instabilities on algebraic spin liquids, Phys. Rev. B **78**, 054432 (2008).

[64] R. K. Kaul and S. Sachdev, Quantum criticality of u(1) gauge theories with fermionic and bosonic matter in two spatial dimensions, Phys. Rev. B **77**, 155105 (2008).

[65] S. M. Chester and S. S. Pufu, Anomalous dimensions of scalar operators in QED$_3$, J. High Energy Phys. 08 (2016) 069.

[66] Y. Huh, P. Strack, and S. Sachdev, Conserved current correlators of conformal field theories in $2+1$ dimensions, Phys. Rev. B **88**, 155109 (2013); **90**, 199902(E) (2014).

[67] Y. Huh and P. Strack, Stress tensor and current correlators of interacting conformal field theories in $2+1$ dimensions: Fermionic Dirac matter coupled to U(1) gauge field, J. High Energy Phys. 01 (2015) 147; 03 (2016) 54(E).

[68] V. Borokhov, A. Kapustin, and X.-k. Wu, Topological disorder operators in three-dimensional conformal field theory, J. High Energy Phys. 11 (2002) 049.

[69] S. S. Pufu, Anomalous dimensions of monopole operators in three-dimensional quantum electrodynamics, Phys. Rev. D **89**, 065016 (2014).

[70] E. Dyer, M. Mezei, and S. S. Pufu, Monopole taxonomy in three-dimensional conformal field theories, arXiv:1309.1160.

[71] E. Dupuis, R. Boyack, and W. Witczak-Krempa, Anomalous dimensions of monopole operators at the transitions between Dirac and topological spin liquids, arXiv:2108.05922.

[72] M. Berkooz, R. Yacoby, and A. Zait, Bounds on $\mathcal{N}=1$ superconformal theories with global symmetries, J. High Energy Phys. 08 (2014) 008; 01 (2015) 132(E).

[73] Y. Nakayama, Bootstrap experiments on higher dimensional CFTs, Int. J. Mod. Phys. A **33**, 1850036 (2018).

[74] H. Iha, H. Makino, and H. Suzuki, Upper bound on the mass anomalous dimension in many-flavor gauge theories: A conformal bootstrap approach, Prog. Theor. Exp. Phys. **2016**, 053B03 (2016).

[75] D. Poland, D. Simmons-Duffin, and A. Vichi, Carving out the space of 4D CFTs, J. High Energy Phys. 05 (2012) 110.

[76] A. Dymarsky, J. Penedones, E. Trevisani, and A. Vichi, Charting the space of 3D CFTs with a continuous global symmetry, J. High Energy Phys. 05 (2019) 098.

[77] A. Dymarsky, F. Kos, P. Kravchuk, D. Poland, and D. Simmons-Duffin, The 3d stress-tensor bootstrap, J. High Energy Phys. 02 (2018) 164.

[78] M. Reehorst, E. Trevisani, and A. Vichi, Mixed scalar-current bootstrap in three dimensions, J. High Energy Phys. 12 (2020) 156.

[79] R. Rattazzi, S. Rychkov, and A. Vichi, Bounds in 4D conformal field theories with global symmetry, J. Phys. A **44**, 035402 (2011).

[80] S. El-Showk, M. F. Paulos, D. Poland, S. Rychkov, D. Simmons-Duffin, and A. Vichi, Solving the 3D Ising model with the conformal bootstrap, Phys. Rev. D **86**, 025022 (2012).

[81] N. B. Agmon, S. M. Chester, and S. S. Pufu, The M-theory archipelago, J. High Energy Phys. 02 (2020) 010.

[82] S. M. Chester, R. Dempsey, and S. S. Pufu, Bootstrapping $\mathcal{N}=4$ super-Yang-Mills on the conformal manifold, arXiv:2111.07989.

[83] L. Iliesiu, F. Kos, D. Poland, S. S. Pufu, D. Simmons-Duffin, and R. Yacoby, Bootstrapping 3D fermions, J. High Energy Phys. 03 (2016) 120.

[84] L. Iliesiu, F. Kos, D. Poland, S. S. Pufu, and D. Simmons-Duffin, Bootstrapping 3D fermions with global symmetries, J. High Energy Phys. 01 (2018) 036.

[85] S. Albayrak, D. Meltzer, and D. Poland, More analytic bootstrap: Nonperturbative effects and fermions, J. High Energy Phys. 08 (2019) 040.

[86] S. Albayrak, D. Meltzer, and D. Poland, The inversion formula and 6j symbol for 3d fermions, J. High Energy Phys. 09 (2020) 148.

[87] T. T. Wu and C. N. Yang, Dirac monopole without strings: Monopole harmonics, Nucl. Phys. **B107**, 365 (1976).

[88] T. T. Wu and C. N. Yang, Some properties of monopole harmonics, Phys. Rev. D **16**, 1018 (1977).

[89] A. Onishchik, D. Leites, and E. Vinberg, *Lie Groups and Algebraic Groups*, Springer Series in Soviet Mathematics (Springer, Berlin, Heidelberg, 2012).

[90] M. S. Costa and T. Hansen, Conformal correlators of mixed-symmetry tensors, J. High Energy Phys. 02 (2015) 151.

[91] M. S. Costa, T. Hansen, J. a. Penedones, and E. Trevisani, Projectors and seed conformal blocks for traceless mixed-symmetry tensors, J. High Energy Phys. 07 (2016) 018.

[92] F. Kos, D. Poland, and D. Simmons-Duffin, Bootstrapping mixed correlators in the 3D ising model, J. High Energy Phys. 11 (2014) 109.

[93] S. Giombi, S. Prakash, and X. Yin, A note on CFT correlators in three dimensions, J. High Energy Phys. 07 (2013) 105.

[94] M. S. Costa, J. Penedones, D. Poland, and S. Rychkov, Spinning conformal correlators, J. High Energy Phys. 11 (2011) 071.

[95] D. Simmons-Duffin, Projectors, shadows, and conformal blocks, Projectors, shadows, and conformal blocks, J. High Energy Phys. 04 (2014) 146.

[96] D. Karateev, P. Kravchuk, and D. Simmons-Duffin, Harmonic analysis and mean field theory, J. High Energy Phys. 10 (2019) 217.

[97] C. Lanczos, An iteration method for the solution of the eigenvalue problem of linear differential and integral operators, J. Res. Natl. Bur. Stand. **45**, 255 (1950).

[98] D. Simmons-Duffin, A semidefinite program solver for the conformal bootstrap, J. High Energy Phys. 06 (2015) 174.

[99] W. Landry and D. Simmons-Duffin, Scaling the semidefinite program solver SDPB, arXiv:1909.09745.

[100] D. Simmons-Duffin, P. Kravchuk, A. Liu, and R. S. Erramilli, hyperion-projects, https://gitlab.com/pkravchuk/hyperion-projects.

[101] https://gitlab.com/bootstrapcollaboration/scalar_blocks.

[102] N. Su, simpleboot, https://gitlab.com/bootstrapcollaboration/simpleboot.

[103] M. Go and Y. Tachikawa, Autoboot: A generator of bootstrap equations with global symmetry, J. High Energy Phys. 06 (2019) 084.